PV Performance Modeling Methods and Practices

Results from the 4th PV Performance Modeling Collaborative Workshop

PVPS

PV Performance Modeling Methods and Practices

Results from the 4th PV Performance Modeling

Collaborative Workshop

Author

Joshua S. Stein PhD (jsstein@sandia.gov)

Sandia National Laboratories

Editor

Boris Farnung (Boris.Farnung@ise.fraunhofer.de)

Fraunhofer ISE

Contributing Authors

Marion Schroedter-Homscheidt
Karel De Brabandere
Marcel Suri
Jan Remund
Manajit Sengupta
Elke Lorenz
Anton Driesse
Stefan Winter
Annette Hammer
Thomas Huld
Mitchell Lee
Giorgio Belluardo
Fotis Mavromatakis
Benjamin Duck
Markus Schweiger
Werner Herrmann
Bruce H. King
Janine Freeman
Teresa Zhang
Gianluca Corbellini
Christian Reise
Hendrik Holst
Jose E. Castillo-Aguilella
Bruno Wittmer
Tomas Cebecauer
Aron P. Dobos
Paul Gibbs
Angele Reinders
Matthew Boyd
Gabi Friesen
Benjamin Matthiss
Steve Ransome
Jürgen Sutterlueti
Yuzuru Ueda
Roger French

Table of Contents

Foreword

The International Energy Agency (IEA), founded in November 1974, is an autonomous body within the framework of the Organization for Economic Co-operation and Development (OECD) which carries out a comprehensive programme of energy co-operation among its member countries. The European Union also participates in the work of the IEA. Collaboration in research, development and demonstration of new technologies has been an important part of the Agency's Programme.

The IEA Photovoltaic Power Systems Programme (PVPS) is one of the collaborative R&D Agreements established within the IEA. Since 1993, the PVPS participants have been conducting a variety of joint projects in the application of photovoltaic conversion of solar energy into electricity.

The mission of the IEA PVPS Technology Collaboration Programme is: To enhance the international collaborative efforts which facilitate the role of photovoltaic solar energy as a cornerstone in the transition to sustainable energy systems. The underlying assumption is that the market for PV systems is rapidly expanding to significant penetrations in grid-connected markets in an increasing number of countries, connected to both the distribution network and the central transmission network.

This strong market expansion requires the availability of and access to reliable information on the performance and sustainability of PV systems, technical and design guidelines, planning methods, financing, etc., to be shared with the various actors. In particular, the high penetration of PV into main grids requires the development of new grid and PV inverter management strategies, greater focus on solar forecasting and storage, as well as investigations of the economic and technological impact on the whole energy system. New PV business models need to be developed, as the decentralised character of photovoltaics shifts the responsibility for energy generation more into the hands of private owners, municipalities, cities and regions.

IEA PVPS Task 13 engages in focusing the international collaboration in improving the reliability of photovoltaic systems and subsystems by collecting, analyzing and disseminating information on their technical performance and failures, providing a basis for their technical assessment, and developing practical recommendations for improving their electrical and economic output.

The current members of the IEA PVPS Task 13 include:

Australia, Austria, Belgium, China, Denmark, Finland, France, Germany, Israel, Italy, Japan, Malaysia, Netherlands, Norway, SolarPower Europe, Spain, Sweden, Switzerland, Thailand and the United States of America.

This report focusses on data, methods, and models for predicting the performance of photovoltaic systems in the field. Such performance varies as a function of component characteristics, system design, site characteristics, and weather and climate data. These topics are documented and organized by the PV Performance Modeling Collaborative (PVPMC). The report is divided into two main sections: (1) a section describing a set of standardized modeling steps for photovoltaic performance modeling, and (2) a summary of presentations made on these topics at the 4th PV Performance Modeling Collaborative Workshop held in Cologne, Germany at the headquarters of TÜV Rheinland on October 22-23, 2015. These summaries provide a good overview of achievements in this area from IEA member countries.

The editor of the document is Boris Farnung, Fraunhofer ISE, Freiburg, Germany.

The report expresses, as nearly as possible, the international consensus of opinion of the Task 13 experts on the subject dealt with. Further information on the activities and results of the Task can be found at: http://www.iea-pvps.org.

Acknowledgements

This technical report received valuable contributions from many IEA-PVPS Task 13 members and other international experts, all of whom are listed as contributing authors. We are thankful to all the presenters at the 4th PVPMC workshop (named in later sections of this report). In addition, we thank the following individuals for their careful reviews and suggestions:

- Ulrike Jahn   TÜV Rheinland Energy
- Cathy Zhou   TÜV Rheinland Energy
- Nils Reich   Fraunhofer ISE
- Helen Rose Wilson   Fraunhofer ISE
- Bert Herteleer   CAT Projects
- Wilfried van Sark   Utrecht University

List of Abbreviations

AM	relative air mass
AMa	absolute air mass
AOD	aerosol optical depth
AOI	angle of incidence
APE	average photon energy
AVHRR	Advanced Very High Resolution Radiometer
CAMS	Copernicus Atmospheric Monitoring Service
CMV	PV power forecasts based on satellites
DHI	diffuse horizontal irradiance
DNI	direct normal irradiance
EURAC	European Academy
FARMS	Fast All-sky Radiation Model for Solar applications
GHI	global Horizontal Irradiance
GOES	Geostationary Operational Environmental Satellites
GSIP	Global Solar Insolation Project
ISFH	Institute for Solar Energy Research Hamelin
JRC	Joint Research Center
KNMI	Koninklijk Nederlands Meteorologisch Instituut
LCE	life cycle emissions
LCOE	Levelized cost of electricity
LFM	loss factors model
MACC	Monitoring Atmospheric Composition and Climate
MPP	maximum power point
MPPT	maximum power point tracking
MPR	module performance ratio
MSG	Meteosat Second Generation Satellite
NOAA	National Oceanic Atmospheric Agency
NREL	National Renewable Energy Laboratory
NSRDB	National Solar Radiation Data Base
NWP	numerical weather predictions
PATMOS-x	Pathfinder Atmospheres-Extended algorithm
PSM	physical solar model
PV	photovoltaic
PVPMC	Photovoltaic Performance Modeling Collaborative
PWV	precipitable water vapor
Pwat	precipitable water content
QE	quantum efficiency
SOLIS	Synoptic Optical Long-term Investigation of the Sun
SMARTS	Simple Model of the Atmospheric Radiative Transfer for Sunshine
SR	spectral response
STC	standard test conditions
TMY	typical meteorological year

Executive Summary

In 2014, the IEA PVPS Task 13 added the PVPMC as a formal activity to its technical work plan for 2014-2017. The goal of this activity is to expand the reach of the PVPMC to a broader international audience and help to reduce PV performance modeling uncertainties worldwide. One of the main deliverables of this activity is to host one or more PVPMC workshops outside the US to foster more international participation within this collaborative group.

This report reviews the results of the first in a series of these joint IEA PVPS Task 13/PVPMC workshops. The 4th PV Performance Modeling Collaborative Workshop was held in Cologne, Germany at the headquarters of TÜV Rheinland on October 22-23, 2015.

Approximately 220 solar energy experts from over 30 countries and four continents gathered for two days at the headquarters of TÜV Rheinland in Cologne Germany to discuss and share results related to predicting the performance and monitoring the output from solar photovoltaic (PV) systems. The workshop was divided into six topical sessions exploring advances in the areas of solar resource assessment, effects of irradiance spectrum on PV performance, soiling losses, bifacial PV performance, modeling tools, and monitoring applications. This workshop is the fourth and largest in a series of workshops organized by the PV Performance Modeling Collaborative or PVPMC (pvpmc.sandia.gov), a group started by Sandia National Laboratories in 2010 to bring together stakeholders with the aim of advancing the "state of the art" in PV performance prediction. The PVPMC collects information from the community and shares it on the web and in a set of open source code libraries in Matlab and Python.

Highlights from the workshop include the following:

- Validation and comparison of four satellite irradiance products across Europe show that these data sets are becoming more accurate and that differences between different products are becoming smaller.
- A number of new spectral irradiance data sets are being developed from satellite data sources. The general availability of such data has promise to reduce uncertainty in PV performance modeling since spectral mismatch is one of the major sources of uncertainty in current tools.
- Two new spectral mismatch models were introduced at the workshop that utilize readily available meteorological data such as precipitable water, clearness index, and air mass to better estimate the spectral mismatch in PV performance. Model developers at the workshop expressed their interest in including such models in future releases of software packages.
- Soiling from dust and snow continue to be major causes of energy loss for PV systems, especially in certain regions. Estimating these losses in detail in performance predictions continues to be a challenge.
- Modeling and field data for bifacial PV modules and systems were presented. It is increasingly clear that significant performance gains are available from bifacial technologies; however, current modeling tools are unable to accurately predict energy production from bifacial modules.
- Field monitoring of PV systems is still in need of standardized methods to ensure high quality data is collected. Several experts in this area presented examples of good practice, but these examples are not typical of system monitoring in general.

This report begins with a technical overview of PV performance modeling steps and then proceeds to summarize each of the technical presentations made at the workshop. Original presentation files are all available on the PVPMC website [1].

1 Introduction

The broad application of photovoltaic (PV) technologies to the energy system is still a relatively new field and as such, best practices and innovative methods and policies are actively being developed and tested in different countries. The latest information on new advances in methods and algorithms can be difficult to obtain, especially if presented at industry conferences, in academic journals, or workshops, which are usually only accessible to a limited group of stakeholders.

One area for which efficient sharing of this information is of particular importance is PV performance and reliability modeling. Because nearly all PV system investment is made before systems begin producing energy and revenue, PV plant or technology investment risk largely depends on the confidence that investors have that the plant/technology will perform in the field as predicted for the expected lifetime. The cost of financing this risk is significantly influenced by uncertainty—either real or perceived—in long-term performance calculations. Disseminating best practices in this area is critical for reducing costs associated with perceived uncertainty. Eliminating perceived uncertainty will result in greater focus on real uncertainties that are known, measurable, and easier to quantify and address: for example, the uncertainty of what the weather and irradiance will be in the future.

The lack of available information about PV performance modeling methods is an important contributor to perceived uncertainty. This was one outcome of a blind study conducted at Sandia National Laboratories' first PV Performance Modeling Workshop in 2011 [2]. For this study, 20 participants were provided with technical descriptions of three PV systems and one year of measured weather and irradiance data and were asked to predict the performance of the systems using the model of their choice. The participants represented a range of PV professionals from PV model developers, integrators, independent engineers, and academia. Together, they applied a total of seven different performance models, and several participants applied more than one model. The results were combined and compared to the actual performance of the system, which was carefully monitored—but not shared with the participants before the study. The results were similar for all three systems.
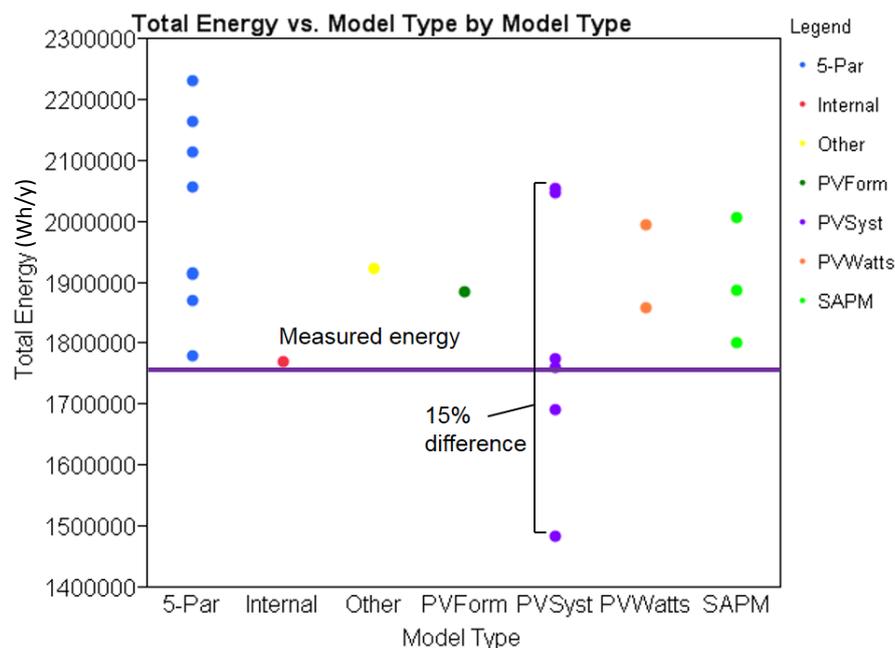
Figure 1: Example results of a blind modeling study that led to the start of the PV Performance Modeling Collaborative.

Figure 1 shows an example for one of the systems. Most of the models over-predicted system performance. The variation of results did not depend on which model was used, but rather who ran the model and "how" the model was set up and parameterized. PV performance models require numerous of inputs and sub-model choices to be made, and it was found that these choices made by model operators result in a significant amount of uncertainty. These results led to the formation of the Photovoltaic Performance Modeling Collaborative (PVPMC), and an ever-growing community interested in better understanding and reducing the uncertainty inherent in PV performance modeling.

Table 1: List of PVPMC Workshops.

Workshop	Location	Date
1st PVPMC Workshop	Albuquerque, NM USA	20-21 September 2011
2nd PVPMC Workshop	Santa Clara, CA USA	1-2 May, 2013
3rd PVPMC Workshop	Santa Clara, CA USA	4 May 2014
4th PVPMC Workshop	Cologne, Germany	22-23 October 2015
5th PVPMC Workshop	Santa Clara, CA USA	9 May 2016
6th PVPMC Workshop	Freiburg, Germany	24-25 October 2016
7th PVPMC Workshop	Lugano, Switzerland	30 April 2017
8th PVPMC Workshop	Albuquerque, NM USA	9-10 May 2017

In 2014, the IEA PVPS Task 13 added the PVPMC as a formal activity to its technical portfolio for 2014-2017. The goal of this activity is to expand the reach of the PVPMC to a broader international audience and help to reduce PV performance modeling uncertainties worldwide. One of the main deliverables of this activity is to host one or more PVPMC workshops outside the US to foster more international participation in this collaborative group.

This report reviews the results of the first in a series of these joint IEA PVPS Task 13/PVPMC workshops. The 4th PV Performance Modeling Collaborative Workshop was held in Cologne, Germany at the headquarters of TÜV Rheinland on October 22-23, 2015.

Approximately 220 solar energy experts from over 30 countries and four continents (Figure 2) gathered for two days at the headquarters of TÜV Rheinland in Cologne Germany to discuss and share results related to predicting the performance and monitoring the output from solar PV systems. The workshop was divided into six topical sessions exploring advances in the areas of solar resource assessment, effects of irradiance spectrum on PV performance, soiling losses, bifacial PV performance, modeling tools, and monitoring applications. This workshop is the fourth and largest in a series of workshops organized by the PVPMC (pvpmc.sandia.gov), a group started by Sandia National Laboratories in 2010 to bring together stakeholders with the aim of advancing the "state of the art" in PV performance prediction. The PVPMC collects information from the community and shares it on the web and in a set of open source code libraries in Matlab and Python.
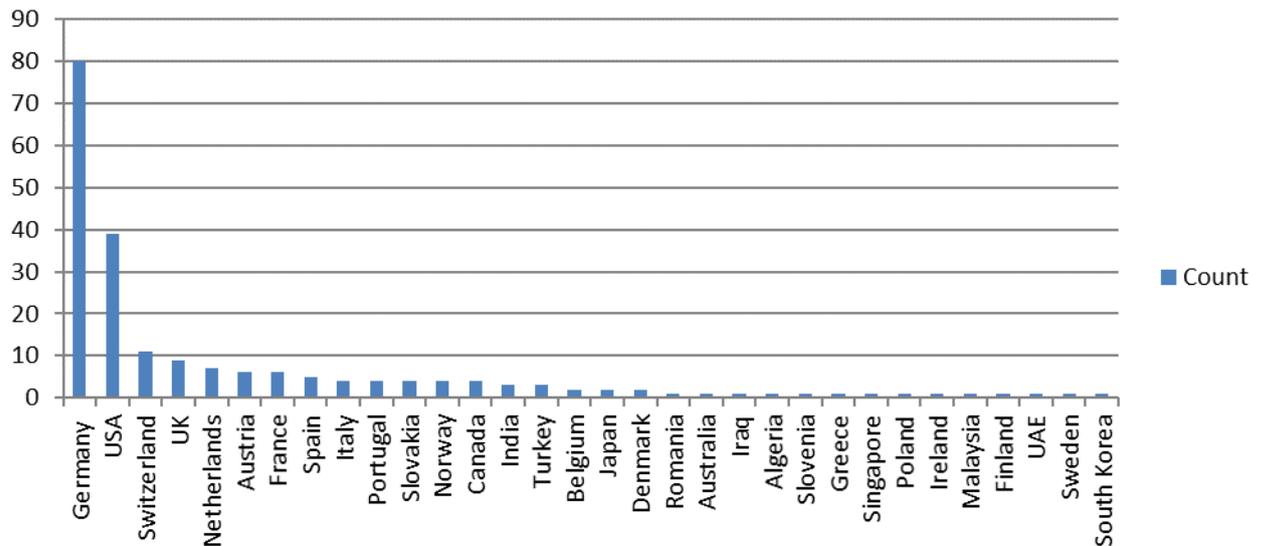
Figure 2: Participants by country at the 4th PV Performance Modeling Workshop in Cologne, Germany.

Highlights from the workshop include the following:

- Validation and comparison of four satellite irradiance products across Europe show that these data sets are becoming more accurate and that differences between different products are becoming smaller.
- A number of new spectral irradiance data sets are being developed from satellite data sources. The general availability of such data has promise to reduce uncertainty in PV performance modeling since spectral mismatch is one of the major sources of uncertainty in current tools.
- Two new spectral mismatch models were introduced at the workshop that utilize readily available meteorological data such as precipitable water, clearness index, and air mass to better estimate the spectral mismatch in PV performance. Model developers at the workshop expressed their interest in including such models in future releases of software packages.
- Soiling from dust and snow continue to be major causes of energy loss for PV systems, especially in certain regions. Estimating these losses in detail in performance predictions continues to be a challenge.
- Modeling and field data for bifacial PV modules and systems were presented. It is increasingly clear that significant performance gains are available from bifacial technologies; however, current modeling tools are unable to accurately predict energy production from bifacial modules.
- Field monitoring of PV systems is still in need of standardized methods to ensure high quality data is collected. Several experts in this area presented examples of good practice, but these examples are not typical of system monitoring in general.

Clear consensus was expressed by the participants on one point: The Solar Energy Team of TÜV Rheinland did a fantastic job of hosting the modeling workshop. Their high quality, comfortable facilities, and gracious attention to detail allowed all participants to focus on the technical program and use our valuable time together as a group for developing and sustaining collaborations to improve PV performance modeling and monitoring.

Figure 3: Participants at the 4th PV Performance Modeling Collaborative Workshop.

The technical content of the report starts in Section 2 with a brief summary of PV performance modeling steps and methods so that the summaries of the workshop sessions that follow in Section 3 can be read within the technical context of the field. More details on the modeling steps and the various sub-models that are used in each step are available on the PVPMC website's Modeling Steps section (https://pvpmc.sandia.gov). This includes approximately 200 webpages with technical model descriptions contributed by PVPMC members. Finally, conclusions are made with recommendations for future related activities.

2 Performance Modeling of PV Systems

Models, in the context of this report, are mathematical or conceptual representations of real systems. They are generated for the purpose of understanding and predicting behavior that can be measured or observed. In the context of PV systems, models are used to understand and predict energy or power output from PV systems under a wide range of environmental, design, and site conditions. It is wise to view any and all PV performance models with a certain amount of caution as all of these models make simplifying assumptions that result in some degree of mismatch between model results and measurements. Furthermore, all measurements of PV system performance (e.g., current, voltage, temperature, tilt and azimuth angles, etc.) have inherent uncertainty. A favorite quote of modelers, which is attributed to George Box [3], is "Essentially, all models are wrong, but some are useful." The PVPMC's aim is to help modelers learn about and distinguish between available models and find the most useful ones for their purpose.

2.1 Standard Sequence of PV Performance Modeling Steps

The approach followed by the PVPMC to describe PV performance modeling is to follow the energy, which originates from the Sun as light, travels through space and Earth's atmosphere, and reaches a PV array, where it is converted to electrical energy. At each step in this journey, energy is transferred and some portion of it is "lost" (usually as heat). The goal of PV performance models is to calculate or estimate how much of the energy is converted to usable and valuable electrical energy. This is usually done by tracking energy conversion and loss at each of these steps.

The general steps are listed below

1. Define PV system design parameters
2. Choose irradiance and weather data
3. Translate irradiance data to the plane of the array
4. Estimate optical losses from shading, soiling, and reflections on the surface of the array or module
5. Estimate "effective" irradiance
6. Estimate the cell temperature of the PV cells
7. Estimate the current (I) and voltage (V) characteristics of the PV module
8. Estimate the DC wiring and mismatch losses
9. Estimate the DC to AC conversion losses
10. Estimate the AC wiring and transformer losses.

In the sections that follow, we will provide more details about the assumptions and calculations that are made to estimate the quantities listed above. When these areas overlap with presentations made by workshop speakers, we will point these out so that the reader can better choose how to read the presentation summaries presented in Section 3.

It is also worth noting that PV technologies and system designs are evolving and quite varied. For the purpose of clarity, we will assume a conventional grid-connected, flat-plate PV system with a string inverter for the discussion below. For other types of PV technology (e.g., concentrating PV) or system designs (e.g., DC optimizers, and systems based on micro-inverters), some of the steps presented below would have to be altered, although the approach would be similar.

2.2 PV System Design Parameters

For the purpose of modeling PV system performance, the following design and site parameters are generally used. It should be noted that the modeling steps are generally applied to a typical system design of a single inverter connected to x number of strings of y modules each. There is a

wide variety of variants to this typical design, such as micro-inverters, multi-port inverters with separate MPPT trackers, etc. Slight modifications to the modeling steps or order in which the steps are followed are usually required for simulations of these different systems.

Site Parameters

- Latitude and longitude
- Elevation

System Design Parameters

- Inverter model name and performance parameters
- Module model name and performance parameters
- Number of modules per series string
- Number of series strings per array
- Cable lengths, types and cross sections
- Tilt (θ_T) and azimuth of the array (or tracking angle algorithm for tracked arrays)
- Albedo of the ground (or roof) surface)
- Horizon map showing potential for shading from obstructions

2.3 Irradiance and Weather Data Sources

Irradiance and weather data for at least a full year must be gathered in order to run a PV performance model. Time steps of one hour or less are standard. Depending on the location of interest, data is available from a number of public and private sources. This data can be from historical and ongoing ground-based measurement stations and networks, modeled from satellite imagery, or modeled from general weather observations in places where irradiance is not measured directly. Frequently, synthetic annual data sets are made available that are meant to be representative of longer trends in irradiance. These "typical" meteorological years are used to estimate future performance from PV systems. More recently, performance simulations have been run using numerous different irradiance data sets in order to estimate the uncertainty due to estimating future weather conditions.

Ground measurements from well-maintained, calibrated radiometers are considered to be the best and most accurate source of irradiance data. However, such stations are not common and finding such data near the location of interest is usually not possible, unless a station has been installed for that purpose, in which case the length of the record is usually short. Thus uncertainties arise from assuming that the available irradiance is similar to the irradiance expected at the site of interest. Microclimatic differences can be important, especially in areas with topographic variability.

Satellite-based model results have improved significantly in recent years and offer a good compromise to sparse ground-based data. Available in grids that cover most inhabited land areas, this data is generally available on an hourly basis and sometimes every 30 or even 15 minutes. Various sources exist for this data, including government agencies, such as NASA, NOAA, German Aerospace Agency, and others. The finest resolution data (in time and space) is available from private companies (e.g., SolarGIS, Clean Power Research, etc.) for a fee.

Irradiance data is reported as three components: direct normal irradiance (DNI), global horizontal irradiance (GHI), and diffuse horizontal irradiance (DHI). These components are typically made with broadband instruments. From these components, the intensity on the plane of the PV array can be estimated using transposition models. Since it is easier to measure GHI, it is common practice to estimate DNI and DHI from GHI using a decomposition model (e.g., DISC [4], DIRINT [5]). Use of such models introduces additional uncertainty.

2.4 Translating Irradiance to the Plane of the Array

Irradiance on the plane of the array is equal to the sum of the beam irradiance, the sky diffuse irradiance and the ground-reflected irradiance. Beam irradiance is calculated as DNI*cos(AOI), where AOI is the angle of incidence of direct irradiance from the Sun to the plane of the array. Ground-reflected irradiance depends on GHI, the tilt angle of the array, and the reflectivity of the ground, typically expressed as the albedo. Typical values for common surface types are available on the PVPMC website [6].

Sky diffuse irradiance has been the subject of many studies aimed at developing models to estimate it from measured irradiance components, array tilt (θ_T), and other factors. The simplest formulation assumes that the intensity of the diffuse light is equal in all parts of the sky. This isotropic model estimates diffuse sky irradiance on the plane of the array as:

$$E_{sd} = DHI \left[\frac{1 + cos(\theta_T)}{2} \right]$$

In fact, the isotropic model of the sky is not very accurate. Due to scattering processes in the atmosphere, the intensity of the diffuse light is enhanced near the position of the Sun. Models that include the effects of this circumsolar brightening more accurately estimate the diffuse light available to a PV array. One of the most widely used models that include circumsolar brightening was proposed by Hay and Davies [7]. It has the following form:

$$E_{sd} = DHI \left[\frac{DNI}{E_a} cos(AOI) + \left(1 - \frac{DNI}{E_a} \right) \frac{1 + cos(\theta_T)}{2} \right]$$

where E_a is extraterrestrial irradiance in (W/m^2), which can be estimated from the day of year, since Earth's orbit is elliptical [8]. The additional terms and factors in the Hay and Davies model are intended to account for the brightening around the solar disk.

Many other models have been proposed, some of which include a term to represent a slight brightening of the sky at the horizon (e.g., [9-10]).

2.5 Estimation of Shading, Soiling, and Reflection Losses

The light that is incident on the plane of the array (incident on the top surface of the module) is not the same as the light that is available for conversion to energy by the PV system. Physical objects surrounding the array such as buildings, poles, and other parts of the PV system can obstruct the light that is able to reach the PV array. One of the goals of system design is the minimization of shading, but some shading may be unavoidable, especially in residential rooftop systems. The effect of shading is quantified by use of a horizon map, which indicates the position of obstructing objects in relation to the path of the Sun across the sky throughout the year. Times when the system is shaded can be estimated; the effect is typically simulated by subtracting the direct beam irradiance from the in-plane value for those times. The effects of shading on a part of the PV array is more complicated to account for and depends on the location of the series strings in the array and other electrical wiring details.

Dust and debris on the surface of the PV modules reduces the available light. The composition of the dust and the environment and climate of the site all play a role in the severity of this effect. Certain parts of the world are much more affected by these "soiling" losses. Section 3.3 of this report provides more details.

The amount of light that is reflected by the front of the PV modules varies with the angle of incidence of the light on the surface. Angles from 0° to about 50° generally result in very little reflec-

tion, but for angles greater than 50°, reflections increase as the angle increases. *Figure 4* shows this effect as predicted using a model developed by Martin and Ruiz [11]. The angular factor is the fraction of the light transmitted through the module surface to the PV cells. Lower values of a_r are used to represent the effect of antireflective coatings on the front glass pane, which maintains an angular factor near 1 at higher angles of incidence.
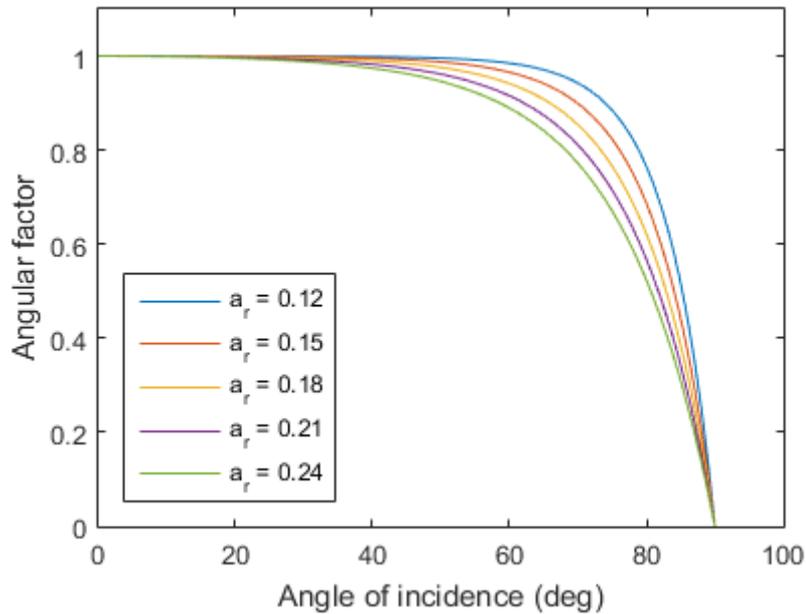
Figure 4: Relative reflectance of a module surface as a function of incidence angle and empirical parameter, a_r, for a model developed by Martin and Ruiz [11].

2.6 Effective Irradiance

Effective irradiance (*Ee*) is the light that is directly available to be converted into electrical current by the PV material. It is essentially the POA irradiance minus several loss factors including:

- Soiling losses
- Reflection losses
- Shading losses
- Spectral losses

All of these losses have been discussed above except for spectral losses. Spectral losses are due to the fact that PV materials are able to absorb light only in a limited range of the solar spectrum. *Figure 5* shows a representation of the solar spectrum. Outside Earth's atmosphere, the solar spectrum is similar to the radiation emitted by a blackbody source at 5778°C. Atmospheric constituents such as water (H_2O), CO_2, ozone, and other gases absorb light in certain wavelengths and alter the extraterrestrial spectrum at Earth's surface. The terrestrial spectrum changes over time and location due to variability in the atmosphere and as a function of the path length of the Sun's direct beam through the atmosphere. This path length is represented by a relative, non-dimensional quantity called optical air mass (AM) and calculated as a function of the solar zenith angle and the ground elevation. In space, the air mass value is zero and at sea level with the Sun at a zenith angle of zero degrees (directly overhead), the air mass value is equal to 1.

The response of a PV device to various wavelengths of light is called the Spectral Response (SR) and is in units of A/W. *Figure 6* shows typical spectral response curves for a number of different PV technologies.
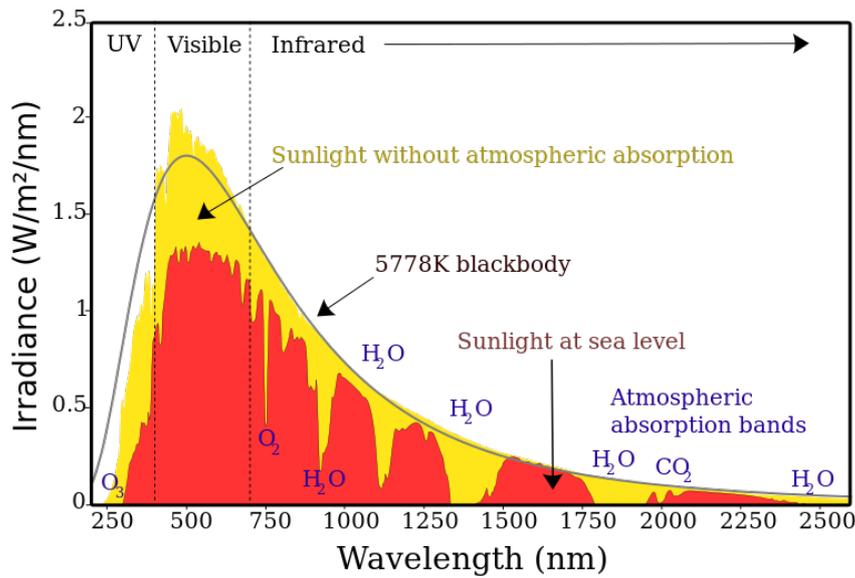
Figure 5: Typical solar spectrum. Source: [12]
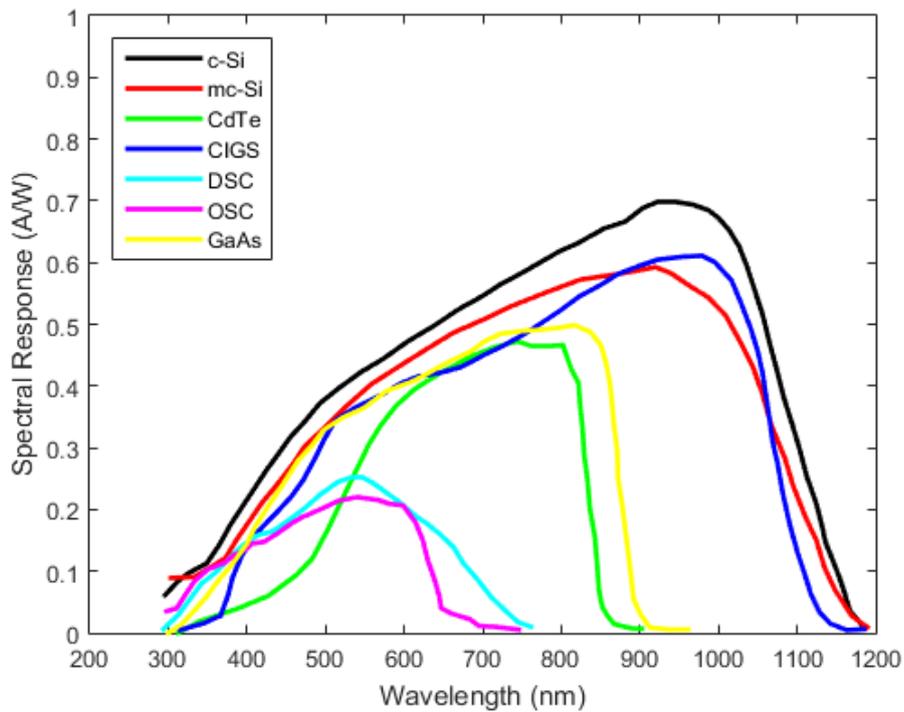
Figure 6: Representative spectral response curves for typical PV cell technologies from the PVPMC website [13]).

One expression for E_e is:

$$E_e = f_1\left\{\left(E_b f_2 + f_d(E_{sd} + E_g)\right)/E_0\right\}SF$$

where f_1 is a factor accounting for the spectral effects, f_2 is a function of AOI that describes the reflection effects (e.g., *Figure 4*), f_d is the fraction of the diffuse irradiance used by the module and typically equals 1 for flat plate modules but can be <1 for concentrating PV modules. *SF* is the soiling factor (dimensionless), which is the fraction of light that is not obstructed by the soiling

19

layer on the PV device. E_0 is the reference irradiance (1 000 W/m^2). E_b, E_{sd}, and E_g are beam, sky-diffuse, and ground reflected broadband irradiances, respectively.

The spectral factor f_1 is usually expressed as a function of quantities that are easily measured, such as air mass [14], air mass and relative humidity (see Section 3.2.2), or air mass and clearness index (see Section 3.2.5).

2.7 Estimation of cell temperature

The operating temperature of PV modules and the cells inside the modules affects the performance of the PV system. Typical PV cells lose efficiency as temperatures rises. Typical rates are -0.3 to -0.5% per °C above STC. For this reason, it is necessary to estimate the operating temperature of the PV modules in the array as it changes during the day. Modules change temperature in response to changes in the plane-of-array (POA) irradiance, ambient air temperature, wind speed, and even relative humidity (humid air has a higher heat capacity). Most module and cell temperature models assume a steady-state temperature balance and therefore should be used with time steps greater than ~15 min. Transient thermal models have been developed, but are not yet available in commercial PV performance models.

2.7.1 Faiman Module Temperature Model

A popular model for module temperature that is used in the PVsyst model is based on Faiman [15] and has the following form:

$$T_c = T_a + \frac{\alpha E_e(1 - \eta_m)}{U_0 + U_1 WS}$$

where T_a is air temperature (°C), α is the absorptance of the module (typical value is 0.9), η_m is the efficiency of the module (typically 0.08-0.2), WS is the wind speed (m/s). U_0 is the constant heat transfer coefficient (Wm^{-2}°C^{-1}) and U_1 is the convective heat transfer coefficient (Wm^{-3} s °C^{-1}). Typical values for U_0 and U_1 range from 23.5 to 26.5 Wm^{-2} °C^{-1} and 6.25 to 7.68 Wm^{-3} s °C^{-1}, respectively. Other module temperature models are also available (e.g., [14; 16-18].

2.8 Current and Voltage (I-V) Models

A PV cell, module, or series string of modules under illumination has a characteristic relationship between the current generated by the device and the voltage applied to the circuit. The characteristic is called the IV curve and estimating this curve or points on the curve is the aim of the models described in this step. There are three basic types of IV models: equivalent circuit diode models, semi-empirical "point" models, and simple efficiency models.

2.8.1 Diode Equivalent-Circuit Model

Diode equivalent-circuit models assume that the performance of a PV module can be represented by a circuit such as the one shown in *Figure 7*. Versions of this basic circuit with more than one diode are also popular.
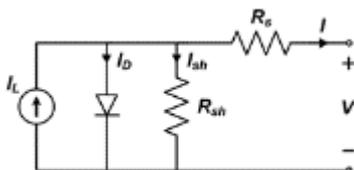

Figure 7: Single-diode equivalent circuit.

The current-voltage (I-V) characteristic of this circuit used to describe PV module performance is described as:

$$I = I_L - I_0 \left[exp \left(\frac{V + IR_s}{nN_sV_T} \right) - 1 \right] - \frac{V + IR_s}{R_{sh}}$$

where I_L is the light-generated current (A), I_0 is the diode reverse saturation current (A), R_s is the module series resistance (Ω), R_{sh} is the module shunt resistance (Ω), n is the diode ideality factor, N_s is the number of cells in series in the module, and V_T is the thermal voltage, $V_T = \frac{kT_c}{q}$, where k is Boltzmann's constant (1.381x10^{-23} J/K) and q is the elementary charge (1.602x10^{-19} C). This equation needs five module parameters to solve for current and voltage (I_L, I_0, n, R_s, and R_{sh}). Several of these parameters vary with irradiance and temperature. When these relationships are defined mathematically, a module performance model is made (e.g., [19-20]). The technical manuals for such performance models should provide these details.

2.8.2 Fixed-Point Models

There are several examples of fixed-point module and system models. These models are limited in that they only provide selected points on the I-V curve for a module. The Sandia Photovoltaic Array Performance Model [14] predicts I-V values for five points shown in *Figure 8*.
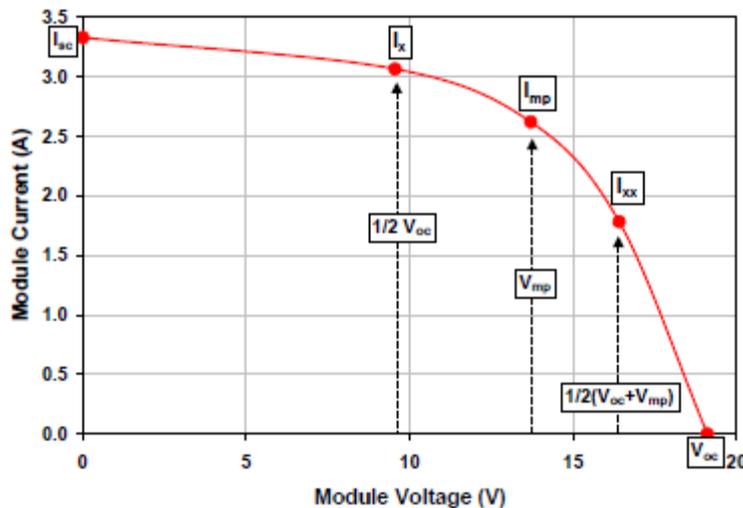
Figure 8: Five points determined by the Sandia PV Array Performance Model.

The Loss Factors Model [21-22] can estimate the maximum power point, V_{oc} and I_{sc}. Other simpler models, such as for instance PVWatts [23], are designed to estimate only the maximum power point (P_{mpp}) and do not resolve the current or voltage separately.

2.9 DC Wiring and Mismatch Losses

PV systems usually have a device that controls the operating voltage in order to maximize the power delivered from the system. The voltage is set and controlled by the device (usually an inverter, optimizer, or charge controller), but the actual voltage at the PV cell is altered by the resistance of the DC cables, which is affected by cable length, cable cross-section, and temperature.

To obtain maximum power from a PV array, the operating voltage must be controlled by a maximum power point tracking (MPPT) algorithm, which continuously adjusts the voltage and seeks to maximize power. The maximum power voltage (V_{mpp}) varies with irradiance and temperature. Usually MPPT is controlled by the inverter for grid-tied systems, or the voltage is controlled by a

charge controller for off-grid, battery-connected applications. MPPT losses can occur when the MPPT controller cannot rapidly find the MPP. Typically, these losses are very low (<0.5%).

DC losses due to resistance in the wiring and interconnections can lead to current and power losses. To minimize these losses, PV designers can connect PV modules in series, thus increasing the voltage while keeping the current fixed to the current at maximum power I_{mpp} of a single module. Since resistance losses increase with the square of the current, this configuration keeps these losses low without increasing the costs associated with thicker cables. A consequence of connecting modules in series is that any mismatch between the I-V characteristics of the module population can lead to mismatch losses. For example, in a series-connected string of modules, since the current flowing through all the modules has to be equal, the module with the lowest current will limit the current in the string. Such mismatch can occur from module inconsistencies or from uneven soiling or partial shading. Module manufacturers bin their modules to minimize mismatch and system designers try to avoid string configurations that are affected by partial shading. If these situations cannot be easily avoided, system designers can use module scale power electronics such as microinverters or module-scale DC-DC converters that perform MPPT for each module separately, thus avoiding many of the mismatch losses, but at a higher cost. Most PV performance modeling applications assume that MPPT and DC losses will be estimated outside the software and are entered as system derating factors.

2.10 DC to AC Conversion Efficiency

In the case of grid-connected PV systems, the PV array is connected to an inverter to convert DC power to AC power. This conversion is associated with losses which depend on the inverter used, the operating DC power and AC and DC voltages. Models to estimate this change in inverter efficiency are used to estimate these losses.

Most PV systems are connected to the grid and produce AC power. One of the inverter's primary functions is to convert DC power to AC power. This conversion process results in power losses that need to be taken into account in the modeling of PV system performance. These losses are expressed in terms of inverter conversion efficiency, which is equal to P_{AC}/P_{DC}. Inverter efficiency varies with both DC power level and DC voltage and this variation depends strongly on the manufacturer and inverter design. *Figure 9* shows an example of this variation for a typical inverter.
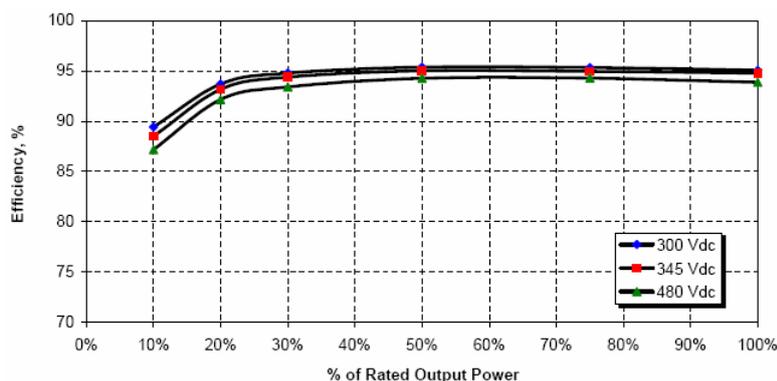
Figure 9: Example of an inverter efficiency profile.

Inverter performance models aim to represent this complex behavior mathematically. Models are based on measurements made by testing labs that measure efficiency at specific DC power and voltage levels. Model parameters are derived from fitting these curves. The Sandia Photovoltaic Inverter Performance Model [24] is one such model.

$$P_{AC} = \left\{ \frac{P_{AC0}}{A-B} - C(A-B) \right\} (P_{DC} - B) + C(P_{DC} - B)^2, \text{ where}$$

$$A = P_{DC0}\{1 + C_1(V_{DC} - V_{DC0})\},$$

$$B = P_{s0}\{1 + C_2(V_{DC} - V_{DC0})\}, \text{ and}$$

$$C = C_0\{1 + C_3(V_{DC} - V_{DC0})\}.$$

P_{DC} is the DC power (W), V_{DC} is the input voltage (V), V_{DC0} is the DC voltage level (V) at which the AC power rating is achieved at reference conditions, P_{AC0} is the AC power rating (W) at reference conditions, P_{S0} is the DC power (W) required to start the inverter process, or self-consumption by the inverter. The C_1, C_2 and C_3 parameters are fitting coefficients. Other inverter models are also available (e.g., [25]).

2.11 AC Wiring and Transformer Losses

The final step in modeling the performance of a PV system is to account for any AC losses between the inverter and the final revenue meter that determines how much AC electricity is available. For small systems (e.g., residential) the meter is directly adjacent to the inverter and AC losses are negligible. However, for large systems, it is not uncommon to have an AC distribution system between the inverters and the meter. Transmission-connected, utility-scale systems may have additional transformers. These wires and transformers will introduce losses to the system output that need to be considered. A few PV performance models simulate these losses directly but many models that are focused primarily on smaller residential and commercial systems simply include a derating factor that decreases the AC output by a constant percentage.

PVsyst includes a simple model for transformer losses [26] that account for:

- Iron losses due to hysteresis and eddy currents in the core of the transformer, which are proportional to grid voltage squared and are usually about 0.1% of the rated power. Some systems install a switch to disconnect the transformer from the grid at night to avoid these losses when the PV system is not producing power.
- Ohmic losses within the wire coils of the transformer, which are proportional to I^2R. These losses are thus dependent on the system current and are usually several times higher than the iron losses on an annual basis.

Current systems are often more complex than the initial software designs, which were aimed at single-inverter designs. In some cases, the software user must either accept the default provided by the software, or has to leave the software to determine a loss value to input back into e.g., PVsyst.

3 Workshop Presentation Summaries

Due the increasing popularity of the PVPMC Workshops and a limit of two days for the workshop, a competitive review process was applied to select a balanced program of high quality presentations. Interested presenters submitted brief abstracts describing their presentations and the workshop organizers reviewed the submissions and built a program of oral and poster presentations. These are summarized in the sections below. All presentations are available on the PVPMC website [1].

The workshop started with two introductory presentations by Florian Reil from TUV Rheinland Energy and Joshua S. Stein from Sandia National Laboratories.

3.1 Session 1: Solar Resource Data and Uncertainty

This session was chaired by Clifford Hansen from Sandia National Laboratories.

Table 2: List of presentations and speakers for Session 1.

Title	Presenter	Affiliation	Country
Satellite- and Camera-derived Irradiance Data for Applications in Low Voltage Grids with Large PV Shares	Marion Schroedter-Homscheidt	German Aerospace Center	Germany
Evaluation of Satellite Irradiation Data at 200 Sites in Western Europe	Karel De Bra-bandere	3E	Belgium
Uncertainty of Satellite Based and Ground Based Solar Resource Assessment	Marcel Suri	GeoModel Solar s.r.o.	Slovakia
Accuracy of Meteonorm 7.1	Jan Remund	Meteotest	Switzerland
Next-Generation Satellite Modeling for NREL's National Solar Radiation Data Base (NSRDB)	Manajit Sengupta	National Renewable Energy Laboratory	USA
Local and Regional PV Power Forecasting Based on PV Measurements, Satellite Data and Numerical Weather Predictions	Elke Lorenz	Carl von Ossietzky University Oldenburg	Germany
Dynamic Uncertainty of Irradiance Measurements – Illustrations from a Study of 42 Radiometers	Anton Driesse	PV Performance Labs	Germany
Towards an Energy-based Parameter for Photovoltaic Classification	Stefan Winter	Physikalisch-Technische Bundesanstalt	Germany
Timeseries of Spectrally Resolved Solar Irradiance Data from Satellite Measurements	Annette Hammer	Carl von Ossietzky University Oldenburg	Germany

3.1.1 Satellite- and Camera-derived Irradiance Data for Applications in Low Voltage Grids with Large PV Shares

Marion Schroedter-Homscheidt introduced a new satellite-based, open-source solar resource product developed by the German Aerospace Center. Data from the Meteosat Second Generation meteorological satellite (MSG), which is updated each 15 min (or even 5 minutes in the rapid scan mode), is used as input to the Heliosat-2 and Heliosat-4 algorithms to calculate irradiance at ground level. Additional inputs of air quality, global pollution, UV intensity, and aerosols are obtained from the Copernicus Atmosphere Monitoring Service and are used in the calculations. Data from these calculations is made available to the public for free. The project is still under development but data is already available for download [26].

The talk dealt with satellite-derived irradiance data as the basis to calculate larger solar shares in distribution grids. Load flow and voltage are derived from electricity grid modeling, photovoltaic performance modeling and ground-based or satellite-based irradiance observations.

This paper describes recent results of two European Commission research projects. ENDORSE dealt with 'Energy Downstream Services' [27] and investigated the use of the European Commission's new Copernicus program [28] and its irradiance data as provided in the precursor project MACC (Monitoring Atmospheric Composition and Climate [29]).

CAMS (Copernicus Atmosphere Monitoring Service) provides solar irradiance time series for Europe, Africa, Middle East and parts of South America free for any use. These new services were also introduced to the audience.

Figure 10: CAMS webpage for measured sky irradiance product.

Based on CAMS products, one can also derive cloud physical parameter statistics for each location of interest. These can serve as a more detailed information base than only using irradiance time series. Irradiance is a parameter that averages out all information about the underlying physical processes responsible for the irradiance value. Having insight into clouds allows more detailed

assessment of a location. The same holds for dust aerosols – a climatological analysis of dust aerosol optical effects was also presented.
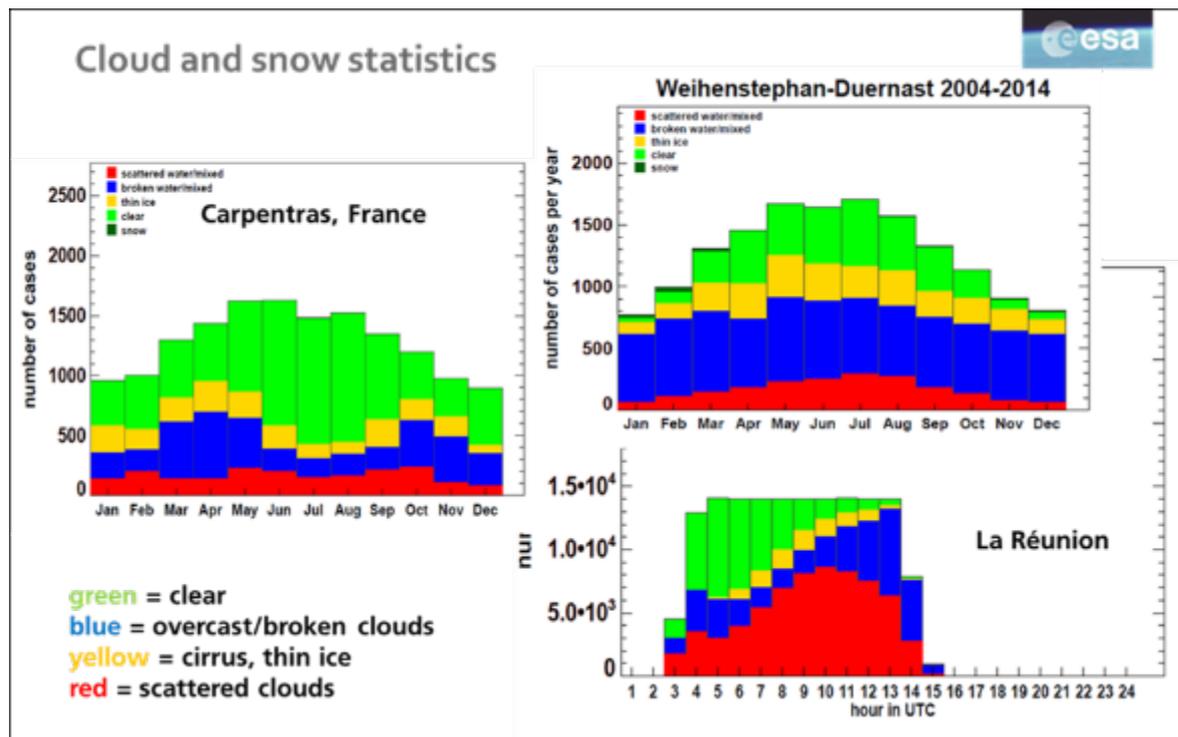
Figure 11: Example of cloud and snow statistics for three locations.

With cloud information being available, nowcasting (forecasting on a <15 min basis) of the cloud cover may be carried out. Algorithms that were developed for large-scale solar thermal concentrating power plants are currently being adapted for use with photovoltaic generation by distributed PV plants which are connected to the distribution grid level in a specific region.

The need for ceilometer-based height assessments of clouds for nowcasting based on sky cameras was discussed briefly, as was the usability of numerical weather prediction output to achieve the same result.

Finally, an application of CAMS/MACC data usage for PV power monitoring at the low-voltage level was discussed. This is work from the European Commission's project Orpheus [30], which deals with the hybrid control of smart grids and e.g. the connection of the solar electricity to the heating sector to use surplus solar production.

The final part of the presentation focused on ideas for applying these data to questions about how best to integrate large amounts of PV into the low-voltage power distribution grids. Using an example from Ulm, Germany, Marion Schroedter-Homscheidt presented a preliminary study on the benefits of satellite-based data for understanding transformer loading from PV systems backfeeding power into the power grid. Preliminary results showed that transformer loading errors were significantly higher when only limited ground-based sensor data was used. Errors were halved when satellite data was employed. Finally, she showed some slides on the benefits and opportunities for using sky cameras to provide data on cloud height and velocities.
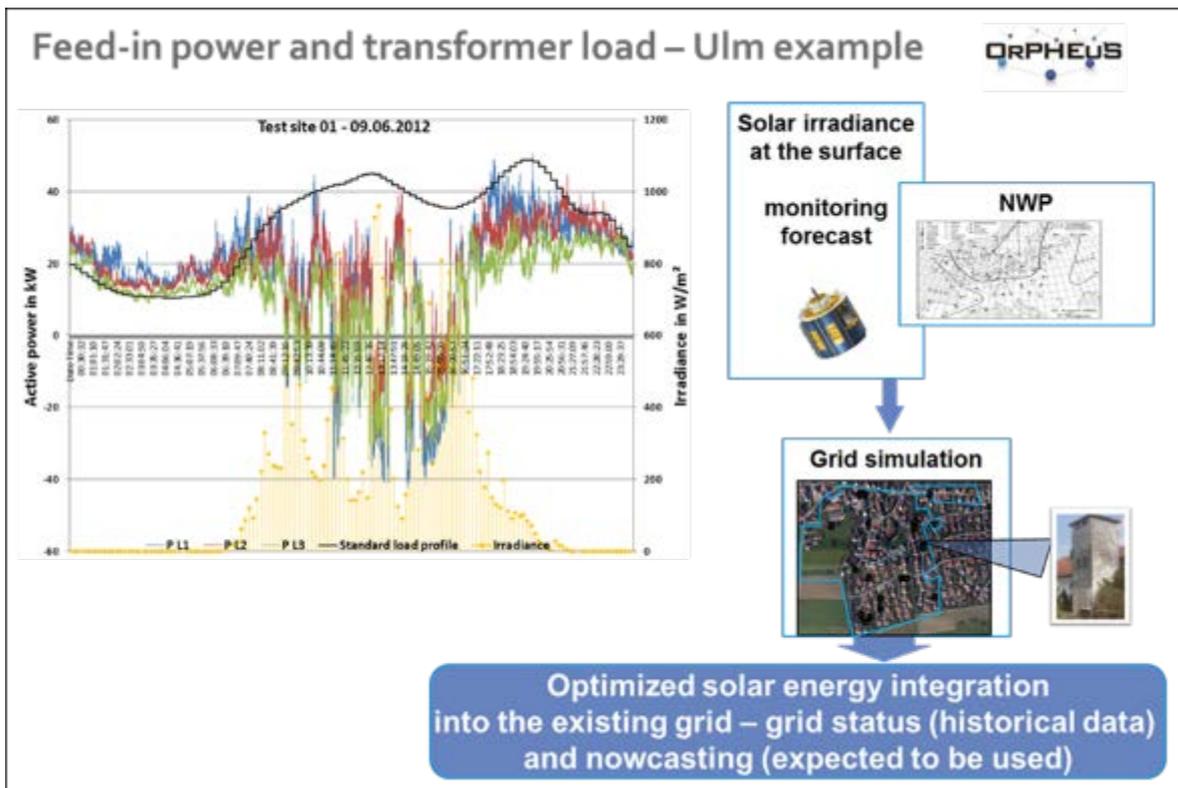
Figure 12: Example of applying the satellite irradiance product to a load flow calculation.

3.1.2   Evaluation of Satellite Irradiation Data at 200 Sites in Western Europe

Karel De Brabandere presented the results of a study comparing different satellite irradiance data sets to ground irradiance data available in Western Europe. The satellite irradiance data examined in the study include: MACC-Rad, HelioClim (v.3, v.4, and v.5), Cpp (KNMI), and GSIP (NOAA). These data are derived from both empirical and physical models. He focused his validation on hourly, daily, and monthly aggregated data from 2011-2015. Ground measurements were from national meteorological stations (160 in France, 12 in Belgium, 31 in the Netherlands). He used three error metrics to compare data: root mean square error, standard deviation of error, and bias error. *Figure 13* shows an example of the results of the comparison for 2012. *Figure 14* shows similar errors for other years. In summary, errors were generally higher for the shorter time scales (e.g., hourly). The Cpp data and the latest version of HelioClim data displayed the lowest overall errors, while the MACC-Rad data displayed the highest bias errors, a fact that was further discussed after the presentation in the Q&A session. One possible explanation was that the MACC-Rad data, unlike the other satellite data, has not been empirically corrected to ground observations. Despite this fact, the MACC-Rad also exhibited a slightly higher standard deviation error as well, especially in cloudy weather conditions, which likely reflects real opportunity for improvements to the algorithms. The HelioClim model showed lower errors with every new version. GSIP data was only available for two months in 2015, but the preliminary results showed it fell in the middle of the group in terms of error metrics.
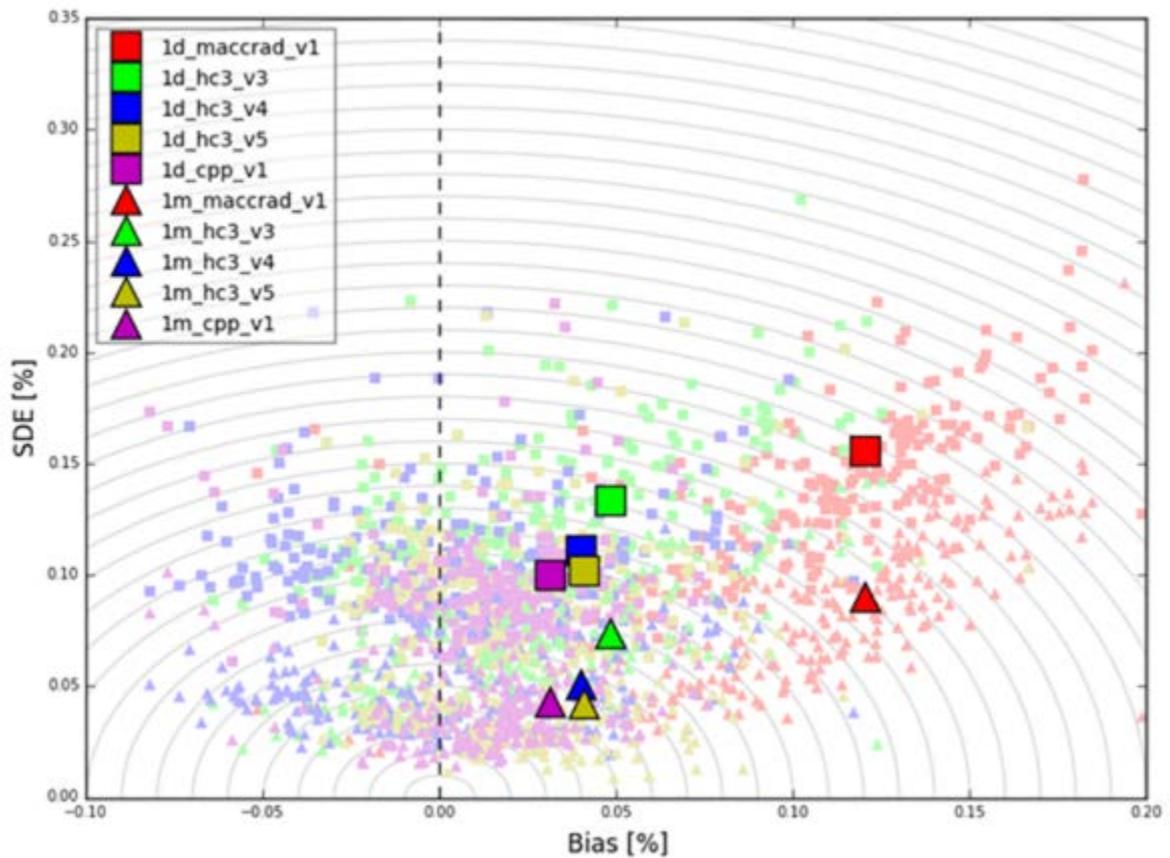
Figure 13: Example of error results from the satellite irradiance comparison for 2012.
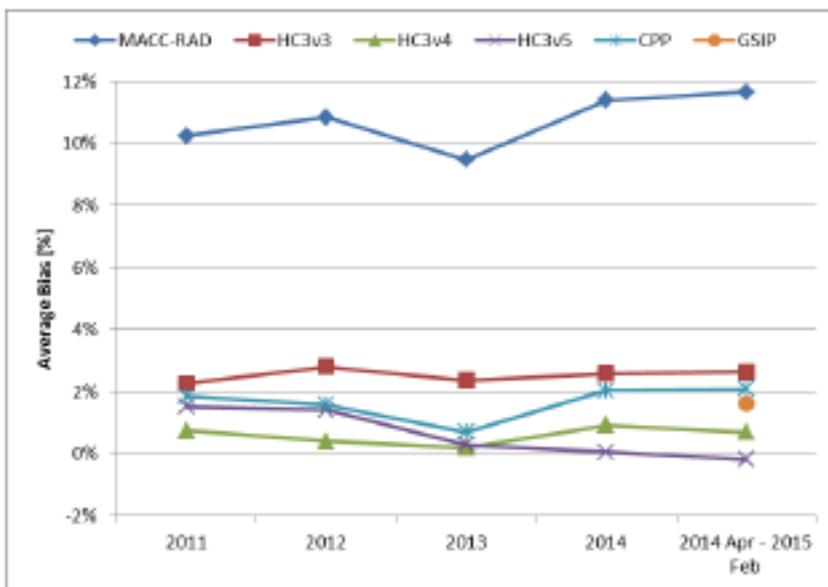
Figure 14: Example of bias error comparison for 2011-2015.

3.1.3   Uncertainty of Satellite Based and Ground Based Solar Resource Assessment

Marcel Suri presented a general overview of the challenges of measuring and modeling irradiance at the surface of Earth. He provided a review of historical practices of ground-based and satellite-based irradiance measurements and discussed the benefits and challenges of these approaches. Uncertainties in solar measurements arise from the instrument accuracy and from the deviations

due to instrument maintenance, soiling, calibration drift, changing site conditions, etc. Thus, only highly accurate and well-maintained sensors should be used. Satellite irradiance data is based on the satellite and atmospheric data inputs that are updated every 10 to 60 minutes and have relatively low spatial resolution. Models used to convert imagery to irradiance are typically semi-empirical and thus tuned to different geographic regions. Satellite pixel size and temporal sampling rates can limit the ability of representing observed variability (for example, microclimatic conditions are difficult to resolve). Uncertainty of the satellite-based models is mostly due to imperfections of the models and the lower resolution of the input satellite and atmospheric data.

After presenting a thorough overview of irradiance measurement and modeling issues, Marcel then proceeded to present the results of an uncertainty analysis of the SolarGIS solar irradiance database. The expected uncertainty for the annual GHI model estimates is comparable to the uncertainty of medium-accuracy pyranometers (*Figure 15*). The uncertainty of low-accuracy and less diligently maintained sensors is typically higher than the uncertainty of SolarGIS GHI. The model uncertainty of the yearly DNI is lower, compared to well-maintained pyrheliometers and RSR instruments (*Figure 16*).

The GHI and DNI model uncertainty can be reduced by site adaptation of the model using at least one year of ground measurements. The short-term ground measurements (for a period of at least one year) from high-accuracy and well-maintained pyranometers, pyrheliometers and RSR instruments are typically used. Table 3Table 3: SolarGIS Uncertainties summarizes yearly uncertainty of the original values of the SolarGIS model, and – for comparison – also the best possible case that can be achieved after site adaptation. The uncertainty represents 80% probability of occurrence, based on the analysis of 200+ validation sites worldwide.
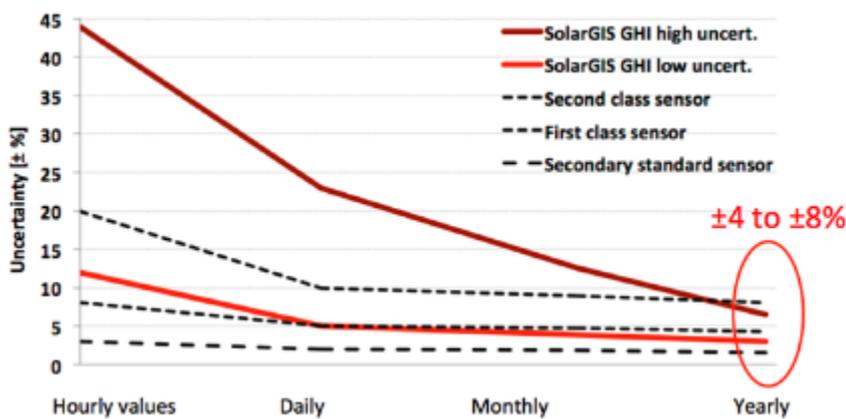
Figure 15: SolarGIS GHI uncertainty as a function of averaging time.
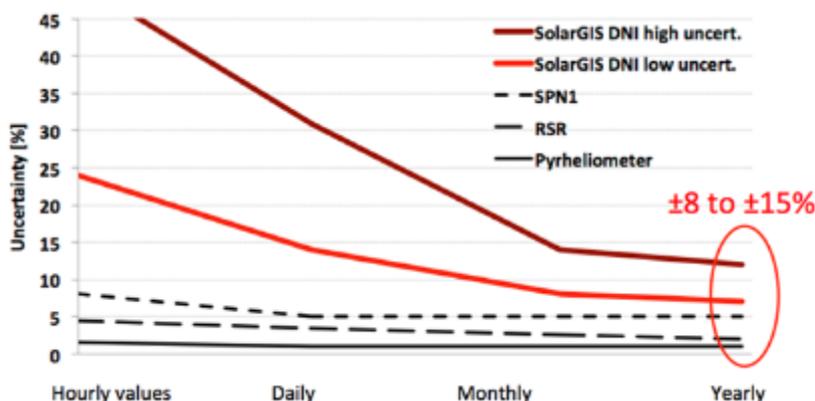
Figure 16: SolarGIS DNI uncertainty as a function of averaging time.

Table 3: SolarGIS Uncertainties.

SolarGIS irradiance product	Uncertainty of the yearly value computed by the original model	Best achievable uncertainty of the yearly value computed by the site-adapted model based on more than 3 years of high-quality ground measurements
GHI	±4 to ±8%	±2.5%
DNI	±8 to ±15%	±3.5%

3.1.4 Accuracy of Meteonorm 7.1

Jan Remund gave a short overview of the accuracy of meteonorm version 7.1 [32], a tool widely used for solar radiation assessments either directly as stand-alone software or as plugin in many PV simulation tools. Although a standard product, the details of data sources and uncertainties are not very well known.

The largest part of uncertainty is linked to the calculation of long-term averages and is caused mainly by the interpolation method. The sources of ground measurements were described briefly (mainly GEBA [32]), as well as the methods used to determine the radiation based on the 5 geo-stationary satellites and the method to mix the two sources.

A second part handled the observed climatological variations. The uncertainty model used in Meteonorm was described, together with the uncertainty and P10/90 information provided to the user. Finally, information was provided on the additional sources of uncertainty for downstream parameters like hourly global radiation on inclined planes.

The purpose of the talk was to educate the audience about the data and algorithms used in Meteonorm and to give them an overview over the uncertainty levels of the results.

The three main points of the talk were:

1. Meteonorm is a combination of a climate database and stochastic weather generator and includes both ground measurements and satellite data
2. Satellite and ground data are mixed to get the optimal results
3. Uncertainty levels are shown for any location, depend on location and are in the range of 2-10% (yearly GHI values, standard deviation).

The software is updated regularly. In 2017, time series of satellite data will be accessible within Meteonorm. It will then contain not only Typical Meteorological Years (TMYs).
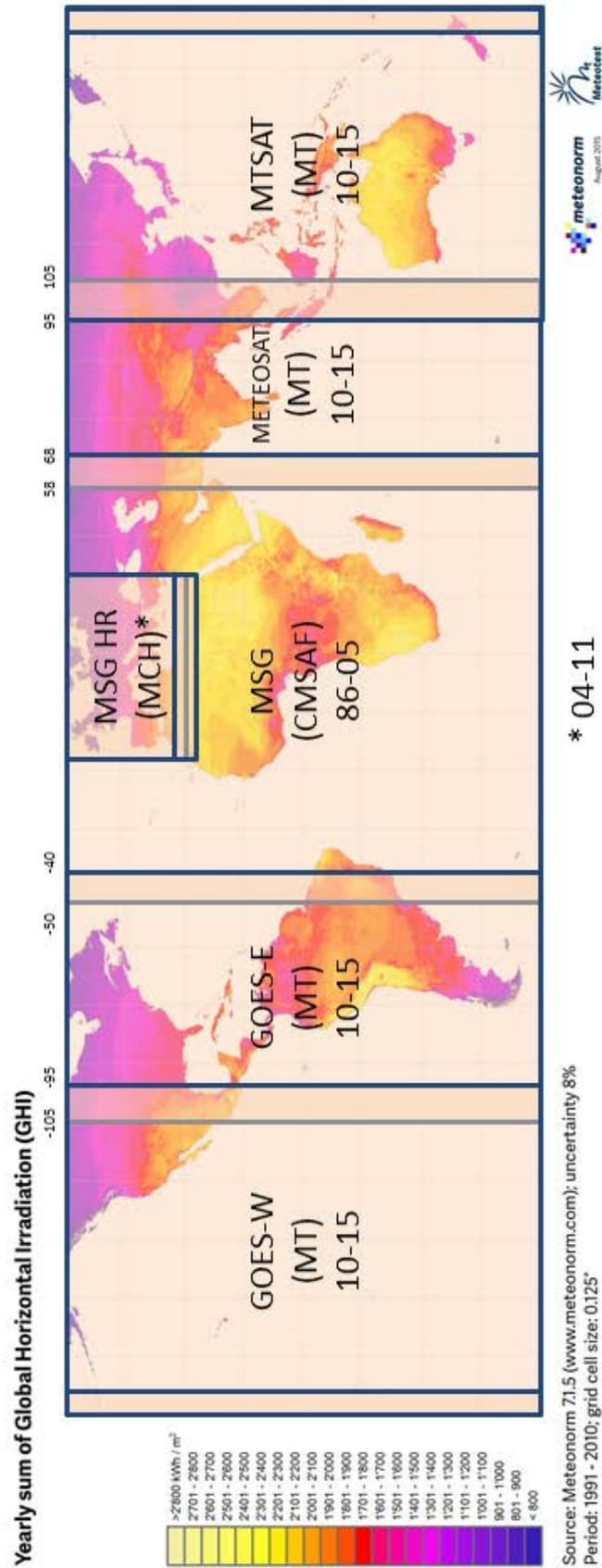
Figure 17: Geostationary satellites used in Meteonorm Version 7.1 with overlapping areas. Sources of satellite data: MT = Meteotest; CMSAF = German Weather Service, MCH = MeteoSwiss.

3.1.5 Next-Generation Satellite Modeling for NREL's National Solar Radiation Data Base

Manajit Sengupta described a new solar resource dataset that is being developed by the National Renewable Energy Laboratory (NREL). Publicly accessible, high-quality, long-term, satellite-based solar resource data is foundational and critical to solar technologies to quantify system output predictions and deploy solar energy technologies in grid-tied systems. Solar radiation models have been in development for more than three decades. For many years, NREL developed and/or updated such models through the National Solar Radiation Data Base (NSRDB).

There are two widely used approaches to derive solar resource data from models: (a) an empirical approach that relates ground-based observations to satellite measurements and (b) a physics-based approach that considers the radiation received at the satellite and creates retrievals to estimate clouds and surface radiation (*Figure 18*). Although empirical methods have been traditionally used for computing surface radiation, the advent of faster computing has made operational physical models viable.
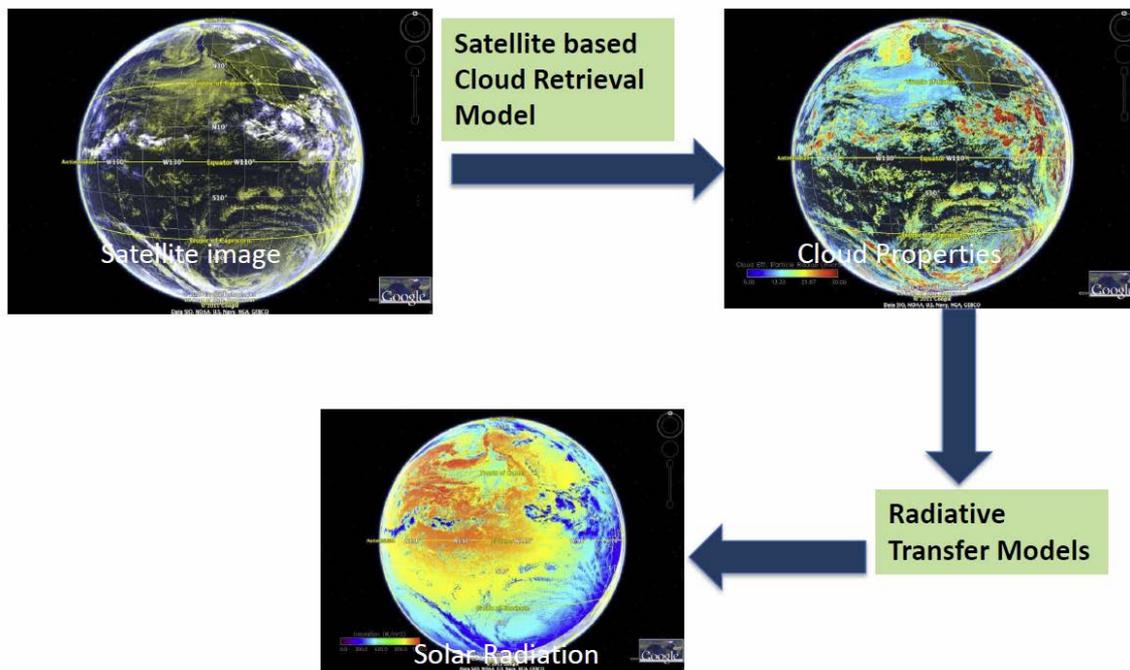
Figure 18: Conceptual data flow for the Physical Solar Model.

The Physical Solar Model (PSM) developed by NREL in collaboration with the University of Wisconsin and the National Oceanic and Atmospheric Administration (NOAA) computes global horizontal irradiance (GHI) using the visible and infrared channel measurements from the Geostationary Operational Environmental Satellites (GOES) system. PSM uses a two-stage scheme that first retrieves cloud properties and then uses those properties to calculate surface radiation. The cloud properties in PSM are generated using the AVHRR Pathfinder Atmospheres-Extended (PATMOS-x) algorithms. Using the cloud mask from PATMOS-x, and aerosol optical depth (AOD) and precipitable water vapor (PWV) from ancillary sources, the direct normal irradiance (DNI) and GHI are computed for clear-sky conditions using the REST2 model. For cloud scenes identified by the cloud mask, the NREL-developed Fast All-sky Radiation Model for Solar applications (FARMS) is used to compute the GHI. The DNI for cloud scenes is then computed using the DISC model (*Figure 19*).
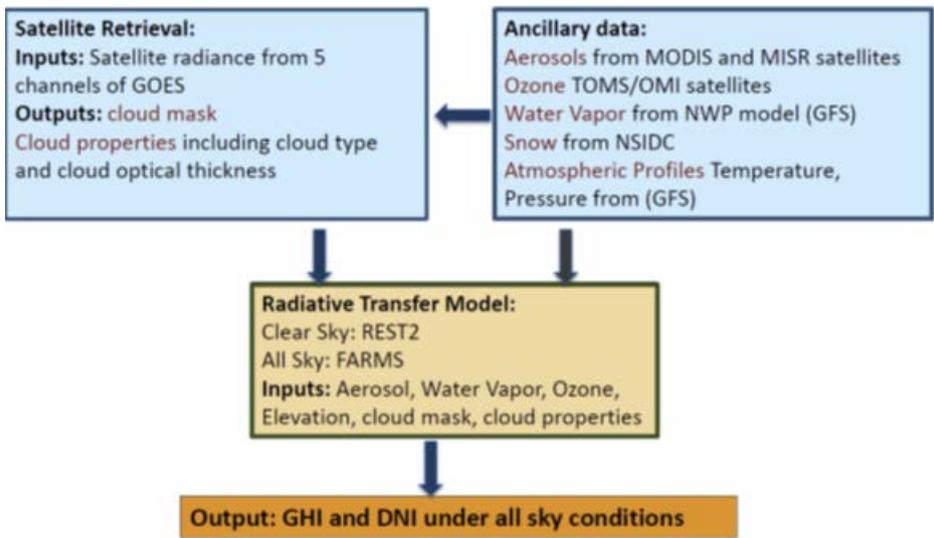
Figure 19: Process models for the Physical Solar Model.

The current NSRDB update has a 4-km x 4-km, 30-minute resolution for the period from 1998 to 2014. This presentation covered the development of the model and an evaluation of the PSM-based NSRDB data set compared to ground measurements. Mean bias errors for seven ground stations are shown in *Figure 20*.
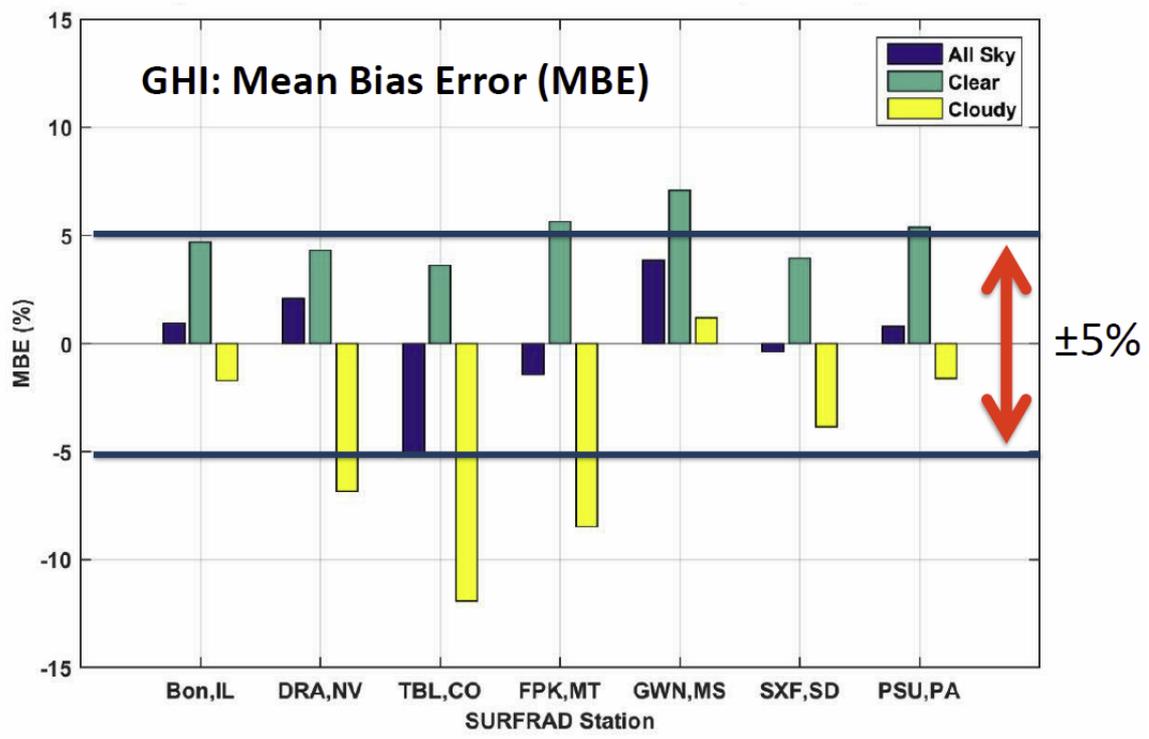
Figure 20: Mean bias errors for the Physical Solar model for seven sites.

3.1.6 Local and Regional PV Power Forecasting Based on PV Measurements, Satellite Data and Numerical Weather Predictions

Elke Lorenz gave an overview of models for PV power forecasting and presented research results for a specific forecasting model utilizing different data sources and methods for PV power prediction for forecast horizons from 15 minutes to several hours. These include the use of PV measurements for very short-term horizons, irradiance forecasts based on cloud motion vectors from

infra-red and visible satellite images for forecasts over several hours, and the combination of data from different numerical weather prediction models for forecasts up to several days ahead. The different data sources are integrated to form a combined PV power forecasting system using parametric simulation models as well as statistical learning methods. The different approaches were evaluated and compared for single PV plants and for regional PV power feed-in using a large data set of PV power measurements.

Important results:

- PV power prediction contributes to successful grid integration of more than 38 GWp PV power in Germany.
- Different prediction models are suitable for different forecast horizons: PV power forecasts based on satellite data (CMV) are significantly better than NWP-based forecasts up to 4 hours ahead. Forecasts based on PV measurements perform best for very short-term horizons (e.g., <15 min).
- A significant improvement compared to single-model forecasts is achieved by combining different forecast models, in particular for regional forecasts.
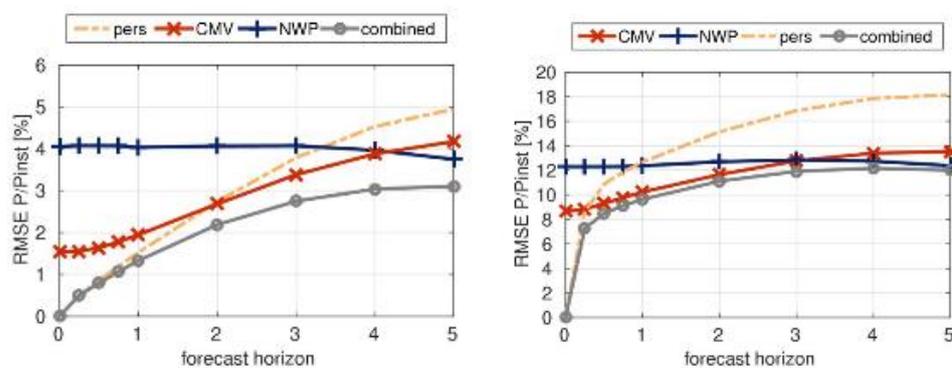
Figure 21: RMSE of forecast PV power versus forecast horizon in hours for different models: Persistence based on measured PV power (orange), cloud motion vector forecast based on satellite data (CMV, red), forecasts based on numerical weather predictions (NWP, blue), combined forecasts (grey). Above: regional forecasts (sum of 921 PV systems distributed in Germany), below: single site forecasts. Data set: 921 PV systems in Germany (Monitoring data base of Meteocontrol GmbH), 15 minute values, March to November 2013.

Follow-on work that is planned:

- Combination of machine learning with PV simulation for integration of additional data sources (additional meteorological parameters, additional NWP systems)
- Probabilistic forecasting: uncertainty information.

3.1.7 Dynamic Uncertainty of Irradiance Measurements – Illustrations from a Study of 42 Radiometers

Anton Driesse introduced the PVSENSOR project, which is an extensive study of commercial instruments designed to measure hemispherical solar irradiance. The overall objective is to develop a better understanding of the instrument strengths and weakness, and to apply this information strategically to reduce uncertainties in PV system performance analysis. As the uncertainty of irradiance measurement usually far exceeds the uncertainty of electrical power measurements, the potential benefits of this work are significant. The work is led by PV Performance Labs at Fraunhofer ISE in Freiburg and is carried out in collaboration with the European Joint Research Center in Ispra, Italy and Sandia National Laboratories in Albuquerque, New Mexico, USA.

The purpose of the presentation was to share insights gained from the ongoing work and to raise awareness of the complexity of uncertainties that are too often hidden behind a single number (or forgotten altogether). Indoor testing carried out in winter 2015 primarily at the JRC focused on isolating specific characteristics, such as temperature dependence, spectral response, dynamic response, linearity, directional response. The first phase of outdoor testing took place in summer 2015 with all sensors mounted on a two-axis tracker at Sandia (*Figure 22*). They were monitored continuously for two months, including several periods in a horizontal position, several periods tracking the Sun, and sometimes being involved in experiments. A period of extended monitoring both at Sandia and at PV Performance Labs in Freiburg, Germany during 2016 will complete the data collection effort.

As the instrument collection includes 20 thermopile pyranometers, 10 photodiode pyranometers, and 12 PV reference cells, plenty of difference should be expected; but the magnitudes of the differences may be surprising. (*Figure 23*) Part of the spread of the instrument readings seen in this graph can be considered to be due to calibration error, which should be constant; the re-mainder of the spread can be explained by various non-ideal instrument characteristics. The presentation used clear-day data segments from both horizontal and tracking periods to draw attention to the clearly visible temperature, angle-of-incidence and spectral effects.

With the most intensive data collection activities completed, greater effort has shifted to the data analysis. This upcoming work involves close comparison of the indoor and outdoor measurements to determine the level of agreement between the observations of various individual characteristics. Next, the project will evaluate how well the combination of those individual characteristics can explain long-term observations, and how their uncertainties contribute to overall uncertainty in the irradiance measurements.

Figure 22: Two sets of sensors mounted on a two-axis tracker at Sandia National Laboratories.
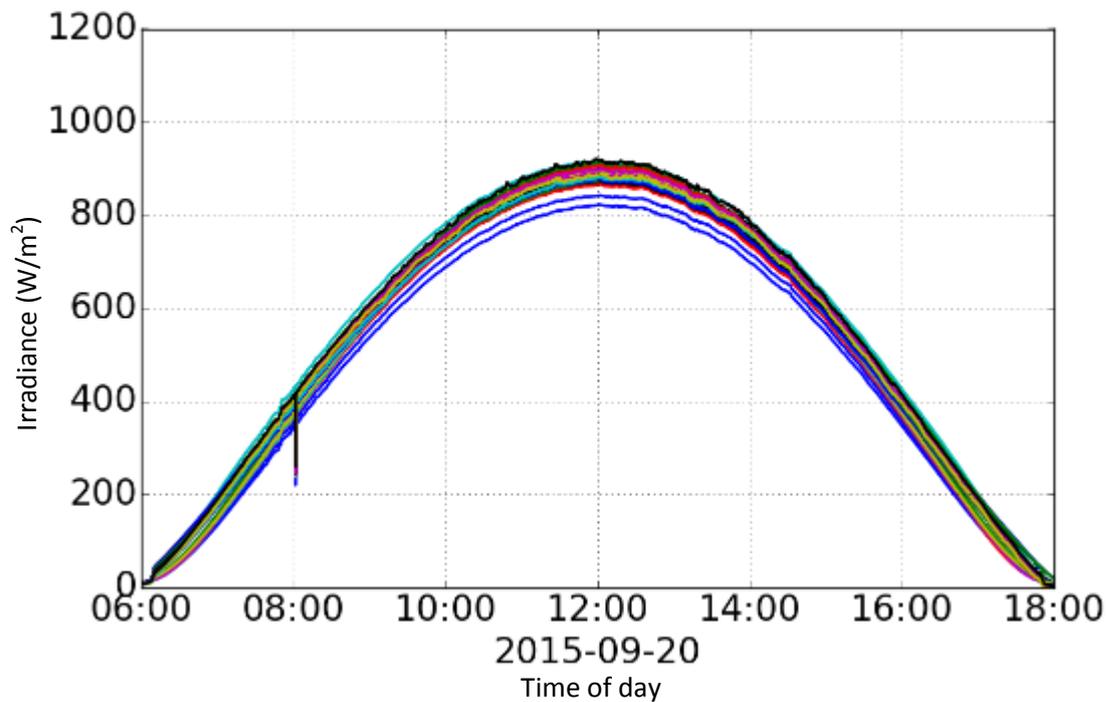
Figure 23: Field measurements of glob al horizontal irradiance from 42 calibrated irradiance sensors on a clear day in Albuquerque, New Mexico USA. The large spread in values represents the uncertainty inherent in available radiometers.

3.1.8   Towards an Energy-based Parameter for Photovoltaic Classification

Stefan Winter outlined a current effort to develop a new energy-based performance metric for comparing different photovoltaic module technologies. In contrast to standard test conditions (STC), which define the power delivered at a specific condition that is rarely achieved in the field, this new metric attempts to estimate the energy delivered from a PV module if it were operated under a defined set of weather and site conditions. Thus, differences in the energy rating of various PV modules should better reflect expected energy differences from systems using these modules. Furthermore, a focus by module manufacturers on maximizing STC ratings may in fact lead to modules that are not optimized for electricity generation in the field. For example, in some cases lower-efficiency modules at STC may produce more energy when placed in the field.

The PhotoClass project supported by the European Union is working to develop such an energy-based rating standard, which is intended to be implemented as part of IEC 61853-3. The project is organized into five work packages. WP1 is focused on developing a modeling method for calculating the energy rating. The approach being developed involves first defining a set of representative climatic data sets (8760 hourly values of irradiance, temperature, wind speed, etc. for certain geographic areas). Second, an orientation, tilt angle, and albedo are specified. Finally, a modeling procedure is defined and the energy yield (kWh), the specific module energy rating (kWh/kW$_p$), and a climatically specific energy rating (dimensionless) are calculated (see *Figure 25*). WP2 focuses on definition of required specifications and selection of reference irradiance devices. WP3 is working on standard methods for characterizing irradiance sensors as a function of time, irradiance, temperature, and angle of incidence. WP4 concentrates on understanding the characteristics of the solar resource and simulators. WP5 is an integrating activity to bring together all the information gained in the other tasks into an international standard (IEC 61853, parts 1-4).
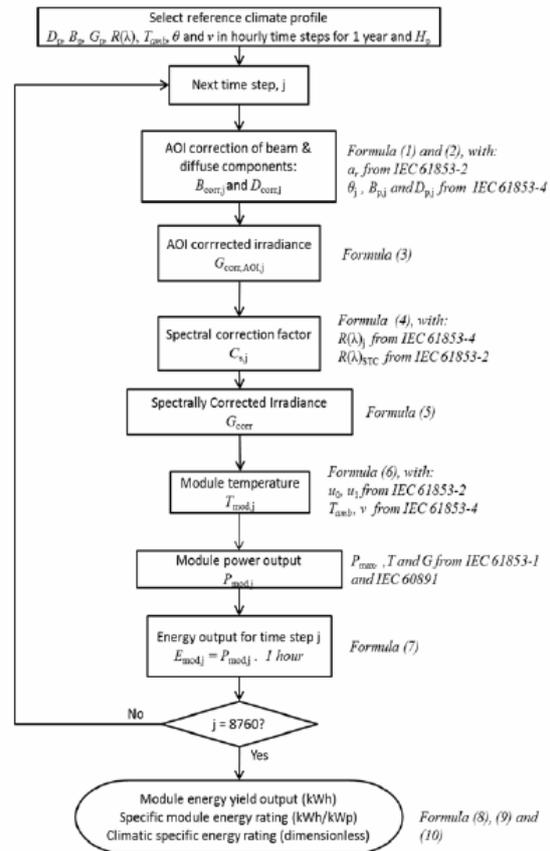
Figure 24: Flow diagram showing the modeling process being developed for Part 3 of IEC 61853.

3.1.9 PVKLIMA- Time Series of Spectrally Resolved Irradiance Data from Satellite Measurements

Annette Hammer presented an overview of a project aimed at characterizing and rating the impact of the solar spectrum on the energy yield of thin-film PV modules. The SOLIS model is used with atmospheric input (aerosol optical thickness and water vapor) from the MACC data set in combination with a cloud index from satellite images. The method is already available [33]; the quality of the method is shown in *Figure 25*.

Open points are the tilt conversion for the different wavelengths and how to handle broken cloud situations.

Optimized treatment of these topics will be developed within the research project PVKLIMA.
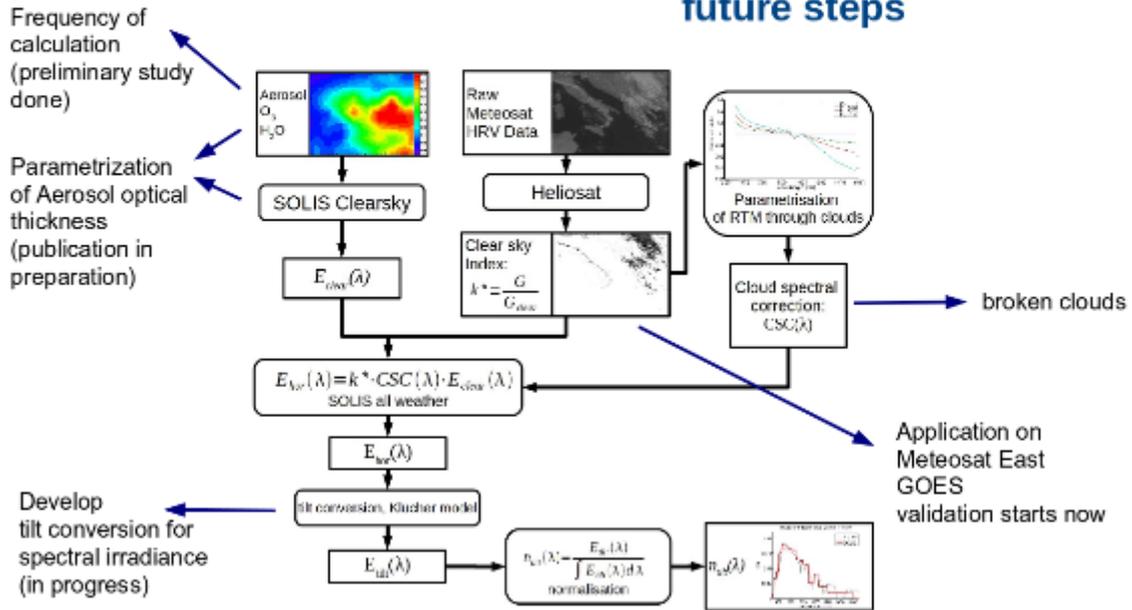
Figure 25: Diagram showing the methods used to estimate spectral irradiance from satellite data.

3.2 Session 2: Spectral Corrections for PV Performance Modeling

This session was chaired by Alex Panchula from First Solar.

Table 4: List of presentations and speakers for Session 2.

Title	Presenter	Affiliation	Country
Satellite-based Estimates of the Influence of Solar Spectrum Variations on PV Performance	Thomas Huld	Joint Research Centre of the European Commission	Italy
Combined Air Mass and Precipitable Water Spectral Correction for PV Modeling	Mitchell Lee	First Solar	USA
Sensitivity Analysis and Uncertainty Evaluation of Simulated Clear-Sky Solar Spectra Using Monte Carlo Approach	Giorgio Belluardo	EURAC research	Italy
Spectral Corrections for PV Performance Modeling	Fotis Mavromatakis	University of Oregon	USA
Improved Prediction of Site Spectral Impact	Benjamin Duck	CSIRO Energy Flagship	Australia
Impact of Spectral Irradiance on Energy Yield of PV Modules Measured in Different Climates	Markus Schweiger	TÜV Rheinland, Solar Energy	Germany

3.2.1 Satellite-based Estimates of the Influence of Solar Spectrum Variations on PV Performance

The presentation by Thomas Huld covered three topics: (1) calculation of the influence of spectral variations on PV power, (2) estimates of spectrally resolved solar radiation from satellite data, and (3) examples of calculations of these effects for different geographic regions.

As shown in *Figure 6*, different PV cell technologies respond differently to light depending on the spectrum. To reconcile these differences for the purpose of converting irradiance to current, a spectral correction factor can be calculated as:

$$C_{S,l} = \frac{\int SR_l(\lambda)G_\lambda d\lambda \int G_{\lambda,STC}d\lambda}{\int SR_l(\lambda)G_{\lambda,STC}d\lambda \int G_\lambda d\lambda},$$

where $SR_l(\lambda)$ is the spectral response at wavelength, λ. G_λ is the spectral irradiance at wavelength, λ, and STC in the subscript indicates the reference spectrum. The overall spectral mismatch (*MM*) of a PV device over time is then:

$$MM = \frac{\sum_{j=1}^{N} C_{s,l}G_j}{\sum_{j=1}^{N} G_j},$$

where *j* is the time step of the calculation (e.g., hour).

To investigate this spectral effect on PV technologies in Europe, Asia, and Africa, spectrally resolved irradiance data were calculated using the SPECMAGIC algorithm, developed by Deutscher Wetterdienst and the University of Oldenburg. Cloud effects are calculated from METEOSAT imagers using a Heliosat-type method. This is then used by SPECMAGIC together with data on aerosols, water vapor and ozone to calculate global and direct irradiance in 24 spectral bands between 300 nm and 2200 nm. SPECMAGIC has been used to process 30 years of METEOSAT data to gen-

erate the CMSAF SARAH data set. Hourly global and direct irradiance values are freely available through the CM SAF web site: www.cmsaf.eu. SARAH version 2 will feature various improvements and also provide spectrally resolved irradiance data.

Next, a Module Performance Ratio (MPR) was defined as the ratio of actual module energy output to the output if the module always had the efficiency measured under Standard Test Conditions (*Figure 26*).

Figure 27 shows the overall potential for seasonal performance changes in c-Si modules due to spectral changes. Relative performance losses can be seen in the Tibetan Plateau of ~5%. *Figure 28* shows a similar map for CdTe modules. It displays relative energy gains in the tropics, which experience high relative humidity. This effect is discussed in more detail within the next presentation by Mitchell Lee of First Solar.
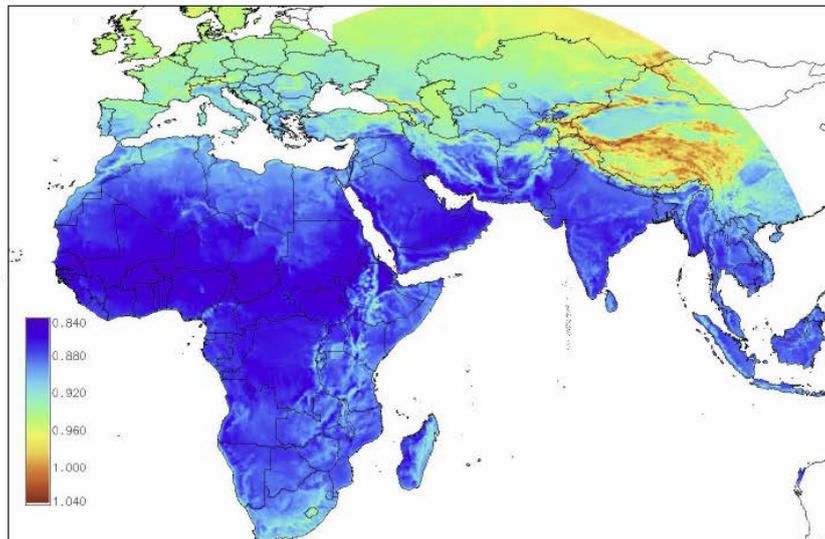

Figure 26: Map showing the Module Performance Ratio for c-Si modules.
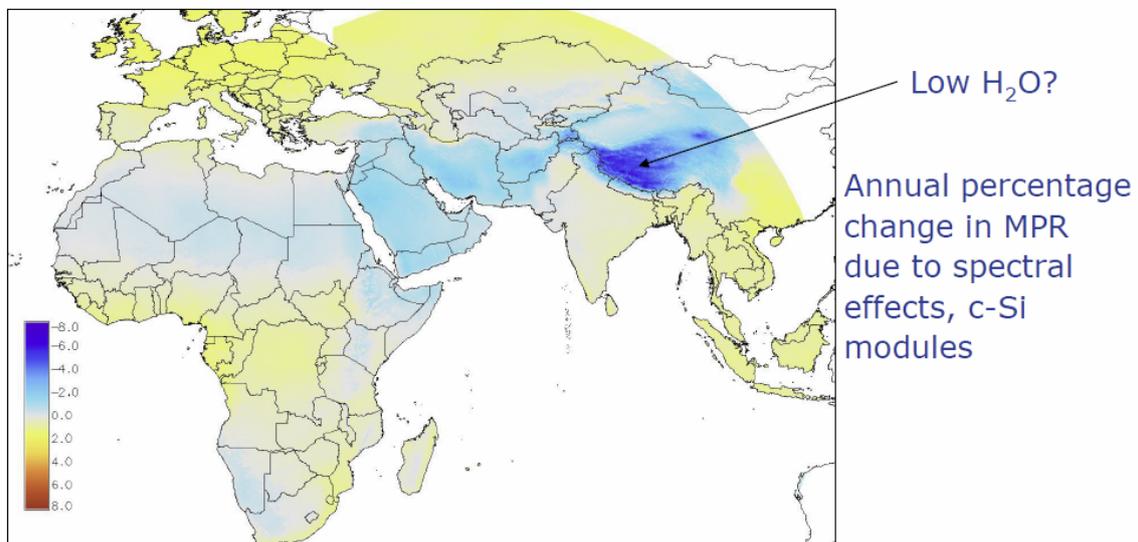
Figure 27: Map showing the annual percent change in Module Performance Ratio due to spectral effects for c-Si modules.
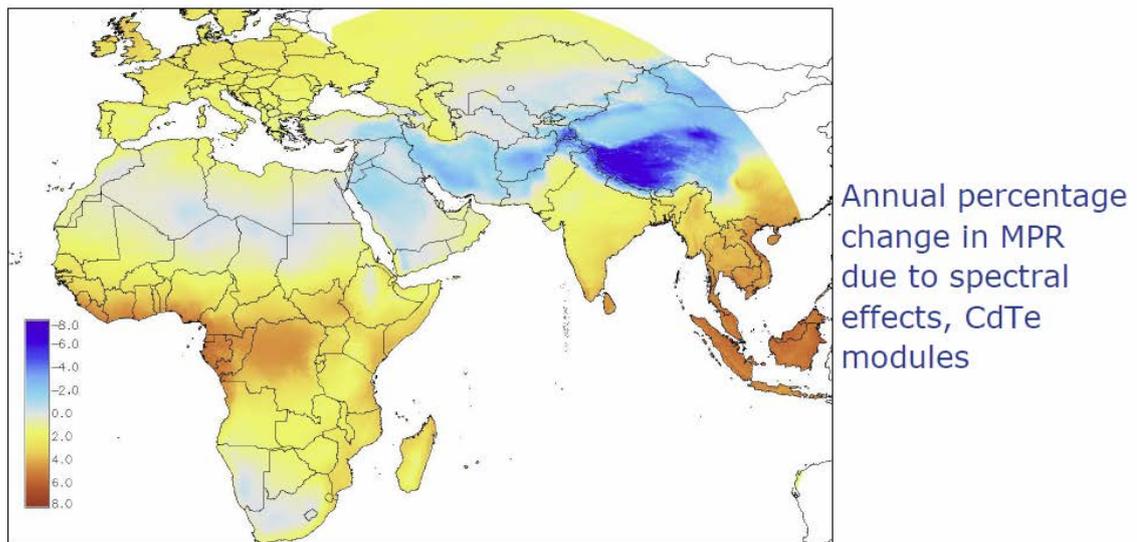
Figure 28: Map showing the annual percent change in Module Performance Ratio due to spectral effects for CdTe modules.

3.2.2   Combined Air Mass and Precipitable Water Spectral Correction for PV Modeling

Mitchell Lee of First Solar presented a new spectral correction method for PV modeling. The spectral correction is applicable to both cadmium telluride (CdTe) and crystalline silicon (c-Si) PV technologies, and is of simple functional form, which enables it to be easily incorporated into standard PV simulation software. The model corrects for changes in spectrum due to air mass and precipitable water content. The model has module-specific coefficients based on the module's quantum efficiency (QE) curve. For modules with similar quantum efficiency curves, the same coefficients can be used.

The spectral correction was developed by use of the Simple Model of the Atmospheric Radiative Transfer for Sunshine (SMARTS). Spectra were simulated for varying precipitable water content (Pwat) from 0.5 cm to 5.0 cm and absolute air mass (AMa) from 0.8 to 4.75. The range of wavelengths used in calculations was 280 nm to 2800 nm, which are the limits of a typical secondary standard pyranometer. All other parameters input into SMARTS were kept at the values from the ASTM G 173 standard. Spectral shift (also known as spectral mismatch) was computed for both modules at each AMa and Pwat value, using the generated spectra and module QE curves as inputs. The three-dimensional surface depending on spectral shift, precipitable water, and air mass was regressed to a simple functional form with module-specific coefficients. The simple functional form allows the spectral correction to be included into PV simulations tools without running SMARTS, or having spectrally resolved irradiance data.

Publically available meteorological and PV field performance data from NREL [34] was used in order to validate the computationally derived spectral model. The data was from three locations: Cocoa, Florida; Eugene, Oregon; and Golden, Colorado, and it spanned 13 months at each location. Spectral shift was estimated using the ratio of module short circuit current, I_{sc}, to plane-of-array irradiance, scaled to equal one under standard test conditions. I_{sc} was also corrected for the effects of temperature, angle of incidence, and soiling. Data was filtered to remove excessively cloudy conditions, low irradiance conditions, and days with minimal data availability. For the c-Si modules, spectral shift was also estimated using an AMa-only method [14], and for the CdTe modules spectral shift was also estimated using a Pwat-only method [35]. Spectral shift derived from I_{sc} was irradiance-weighted to daily resolution and plotted against the spectral shift factor as

estimated using the newly proposed model and previously existing models. In all cases, the newly proposed Pwat and AMa spectral correction was as good as, or better than, existing simple corrections.
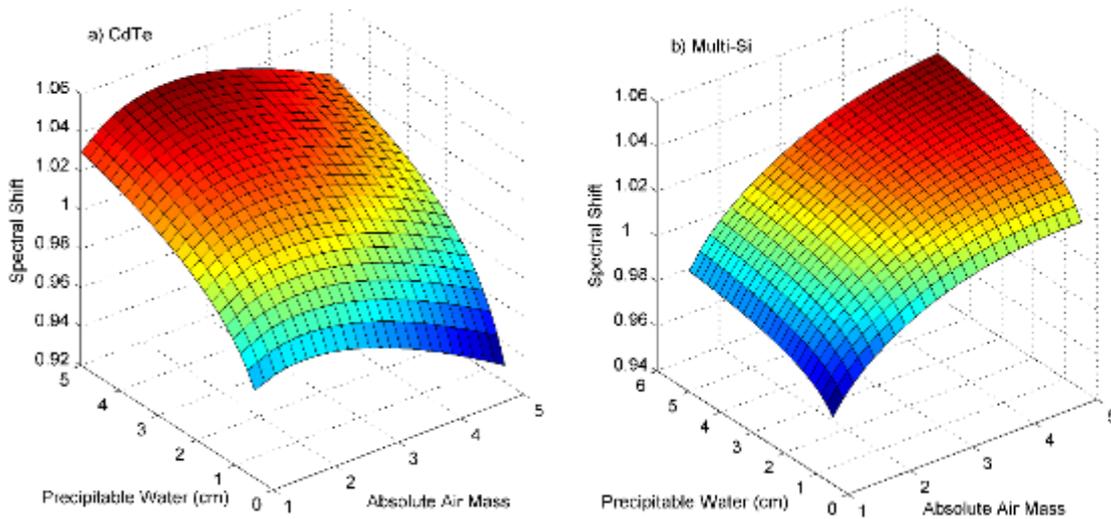
Figure 29: Sensitivity analysis of spectral shift to air mass and precipitable water for a) CdTe PV modules and b) multi-Si PV module.

CdTe

$$M_{now} = 0.542M_{measured} + 0.476$$
$$R^2 = 0.494, MAE = 0.0169$$

$$M_{Proposed} = 0.585M_{measured} + 0.433$$
$$R^2 = 0.698, MAE = 0.0166$$

Multi-Si

$$M_{now} = 0.944M_{measured} + 0.044$$
$$R^2 = 0.428, MAE = 0.0130$$

$$M_{Proposed} = 0.933M_{measured} + 0.060$$
$$R^2 = 0.723, MAE = 0.0077$$
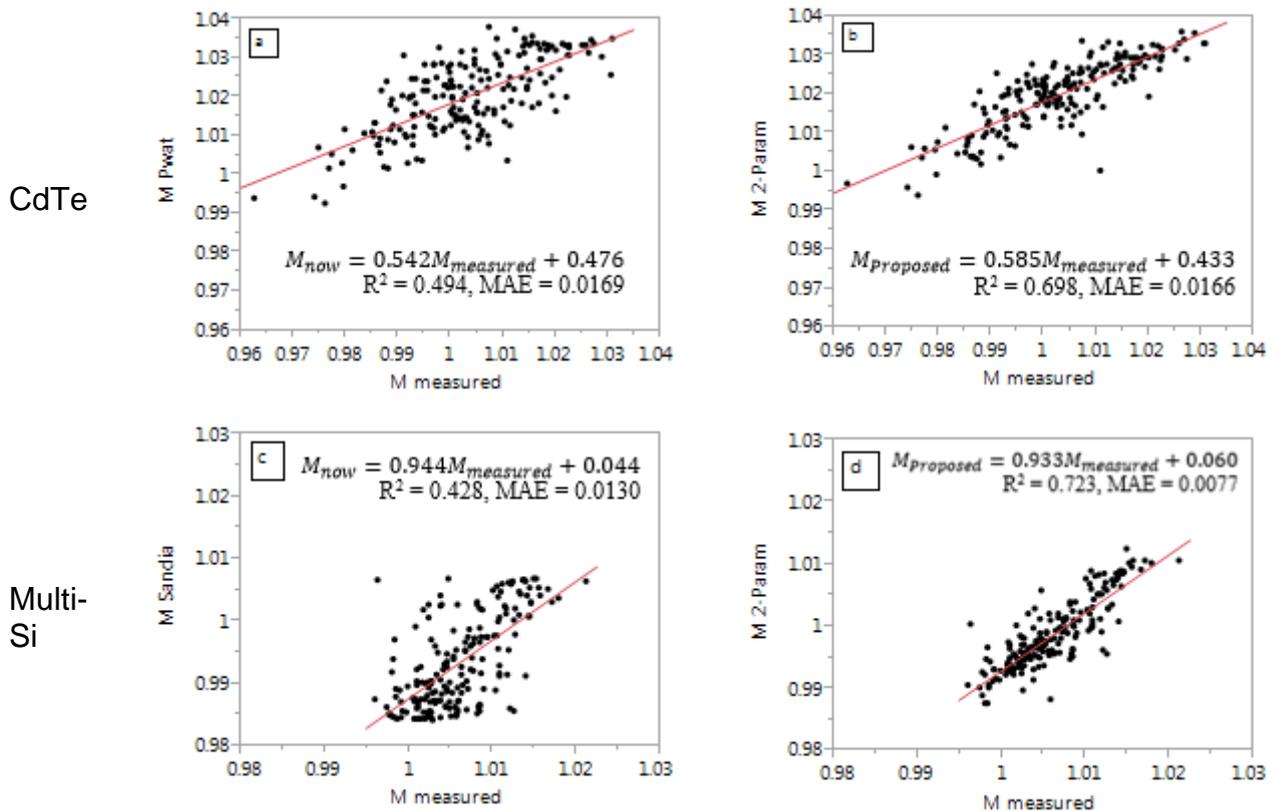
Figure 30: a) CdTe spectral correlation proposed by Nelson et al., [35] versus measured M for the CdTe module. b) M estimated using the proposed spectral model versus measured M for the CdTe module. c) Spectral correction proposed by King et al., [14], versus measured M the multi-Si module. d) M estimated using proposed spectral model versus measured M for the multi-Si module. All M data is from the Cocoa, Florida test site, of daily resolution, and GHI-weighted.

3.2.3 Sensitivity Analysis and Uncertainty Evaluation of Simulated Clear-Sky Solar Spectra Using Monte Carlo Approach

Giorgio Belluardo of EURAC presented the methodology and research results from the calculation of the uncertainty of a Radiative Transfer Model (RTM) using the Monte Carlo technique. RTM are used to calculate the spectral and broadband irradiance on Earth's surface given a set of atmospheric input parameters. While many research studies exist that evaluate the accuracy of such models (i.e. the comparison of RTM-generated spectra with measured spectra), to the authors' knowledge a research gap still exists in the evaluation of the uncertainty propagation from the input parameters to the model output. This is partly explained by the non-integral and not differentiable nature of the Radiative Transfer Equation (RTE) implemented in the RTM, that does not allow the usual law of propagation of error to be applied. Instead, a statistical approach based on the Monte Carlo technique is applied here. The RTM SDISORT implemented in the UVSPEC tool and part of the LibRadtran library is used as the object of the study. The analysis considers the spectral range 280 nm - 2500 nm that encompasses the sensitivity of all commercially available photovoltaic technologies as well as of spectroradiometers.

The procedure starts with the definition of a reference set of SDISORT input parameters, of their associated error bounds (i.e. the maximum error reasonably attributed to an input quantity), and of the Probability Density Function (PDF) of their error. By randomly generating N>>0 number of values for each input quantity according to the defined conditions, it is possible to construct N>>0 input vectors that are fed into SDISORT. The output spectra are statistically analyzed, and the relative uncertainty is calculated for each wavelength as well as for the broadband irradiance (integral of the spectrum). In particular, two options are possible for the generation of the input vectors. In the first, only one input parameter at a time varies, in order to evaluate the contribution of every single input parameter to the uncertainty of SDISORT. In the second, all input parameters vary simultaneously, in order to evaluate the combination of error propagation for the whole set of input parameters. The overall methodology and the two options described are shown in *Figure 31*. Results of the uncertainty of global horizontal spectral irradiance generated with SDISORT for the reference set of input parameters corresponding to the atmospheric conditions at Kanzelhöhe Observatory (Austria, 1526 m asl) on April 25th, 2013 at 10 a.m., are shown in *Figure 32*. The input parameters most influencing this spectral uncertainty are: ozone concentration (especially in the UV-B region), extraterrestrial spectrum (constant contribution considered over the whole range), Ångström turbidity coefficient (in the UV-B and UV-A regions) and water vapor (in the water absorption bands).

Next, specific combinations of input parameters corresponding, respectively, to the maximum and minimum values of uncertainty of the broadband global horizontal irradiance generated with SDISORT are found. This is done in order to consider all possible combinations of input parameters differing from the reference one used in the previous point, and that can occur at a different location and/or at a different time than the reference ones. Results show that the uncertainty of global horizontal broadband irradiance simulated with SDISORT and deriving from the simultaneous propagation of uncertainty of all input parameters is between 2.9% and 5.9%. These values are higher, but still comparable to typical uncertainty values of global irradiance measurements performed with spectroradiometers. Furthermore, it is demonstrated that the upper uncertainty limit would be significantly underestimated if a classic propagation of error was used, because the latter does not take the correlation of input parameters into consideration correctly in such a case.
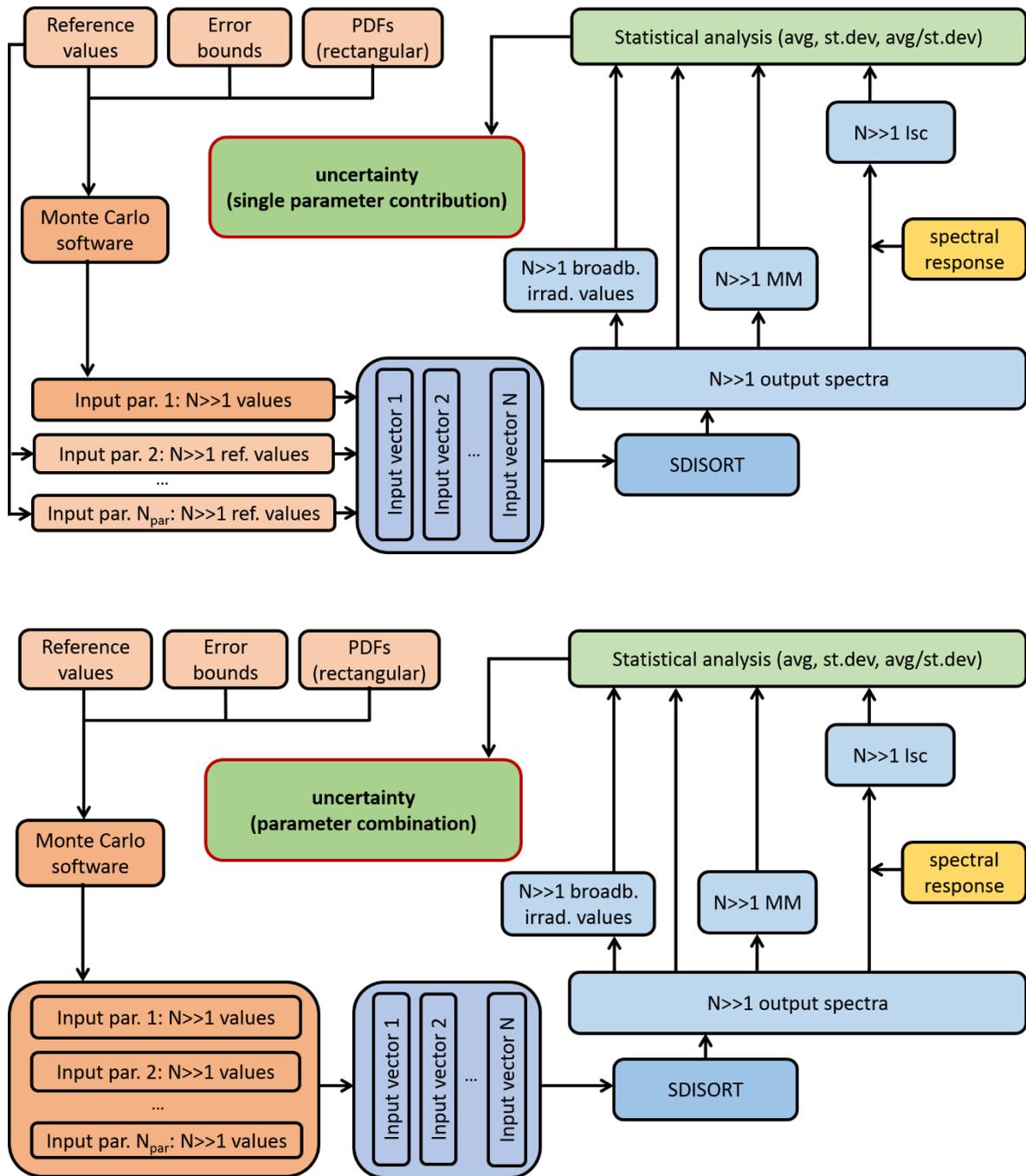
Figure 31: Schematic diagram of the methodology described, that involves the use of the Monte Carlo technique. (top) Propagation of the uncertainty of one specific input parameter. (bottom) Simultaneous propagation of the uncertainties of all input parameters.
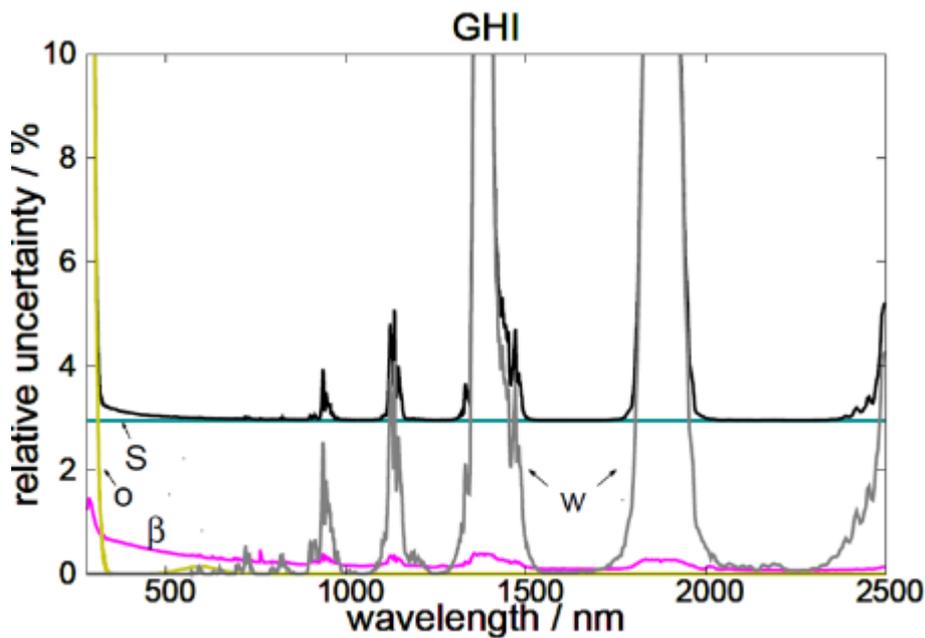
Figure 32: Relative uncertainty of the SDISORT output at varying wavelength, due to the uncertainty of each input parameter (colored lines) and to the combined effect of all input parameters (black line), for global horizontal irradiance. Conditions correspond to the atmospheric state at Kanzelhöhe Observatory (Austria, 1526 m asl) on April 25th, 2013 at 10 a.m.. S: extraterrestrial irradiance, o: ozone concentration; w: precipitable water, ß: Ångström turbidity coefficient.

An interesting follow-up of the present study would be to further investigate the propagation of the uncertainty from the solar spectrum generated with SDISORT to some PV device calibration parameters that are a function of the incident solar spectrum: the short-circuit current (I_{sc}) and mismatch factor (MM). Preliminary results on seven different PV technologies show that the uncertainty of I_{sc} and MM is higher for technologies with narrower spectral responsivity.

The work presented in the talk and its possible follow-up form an important contribution to the clarification of the uncertainty level associated with the estimated solar resource, which is part of the PV chain. It is therefore beneficial also for the bankability of solar energy projects.

3.2.4   Spectral Corrections for PV Performance Modeling

Fotis Mavromatakis provided an overview to illustrate that PV performance predictions based on using air mass as a proxy for spectral effects can be improved. The presenter defined a quantity he called the average PV module response, which is nearly identical to the Module Performance Ratio described earlier (3.2.1). He then showed that this quantity could be calculated using DNI, DHI, or GHI irradiance. *Figure 33* shows an example using DNI and normalized to a 45° solar zenith angle. Other examples using DHI and GHI showed that these effects can differ depending on the irradiance source used.

The talk pointed out a weakness in relying only on air mass as a proxy for spectral effects. This result is consistent with the points made by other presenters in this section.
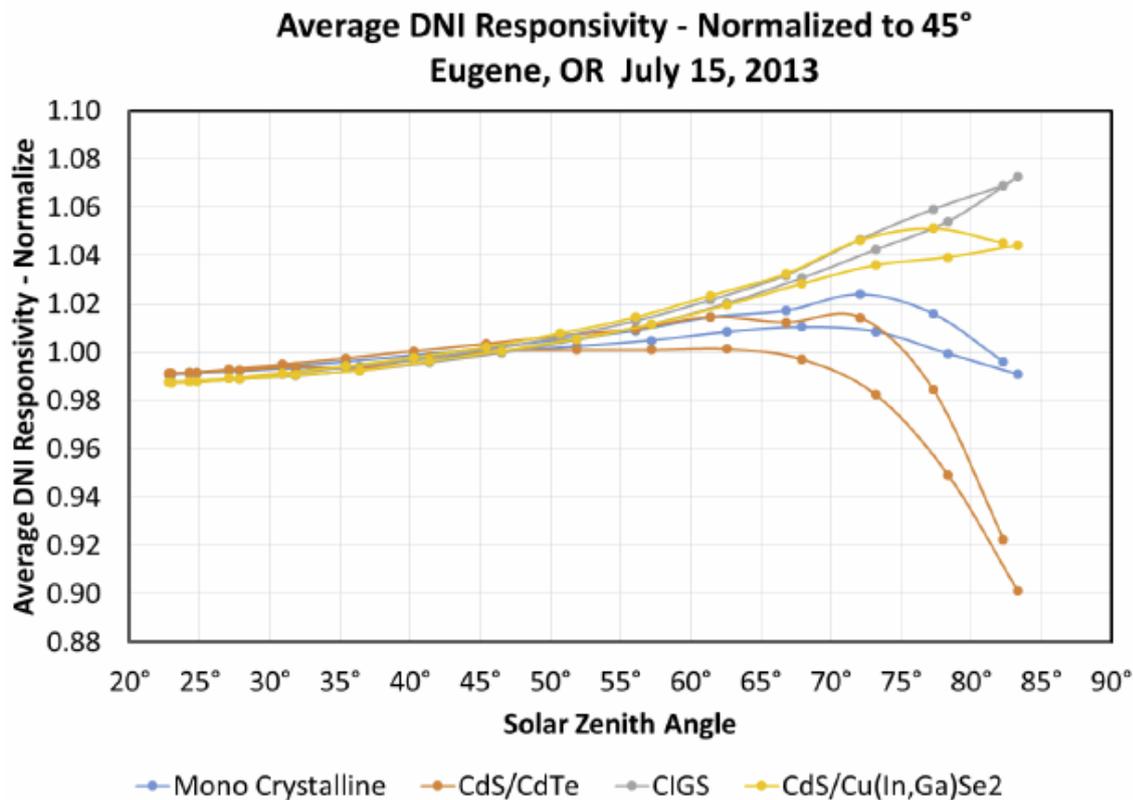
Figure 33: Relative PV module response normalized to 45° solar zenith angle for four different PV cell technologies.

3.2.5   Improved Prediction of Site Spectral Impact

Benjamin Duck presented a new spectral model for improving the accuracy of PV performance modeling. Estimates of the output of deployed PV systems based on pyranometer data are subject to errors introduced by the mismatch between the pyranometer and PV responses to the angular and spectral distribution of irradiance. The importance of applying a spectral correction is dependent upon both the timeframe of interest and location/condition dependent factors. There are two methods most commonly used in literature and incorporated into the most popular PV system performance modeling software. The first method uses the air mass function described in the Sandia Array Performance Model. This captures the spectral correction as a 4th order polynomial as a function of geometric air mass only. Coefficients for the polynomial are available from Sandia and other sources for all major PV technology types and many manufacturers. The second is a model developed by the CREST laboratory at Loughborough University. That model seeks to account for the impact of clouds and atmospheric effects by parameterizing the correction as a function of both geometric air mass and clearness index. The published CREST model only attempts to treat amorphous silicon devices and is not typically applied to other technologies.

This talk presented data showing the application and validation of these two methods against measurements at the CSIRO PV Outdoor Research Facility at Newcastle, Australia. The methods were compared against photovoltaic device performance normalized to standard conditions, and against direct measurements of the incident solar spectrum. A key weakness demonstrated in both methods is the assumption of a unitary correction factor at a geometric air mass of 1.5. This assumption leads to an offset as large as 3.5% between the estimated and measured spectral correction that appears to be relatively independent of season. The authors posit that this offset is likely to be linked to the general atmospheric characteristics of the site and hence that it may be possible to generate a correction value, which is termed the site spectral offset. A single pa-

rameter air mass function is also shown to be inadequate to account for data collected under conditions that do not have completely clear skies.

The CSIRO team developed a modification of the CREST method that uses the module spectral response and data from the Newcastle site to calculate a spectral correction surface (*Figure 34*). This surface has been demonstrated to provide an increase in the accuracy of energy yield predictions for the site. The modification is applied by using the spectral response of the module, rather than a spectral windowing technique, as the basis for calculating the useful irradiance fraction. The result is a value that is equivalent to the spectral mismatch factor. A two-variable polynomial surface is then fit to this data using the parameters of air mass and clearness index, where clearness index is derived from solar radiation measurements and using the Haurwitz model for clear sky global horizontal irradiance [36]. The resulting surface for a crystalline silicon module is shown below.
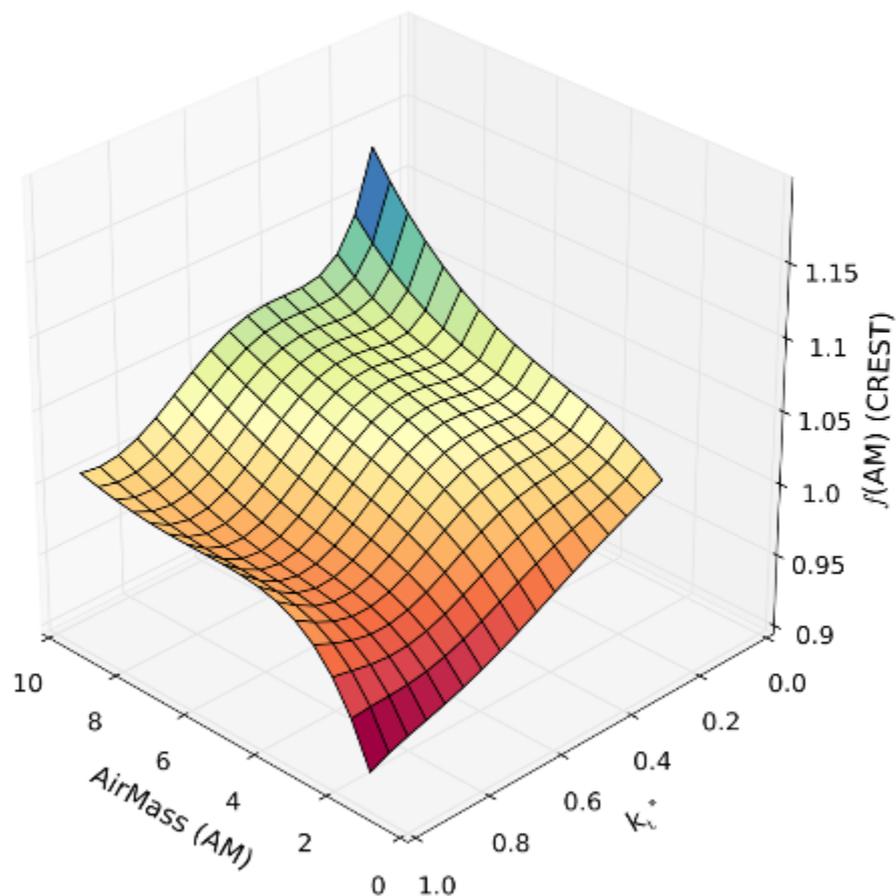
Figure 34: Spectral correction surface based on air mass and the clearness index.

For the Newcastle site, this surface significantly reduces the estimation errors for spectral impact. However, it was noted that there are still some issues with this approach that need to be addressed: 1) the above analysis has been performed only for data taken from a single location. High-quality spectral information from other locations is necessary in order to confirm the exist-

ence of any time-independent spectral offset and the structure of the fitting surface; 2) the pre-diction surface is sensitive to the type of clear sky GHI model adopted. Even making small changes to the coefficients for the model used was shown to affect the surface shape while still providing the same predictive improvements. The sensitivity to the GHI model implies that a surface derived from one site will not be applicable to another unless the GHI modeling procedure is globally ap-plicable; 3) dependencies on other parameters are still present within the dataset. In particular, changes to the clear sky value for spectral mismatch have been noted to have different air mass dependencies that cannot be explained by simple geometric models. A significant correlation has been observed with the atmospheric precipitable water content that is also not captured in the current model.

Main points of presentation:

1.   Current models contain an underlying assumption that spectral mismatch = 1 at air mass = 1.5. This leads to an offset between estimated and measured data. Further, es-timation under non-clear sky conditions leads to significant errors in instantaneous data as no existing models can reproduce these effects for most conventional PV technologies.

2.   A significantly improved spectral impact estimation is possible using an easily imple-mented modification to the CREST approach that accounts for non-clear sky condi-tions and incorporates a site spectral offset value.

3.2.6   Impact of Spectral Irradiance on Energy Yield of PV Modules Measured in Differ-ent Climates

Markus Schweiger of TÜV Rheinland shared the latest results of the national R&D project PV-KLIMA with regard to spectral irradiance measurements in four different climates and an analysis of the impact on the energy yield delivery in comparison to other environmental effects (*Figure 35*).

Figure 35: Outdoor test installations in Germany, Arizona, India and Italy with 15 PV modules op-erating since 2014.

In the first step, the spectral response (SR) of 15 different PV modules was measured in the labor-atory as shown in *Figure 36*. The results revealed significant differences in the SR signal of differ-ent technologies and manufacturers. In the second step, the samples were exposed outdoors in

Cologne (Germany), Ancona (Italy), Tempe (Arizona), Chennai (India) and Thuwal (Saudi-Arabia). Besides the electrical performance of the PV modules, the spectral irradiance was measured in the wavelength range of 300 to 1600 nm in one-minute intervals. Shifts of the solar spectral irradiance were analyzed by the average photon energy factor (APE). Given the spectral response and the average spectral distribution, gains and losses in the energy yield delivery were calculated individually for each sample by the spectral mismatch factor approach (MMF) according to IEC 60904-7, as shown in Table 5.

Table 5. Prospective yield gains or losses for different PV module technologies in different climates due to spectral effects calculated with the spectral MMF approach.

PV	Italy	Arizona	Germany	India
c-Si	< 0.5 %	> -1.2 %	< 1.3 %	< 1.6 %
CIGS	< 0.7 %	> -1.6 %	< 1.8 %	< 2.8 %
CdTe	< 1.0 %	< 1.1 %	< 2.3 %	< 5.3 %
Tandem a-Si (top limited)	< 3.5 %	< 7.0 %	< 4.0 %	< 10.6 %

Spectral irradiance data measured outdoors revealed a red shift in the distribution of the solar spectrum for winter and a blue shift for summer. Also strong daily shifts in the spectral distribution could be shown, depending on air mass, cloud coverage and angle of incidence. Spectral effects almost compensate each other for energy-weighted one-year data of single-junction devices. PV modules with c-Si or CIGS cells did not show a significant dependency on spectral effects. By contrast, PV modules with CdTe cell technology are more sensitive to shifts in the spectral irradiance and gains in the photocurrent of up to +5.3% were observed at the location Chennai.

It is planned to continue the outdoor measurements to generate a long-term database for spectral irradiance data.
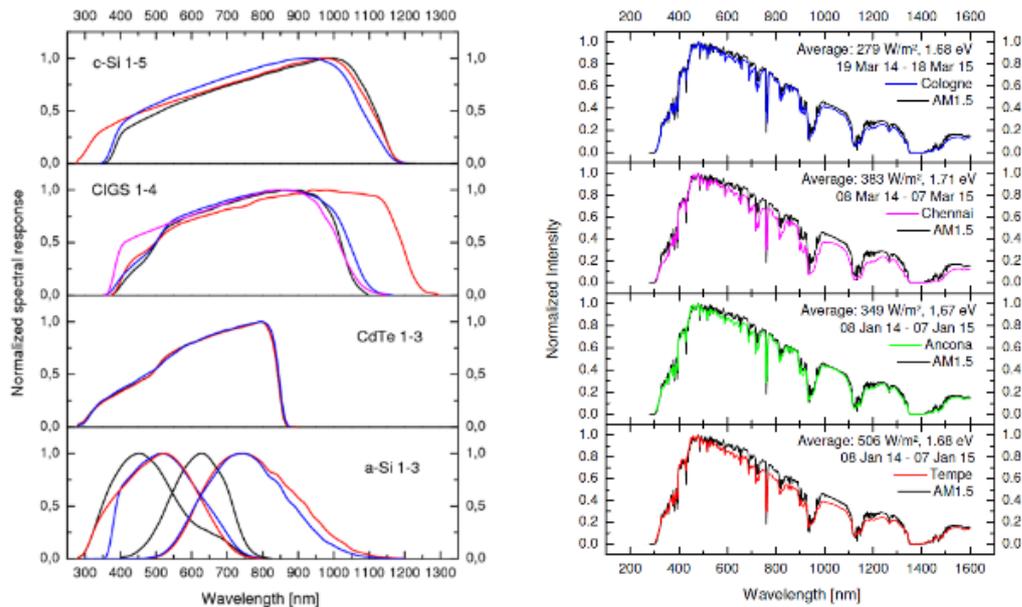
Figure 36: Left: Normalized spectral response signal of the tested sample types. Right: Average annual spectral distribution of irradiance at 4 test sites in comparison to the AM1.5 spectrum.

3.3 Session 3: Soiling and Snow, and Other System Derating Factors

This session was chaired by Ulrike Jahn from TÜV Rheinland.

Table 6: List of presentations and speakers for Session 3.

Title	Presenter	Affiliation	Country
Impact of Soiling on PV Module Performance for Various Climates	Werner Herrmann	TÜV Rheinland, Solar Energy	Germany
Overview of Sandia's Soiling Program: Description of Experimental Methods and Framework for a Quantitative Soiling Model	Bruce H. King	Sandia National Laboratories	USA
Validation of Models for Energy Losses due to Snowfall on PV Systems	Janine Freeman	National Renewable Energy Laboratory	USA

3.3.1 Impact of Soiling on PV Module Performance for Various Climates

Werner Herrmann of TÜV Rheinland presented results of a soiling impact study for PV systems in a range of climates in different regions. During long-term operation of photovoltaic (PV) power plants, soiling of the PV module surface can cause significant energy yield losses, which pose a particular challenge to PV energy yield prediction. PV soiling loss is dependent on the site characteristics such as climatic conditions or the surrounding environment, but also on the glazing characteristics of the PV module. The presentation focused on experimental soiling loss profiles, which have been measured at five test locations of TÜV Rheinland, covering a wide range of climatic conditions (*Figure 37*).

Location	Country	Operation since	Köppen-Geiger climate classification
Ancona	Italy	01 Nov 2013	Cfa (mediterranean)
Tempe	Arizona/USA	15 Dec 2013	Bwh (hot dessert)
Chennai	India	01 Feb 2014	Aw (tropical savanna, hot-humid/dry)
Cologne	Germany	01 Mar 2014	Cfb (temperate)
Thuwal	Saudi-Arabia	11 Mar 2015	Bwh (hot desert, sandstorm impact)
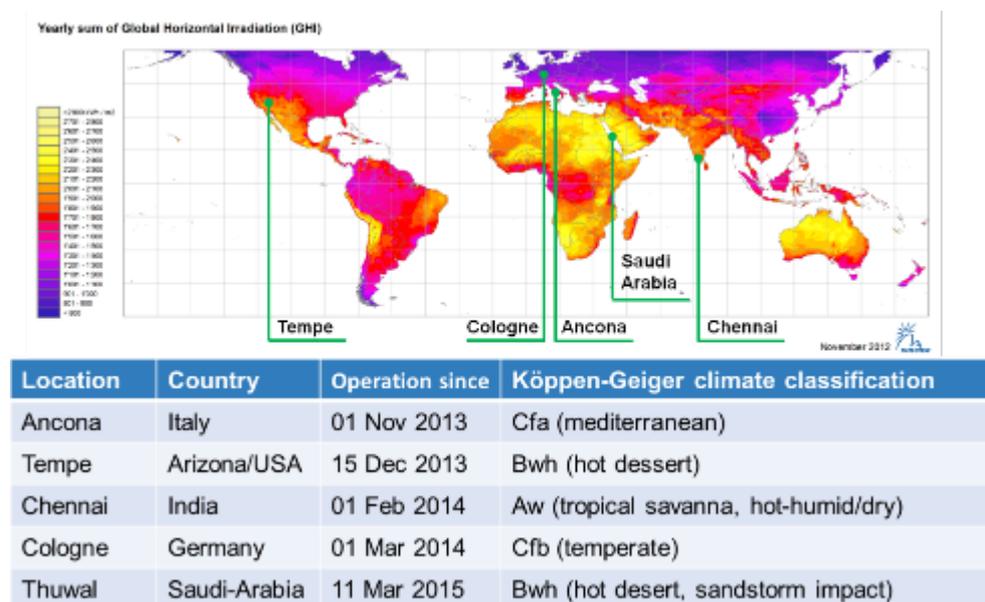
Figure 37: Map and table showing the location, climatic zone, and dates associated with the five soiling stations discussed in the presentation.

Dust was monitored by side-by-side irradiance measurement with two mini-modules, of which one was periodically cleaned whereas the other was exposed to natural soiling. The soiling loss factor was defined as ratio of effective irradiances reaching the cells.

Annual PV soiling loss in Tempe (Hot and dry climate) was <4% in the first year of monitoring. Up to 15% transmission loss was observed, after which rainfall led to nearly full recovery. Annual soiling loss for the tropical test site is lower (<3%). However, the transmission loss at the end of the 3-month dry season was 25%. For temperate climates (Cologne, Ancona) with frequent rainfall, annual PV soiling loss is less than 0.5%. For the desert test site in Saudi Arabia, high soiling rates were observed (average 0.5% transmission loss per day), which indicates that economic operation of a PV power plant requires periodic cleaning.

Dust accumulation on the glass surface changes the angular response of PV modules, resulting in significant angular losses. For test site Tempe, more than 20% of total soiling loss was caused by angular effects. Furthermore, the study clarified that the soiling loss pattern of consecutive years can be subject to significant variation. Accordingly, long-term monitoring programs are required for accurate PV performance modeling and energy yield prediction.

3.3.2 Overview of Sandia's Soiling Program: Description of Experimental Methods and Framework for a Quantitative Soiling Model

Bruce King of Sandia presented an overview of Sandia's research program. Sandia has been at the forefront of the development of quantitative, repeatable methods to study the impact of soil composition and mass loading on the performance of photovoltaic panels since 2012. Their methodology includes procedures for formulating liquid suspensions containing relevant soil components, procedures for spray depositing these liquid suspensions onto test panels, and characterization methodology to quantify the impact that the resulting coatings have on an underlying PV cell. Laboratory work is complemented by three types of soiling stations installed at multiple locations across the US to confirm the influence of soil composition on performance and correlate to laboratory studies. Two stations, built and deployed by University of Colorado-Boulder, include ambient air sampling equipment and glass collection plates to provide better understanding of the interrelationship between suspended particulate matter, natural soil deposition rates and composition. The third type of station, built and deployed by Arizona State University, monitors the impact of soil accumulation on the electrical performance of calibrated PV reference devices. The research has enabled Sandia to present a high-level view of the processes that lead to the suspension of particulates in the atmosphere and their ultimate impact on PV system performance (*Figure 38*).
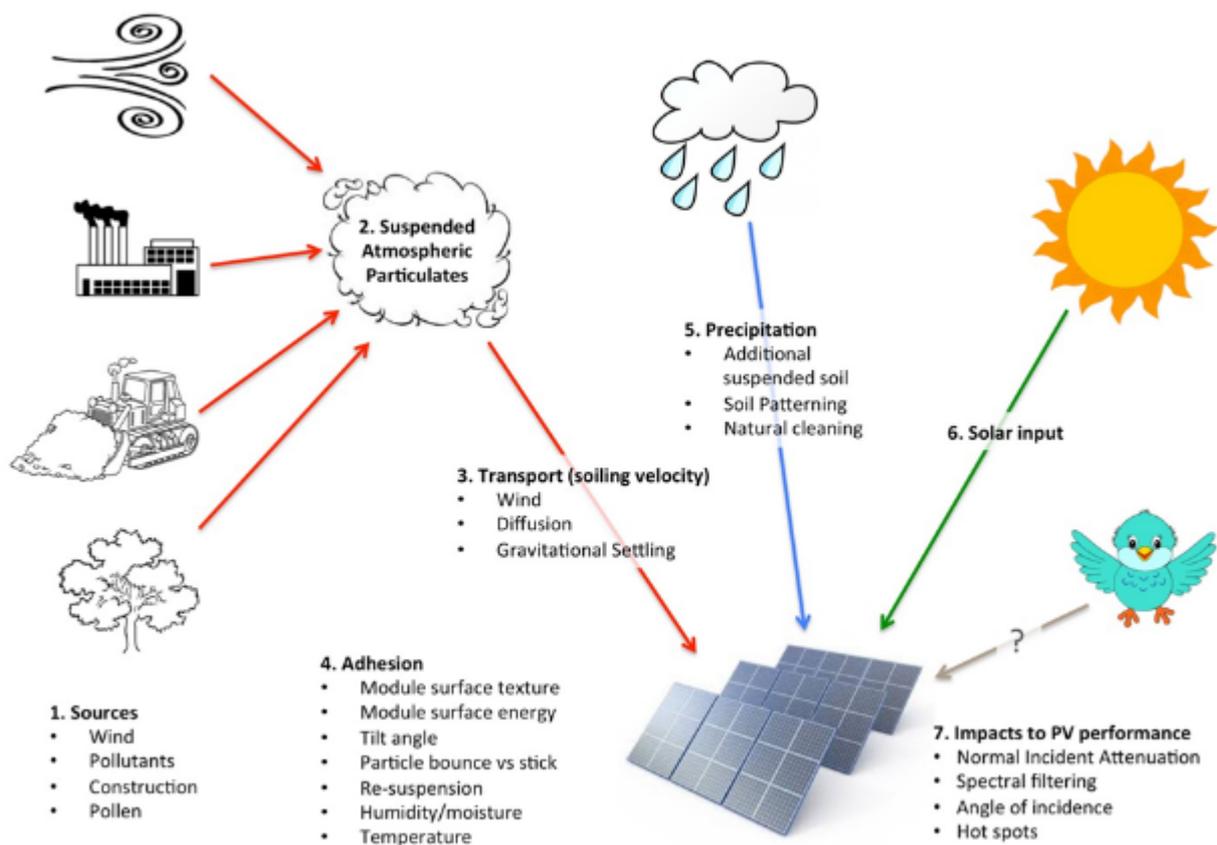
Figure 38: Natural processes affecting soiling of PV panels and subsequent power loss.

Combined indoor and outdoor studies have enabled Sandia to demonstrate that the transmission profile of outdoor soiling conditions can be approximated with a laboratory-synthesized analogue. Examination of soil composition revealed a few important trends. First, soils containing primarily soot and sand provided a neutral response with no impact to the spectrum of the transmitted light. Secondly, these formulations were highly susceptible to the soot content. On a mass basis, soot was found to have a 10-fold impact on transmission loss compared to sand. This finding is particularly relevant to PV systems deployed in areas with significant pollution from combustion. PV systems near industrial areas or airports may be more susceptible to soiling losses than systems located in rural or agricultural areas.

Likewise, examination of soils containing pigment blends was revealing. Yellow Goethite rich soils displayed greater spectral sensitivity overall, absorbing considerably in the UV to green wavelengths (~300 – 500 nm), but very little above ~600 nm. In contrast, red hematite-rich soils displayed a more neutral absorption. The greatest impact to transmission loss came from an intermediate blend of these two, which displayed a strong peak in the UV to green coupled with high absorption from 500 – 1200 nm.

The effect of soiling on angle of incidence response was investigated by applying synthetic (neutral) soil to one half of a customized split reference cell and measuring Angle of Incidence (AOI) response outdoors on a two-axis tracker. A low soiling rate (< 0.5 g/m^2) was observed to have minimal effect on the AOI response compared to a reference curve while a high soiling rate (>3 g/m^2) has a pronounced effect. This effect is in addition to normal attenuation effects due to

the incidence angle and could be a significant consideration for commercial rooftop systems in particular, which are typically deployed at low tilt angles (*Figure 39*).
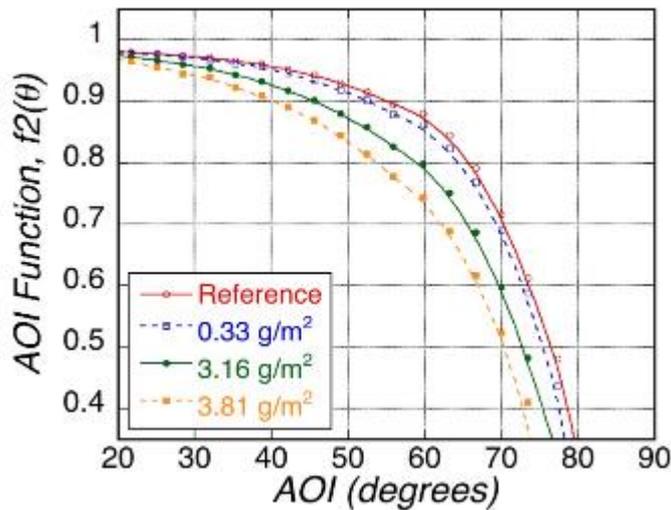

Figure 39: Influence of soil on angle of incidence response of PV panels. High soiling leads to greater reflection losses than observed on clean panels. This loss is in addition to angle-dependent attenuation compared to a normal incidence angle.

An analysis of total suspended particulate concentrations against mass accumulation on glass plates collected from outdoor sites revealed a generally linear trend; higher airborne particulate concentrations lead to greater accumulations. Second, both airborne concentration and mass accumulation were generally higher at one site in Commerce City, CO. This area is generally known to be a heavily industrial area. Preliminary transmission loss measurements across all sites produced a linear response against mass accumulation. While there was scatter in the data, this observation may support a claim that the composition of accumulated soil is rather simple, without a significant spectral component. This claim cannot be verified without compositional analysis of the collected soils. However, if it proves to be true could have significant implications for developing soil mitigation strategies and for performance modeling.

3.3.3   Validation of Models for Energy Losses due to Snowfall on PV Systems

Janine Freeman of NREL presented a very important, yet little discussed, topic: the effect of snow on PV systems. The presentation outlined the importance of modeling snow losses in snowy climates, discussed the implementation of such a model in SAM, and most importantly, discussed the capabilities and limitations of the model from the perspective of results gained using it. It summarized a full report on the topic that was published by NREL [37]; more information can be found in that report.

Due to the potential for increased deployment of PV systems in snowy climates, there is interest in a method capable of estimating PV losses resulting from snow coverage. A handful of snow coverage models have been developed over the last 15 years, but to date, no such models have been incorporated into the PV modeling workflow. With annual energy losses estimated up to 25% by previous research, there is a clear need for snow losses to be factored into energy estimates for snowy climates. In response to this need, NREL has integrated the methodology of the snow model developed in the paper by Marion et al. [34] into NREL's System Advisor Model (SAM). The mechanics of Marion's model can be found in the paper he published on the subject [38], but part of the impetus for choosing his model over others is that the only additional information required from users in order to run the model is a time series of snow depths.

After implementing the snow model in SAM, NREL performed an initial model validation for two systems in snowy climates (Forrestal system in Washington, DC and RSF2 system in Colorado) for which they had system specifications, measured performance data, and snow depth data. After scaling the output to match the summer months so that the effect of the snow model could be analyzed separately from systematic model bias, they compared the energy predicted by SAM with and without the snow model to measured energy, and looked at the results on both an annual and monthly basis (*Figure 40*). These results showed that use of the snow model greatly reduced annual error, but on a monthly basis, it may overpredict the snow loss and make the monthly errors worse, as was seen in December for the RSF2 system. This is consistent with Marion's evaluation of his snow model, and also illustrates the biggest need for future research in this topic: improving accuracy at shorter timescales?

After demonstrating that the model helped to reduce error for two systems, NREL proceeded with a national study to model the potential effect of snow on PV systems throughout the continental U.S. They modeled two typical fixed-tilt systems (tilt=20° and tilt=latitude) for 239 locations in the U.S. using 30 years of historical weather data from the 1961-1990 NSRDB data set. They then took the spread of results seen in that study to create a map of general trends in snow losses for the continental U.S (see *Figure 41*). These loss estimations vary as one would expect, reaching over 20% in the northern regions of the country, and resulting in higher losses for higher elevation sites than their nearby neighbors in the region (for example, Flagstaff AZ compared to Phoenix AZ). This plot may not capture every year, but is meant to represent typical starting losses for users without additional information about their site.

In summary:

- The snow loss model implemented in SAM was shown to reduce annual error for two systems.
- The snow loss model was used to produce a map of typical snow losses for the continental U.S. as a starting point for users without more detailed data.
- Although it reduced error on an annual basis, the model sometimes overpredicted monthly or hourly losses. Future work should strive to improve the model at more granular timescales.
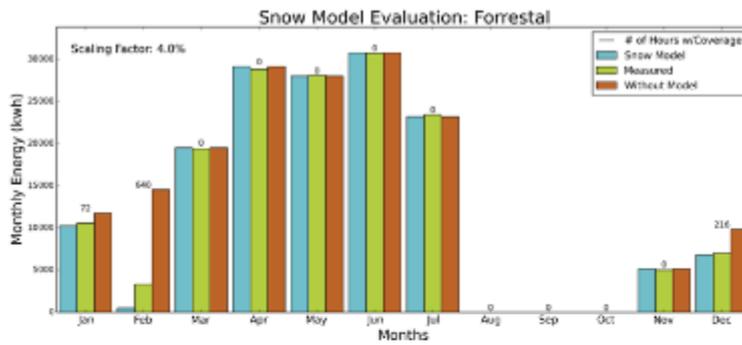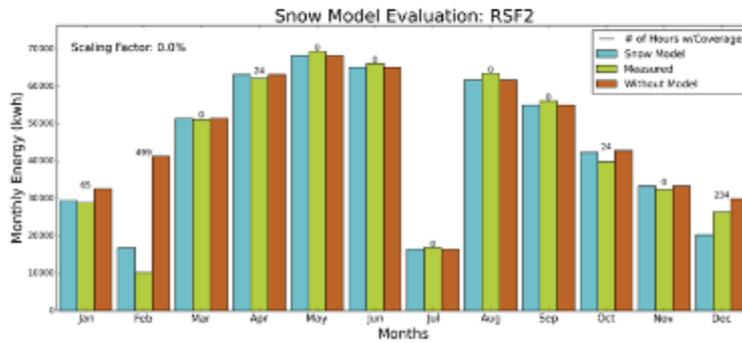
Figure 40: Results from the validation study using Forrestal system in Washington, DC and the RSF2 system in Golden, Colorado.
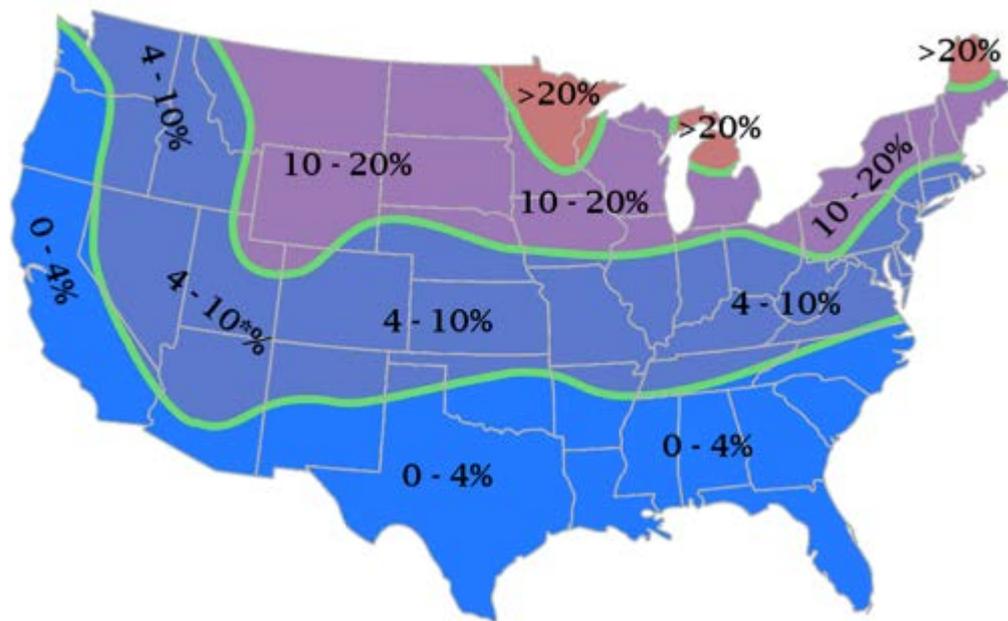
Figure 41: General trends in average snow losses as a percentage of annual energy production. Note: Like-colored regions have similar loss percentages and are labeled in the figure. The specific region around Nevada and the Four Corners is special (indicated by an *) in that high altitude regions, such as Flagstaff, Arizona and Ely, Nevada should be considered to be in the next higher tier of snow losses. This plot is a broad enough generalization that it may apply to either a tilt = latitude or a 20° system.

3.4 Session 4: Bifacial PV Modeling Challenges

This session was chaired by Teresa Zhang from SunEdison.

Table 7: List of presentations and speakers for Session 4

Title	Presenter	Affiliation	Country
Introduction to Bifacial Modeling Challenges	Teresa Zhang	SunEdison	USA
Simulation and Validation of Modeling of Bifacial Photovoltaic Modules	Gianluca Corbellini	SUPSI	Switzerland
Realistic Yield Expectations for Bifacial PV Systems - am Assessment of Announced, Predicted and Observed Benefits	Christian Reise	Fraunhofer-Institut für Solare Energiesysteme ISE	Germany
Modeling of the Expected Yearly Power Yield on Building Facades in Urban Regions by Means of Ray Tracing	Hendrik Holst	Institut für Solarenergieforschung GmbH	Germany
Multi-Year Study of Bifacial Energy Gains Under Various Field Conditions	Jose E. Castillo-Aguilella	Prism Solar Technologies, Inc.	USA

3.4.1 Introduction to Bifacial Modeling Challenges

Teresa Zhang from SunEdison provided a brief introduction to bifacial module technologies. This technology was first introduced in a U.S. Patent in 1966. There were multiple presentations made on bifacial cell technology at the 1st European Photovoltaic Solar Energy Conference in 1977. In 2000, Russia deployed 10 kW of bifacial PV on the International Space Station. In 2009, the first commercial bifacial modules were released by Sanyo (no Panasonic). By 2015 more than 100 patents had been granted for this technology. Tens of MW have been deployed worldwide and more than 10 companies are currently offering bifacial module technology in the market. Multiple existing cell technologies can be made to be bifacial, including HIT, PERC, and, IBC.

There are a number of modeling challenges facing bifacial technologies. These include: (1) a lack of standards for rating and characterizing bifacial modules and (2) the difficulty in estimating the back-surface irradiance resource, which varies spatially and depends on the site characteristics (e.g., albedo) and system design and layout. *Figure 42* shows a selection of deployment options for bifacial PV including rooftop, parking structures, tracking systems, and vertical deployments.

Figure 42: Examples of some of the deployment designs being considered for bifacial PV systems.

3.4.2 Simulation and Validation of Modeling of Bifacial Photovoltaic Modules

The purpose of this talk by Gianluca Corbellini about bifacial PV modules was to describe results of experimental research performed at SUPSI, their indoor and outdoor measurement, together with modeling of performance.

For the outdoor measurement, the bifacial output has been compared with monofacial modules of different technologies (HIT, Poly-Si, CIS, CdTe), during different periods of the year, in Lugano, Switzerland (*Figure 43*). In addition to standard sensors (cell temperatures, front-surface irradiation on the plane of array, global and diffuse horizontal irradiation), dedicated sensors were installed to measure the irradiation on the back surface of the bifacial modules. Moreover, a new method has been used to estimate the cell temperature of bifacial modules, using open circuit voltage, temperature coefficients and irradiation; this model was first validated on a monofacial module where the cell temperature was available.

For the indoor measurement, SUPSI tested the reflectance of the dark room for flash testing in the case of bifacial modules, in particular measuring the irradiance seen by back-surface cells; on this basis, a new method to normalize the nominal power from irradiation of both surfaces of the bifacial modules has been developed.

To understand the performance of bifacial module, it is clearly very important to model the contribution of the back surface, depending on environmental conditions. The new model developed within this research accounts for the contribution of the ground-reflected irradiation on the back surface and for the diffuse component of irradiation. In contrast to ray-tracing modeling, this study aims to obtain a simple model (*Figure 44* and *Figure 45*) that can be run very fast but still with good results.

Summarizing the major outcomes of the research in three points:

- The reflectance of the dark room is needed for indoor testing, to normalize front and back efficiency
- For a single configuration, the simple modeling of irradiation is working well, the tuning of the two parameters should be further investigated
- The gain of bifacial modules with respect to monofacial modules is strongly dependent on the position of the Sun in the sky (*Figure 46*)

Further research will include:

- Modeling of the LCOE for bifacial modules: Design of optimal oriented and configured bifacial modules (AC/DC ratio, distribution of power curve during the day, self-consumption) for typical industrial cases and

- Extension of the existing modeling to other orientations and including the dependence of the height from the ground and the tilt angle

Figure 43: Test stand with different technologies, including bifacial modules at top left and top right

$$P(G_{bf}, T_{bom}) = \frac{P_{STC}}{1000} G_{bf} \cdot \left(1 + \frac{\delta}{100}(T_{bom} - T_{STC})\right) \cdot \left(1 + \sum_{i=1}^{4} a_i \cdot \log^i\left(\frac{G_{bf}}{1000}\right)\right)$$

$$G_{bf} = G_{eff} + k_0 \cdot GR_{back} + k_1 \cdot DHI$$

$$G_{eff} = E_b \cdot IAM_b + E_d \cdot IAM_{diff} + GR_{front} \cdot IAM_{gr}$$

$$GR_{back} = GHI \cdot Albedo \cdot \frac{1 - cos(\pi - tilt)}{2}$$
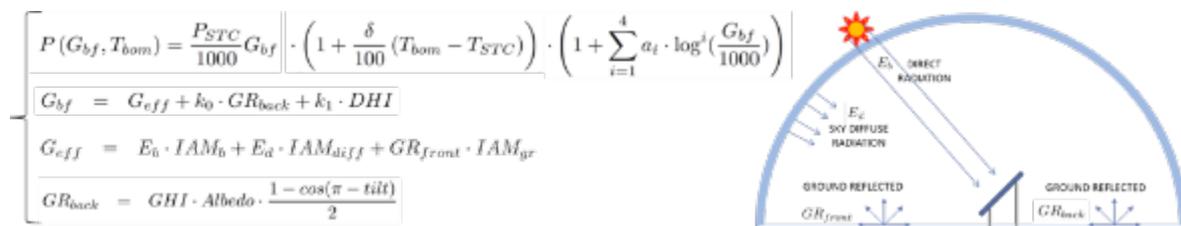
*Figure 44: Modeling of bifacial module performance*
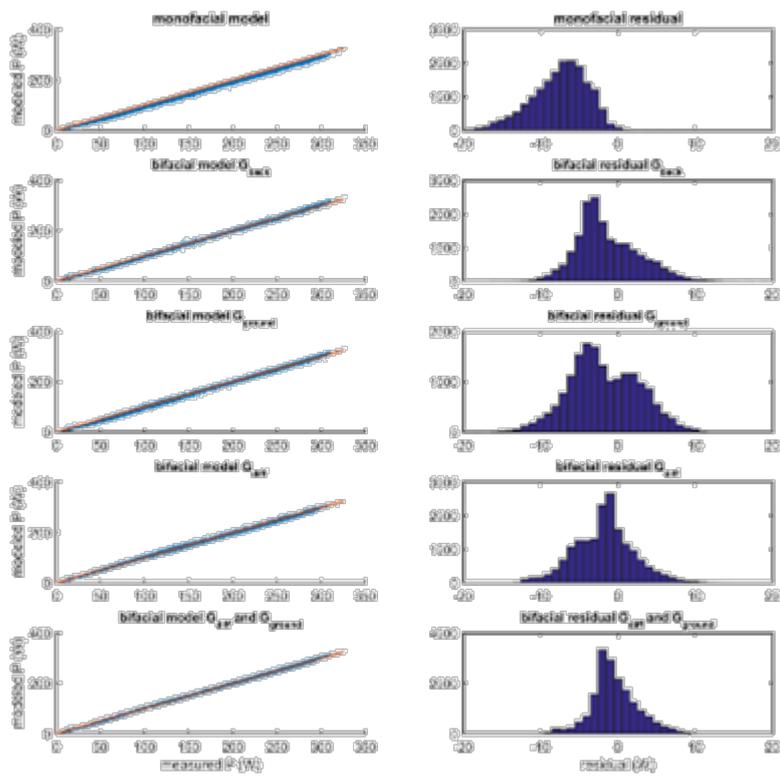
Figure 45: Five modeling approaches for the back-surface contribution
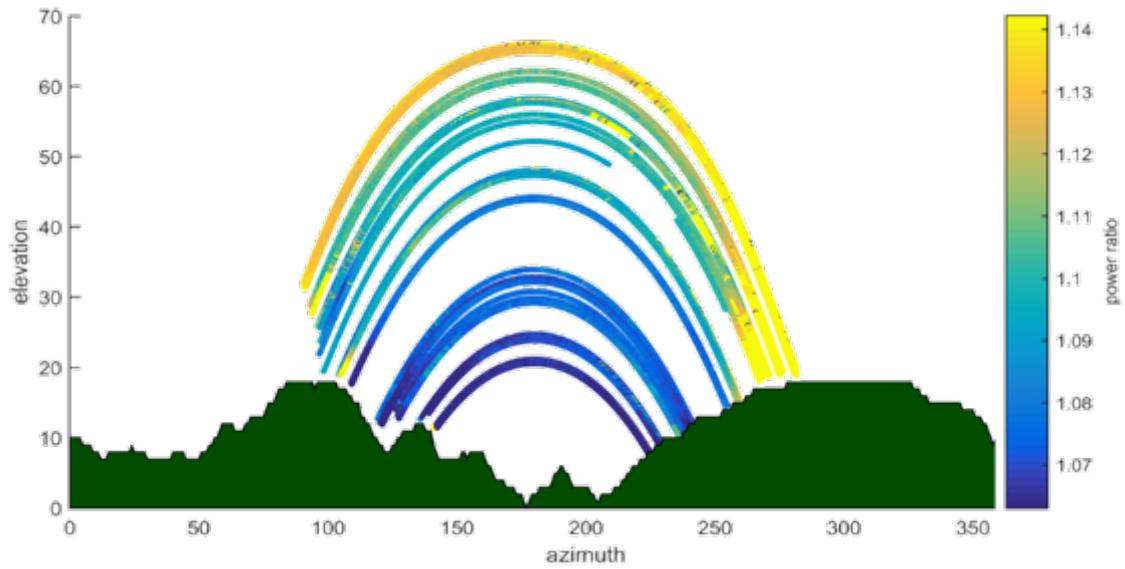

Figure 46: Gain of bifacial modules with respect to monofacial modules (power is normalized by front-surface efficiency)

3.4.3 Realistic yield expectations for bifacial PV systems – an assessment of announced, predicted and observed benefits

Christain Reise of Fraunhofer ISE presented data on realistic expectations of bifacial system performance. Bifacial PV modules are able to convert solar irradiation on both surfaces. Therefore, larger amounts of generated energy are expected – compared to standard (monofacial) modules. Today, bifacial modules are offered by an increasing number of manufacturers, and marketing material sometimes promises quite optimistic bifacial gains.

In fact, bifacial gains are not easy to estimate in advance, as they depend on the spatial distribution of the irradiance incident on the rear module surface. Several site and system specific conditions, such as albedo, module mounting geometry and mounting structure affect this irradiance. Currently, none of the widely utilized PV system simulation tools is able to predict the rear surface contribution of bifacial modules accurately.

Fraunhofer ISE's approach combines simulation tools from different fields of (solar) energy technology, the lighting and daylighting domain and the PV system simulation domain. In this way, we are able to deal with solar geometry, sky radiance distribution, scene geometry, surface properties, PV module properties and wiring scheme without any need for severe approximations in the model definition. The backward ray-tracing software "Radiance" (Berkeley Lab) is used for the optical part of our calculations. Radiance is based on physical relations and physical units of radiance (W/m^2s) and irradiance (W/m^2). The electrical simulations are covered by "Zenit" (Fraunhofer ISE), a detailed software model for all kinds of commercial PV power plants.

Both tools have been independently validated in several exercises. In this contribution, we report on two different validations of the combined procedure. The first set-up deals with the performance of a single bifacial module and uses short-term measurements from a roof test stand at Fraunhofer ISE. The second validation uses long-term performance values from a semi-commercial bifacial PV system monitored by Fraunhofer ISE.

Now, having this validated tool, bifacial gains are evaluated for a systematic list of system configurations, including single modules, single linear rows and arrays of rows of modules, while looking at flat, tilted and vertical mounting options above areas of different albedo. The presented work is based on studies prepared for several clients and on in-house research at Fraunhofer ISE for additional system configurations.

The configuration results are discussed with respect to their bifacial gain in relation to space requirements (expressed by ground cover ratios), mounting systems and overall system output. Reasonable ranges for expectable gains from bifacial modules and PV systems were given in the conclusion of the presentation. In summary, while results from single-module and small-system studies have generally shown the possibility of bifacial gains of between 15% to 25% and even higher, larger bifacial systems with multiple rows and self-shading exhibit smaller gains in the range of 5% to 15%.

3.4.4 Modeling of the Expected Yearly Power Yield on Building Façades in Urban Regions by Means of Ray Tracing

Hendrik Holst presented methods used to simulate annual PV production from BIPV building façades. While roof-top installations of photovoltaic systems are common these days, installations on building façades can provide great advantages, especially in urban regions, where the available façade area easily outnumbers the available area on roofs. Unfortunately, not all areas of a building façade are equally suitable for photovoltaic systems due to shading by neighboring buildings or environmental obstacles. This talk presented the results of optical ray-tracing simulations of the expected yearly power yield that is incident on building façades in urban regions and the hin-

terland. These simulations were executed during the study "Vertikale Solar Fassaden in Hannover" on the behalf of the region of Hannover for LiFE2050.

First, the authors created a light source representing the yearly average irradiation conditions for a location in northern Germany. Our input data are irradiance values, which were measured using a pair of photopyranometers at the Institute for Solar Energy Research (ISFH) in Hamelin, Germany over a period of 14 years (1992-2006). To allow for a realistic representation of the spectral and angular distribution of daylight, they create a daylight model [39-40]. The model includes the impact of the Sun's position as well as clouds on the specular and angular distribution. However, the scattering of light is treated independently of wavelength, therefore neglecting the impact of e.g. aerosols or seasonal changes in the atmospheric composition. As a result of this modeling approach, a partition of the celestial hemisphere is created, as shown in *Figure 47*(a). During the simulation, each interval of this partition contains its own spectral distribution.
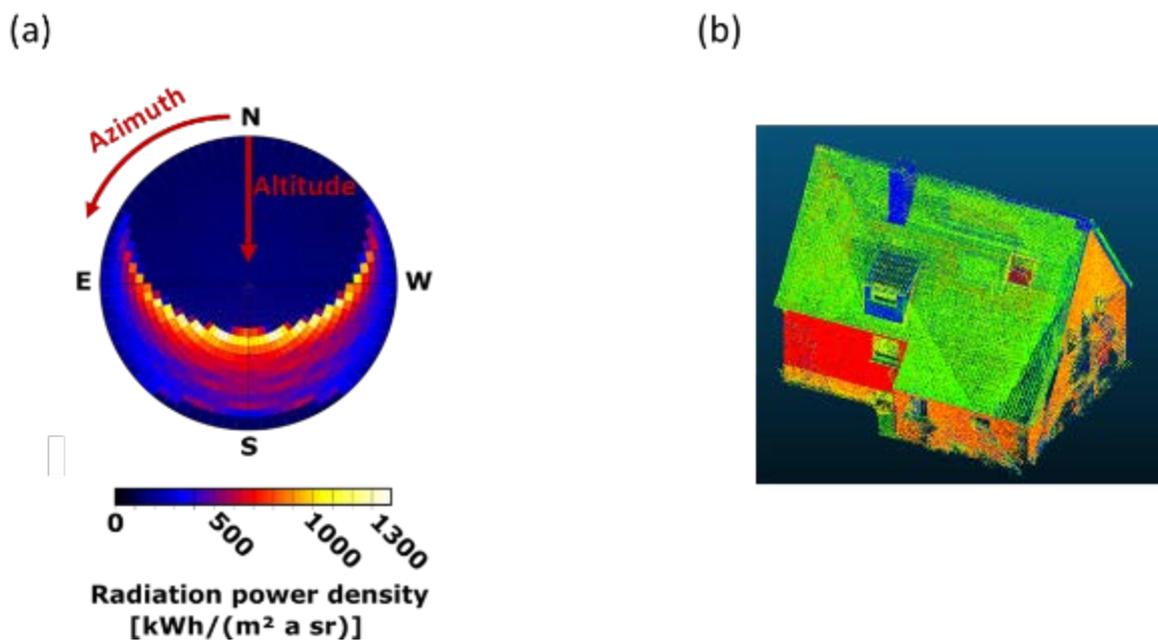

Figure 47: Utilizing our daylight modeling approach, the celestial hemisphere is partitioned into intervals of 5° azimuth and 5° altitude (a). Here, each interval is colored corresponding to the mean annual power density for the location of Hamelin, Germany. Within the simulation, each interval contains its own spectral distribution. A 3D model of buildings is created based upon a point cloud (b) obtained from a laser scan of real building facades.

Using their modular in-house ray-tracing framework DAIDALOS [41] the authors linked the light source with the building models to evaluate the expected yearly power yield that impinges on a building façade. Within the urban hinterland, buildings are typically free-standing houses as shown in *Figure 48*. Under optimum conditions, these buildings can receive yearly solar irradiation yields of up to 100 kWh/(m^2 year) on their south orientated façade, being only partially shaded by building extensions, e.g. the annex shown in *Figure 48*(a). This is significantly reduced as soon as neighboring buildings (b) or environmental obstacles (c) are considered; both provide severe shading and reduce the expected solar irradiation yields on the façade by up to 60%. The simulation times were kept acceptable in the range of 5 to 15 minutes per simulated building. Within the city, buildings typically have more than one floor, providing a large area of façade where photovoltaic (PV) systems could be installed. The reduction by other city buildings for irradiation of façades is again about 60% of the yield, however, as neighboring buildings are more common, a higher percentage of buildings suffers from this effect.
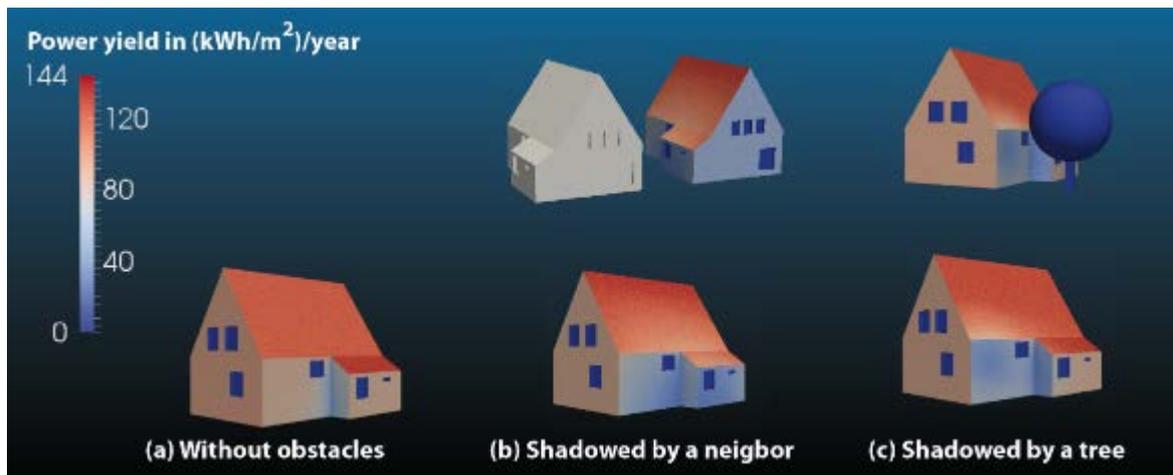
Figure 48: The expected yearly solar irradiation yield incident on the façade of a building in the urban hinterland. Under optimum conditions (a) a yearly irradiation yield of about 100 kWh/(m²year) is predicted for the south-facing side of the building. This is reduced by up to 60% as soon as obstacles like neighboring buildings (b) or environmental structures (c) are shading the façade.

To conclude, the utilization of a realistic daylight model in conjunction with measured façade data allows for a realistic simulation of the expected yearly solar irradiation yield on building facades, while the simulation times were kept acceptable in the range of 5 to 15 minutes per simulated building. The results show that PV modules on façades suffer solar irradiation yield reductions of more than 60% if shading from neighboring buildings occurs.

3.4.5   Multi-Year Study of Bifacial Energy Gains Under Various Field Conditions

Jose Castillo-Aguilella of Prism Solar presented multi-year results from deployed bifacial and monofacial reference systems in locations in New York and Arizona. The data showed that conventionally mounted ground bifacial systems have the potential to generate +17.5% additional energy compared to equally rated monofacial systems. The testing clearly demonstrated that additional increased bifacial energy gains can be realized when the surface reflectivity of the ground is optimized or when the bifacial modules are used in various vertical configurations. The data suggest that vertically mounted bifacial modules can outperform equally rated, traditionally mounted monofacial modules even under adverse ground reflectivity conditions. These field results were compared with Prism Solar's bifacial energy estimation methods.

The main goal of the talk was to present field data from bifacial modules under various installation conditions and show the potential of bifacial modules to increase the kW-h/kW that can be obtained from PV system. To this end, both the Prism Solar bifacial and monofacial references modules and their electrical characteristics were presented, which were chosen such that these characteristics would be as similar as possible. Since the bifacial energy gain, that is the energy being supplied by the rear of a bifacial module, cannot be decoupled directly, the bifacial gain was determined by the increased energy production of the bifacial modules over the monofacial reference modules mounted under the same conditions. Seven combinations of test conditions at two sites were presented, in which the module height, albedo, and the surface albedo were varied. An increase in the energy collected by the bifacial modules was reported as each of the variables under study increased; depending on the various site conditions, the bifacial gain was between 12.31% and 36.8%.

Additional independent data from the TÜV/GTM comparative test trial of energy yield was presented, which further supported the bifacial gains in the 10%-15% for non-optimized bifacial field conditions.

Test Conditions

Test Condition	Date Range	Tilt Angle θ(deg.)	Min Height Ratio h(m)	Albedo α(%)	Azimuth φ(deg)	BGE(%)
1	10/1/2012 to 4/28/2015	30	0.63	10%	180	17.7
2	5/10/2013 to 10/04/2013	30	0.76	77%	180	36.8
3	5/10/2013 to10/04/2013	30	0.2	77%	180	27.3
4	10/06/2013 to 01/14/2015	20	0.2	70%	180	18.41
5	10-31-2013 to 12/31/2014	20	0.2	68%	180	19.57
6	10-31-2013 to 12/31/2014	20	0.2	22%	180	12.31
7	1/1/2014 to 08/01/2015	10	0.3	75%	180	17.85

Figure 49: Bifacial test conditions presented in the presentations

Field data for vertically mounted bifacial and reference modules under various azimuth conditions was also presented with significant bifacial energy gains under all conditions.

	Vertical C6SP South (REF)	Vertical B245 South	Vertical C6SP East	Vertical B245 East	Vertical B245 -45
Average Annual Energy (kWh/kW)	1186	1555	854	1796	1737
Energy Gain Jan 2013 – Jan 2015		31.34%	-27.93%	51.55%	46.54%
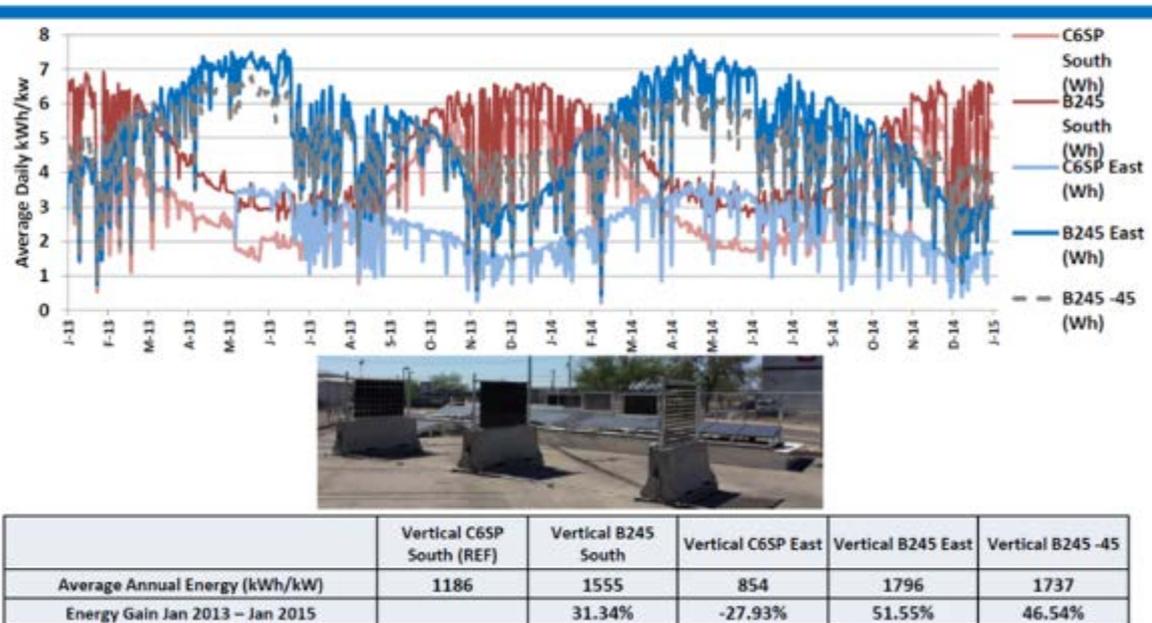
For an additional comparison, the 10 degree tilt monofacial reference system of Test Condition 7 produced an annual yield 1744 kWh/kW

Figure 50: Example comparing yields from monofacial (C6SP) and bifacial arrays (B245)

In addition, the authorhe discussed what should constitute the true STC and bifacial rating of a bifacial module, especially with concerns towards the safety aspect associated with the additional currents and power generated by the bifacial modules, since UL/IEC do not currently address these concerns. The shortcomings of not presenting the bifacial ratio or rear-surface STC parame-

63

ters were demonstrated with an example and how the lack of standard test conditions during flash testing (white/black background, collimation, etc.) can cause major differences in the STC rating of bifacial modules. In terms of safety, the TÜV/Prism BSTC rating was presented; this rating uses calculated front and rear surface performance parameters that take into account STC test conditions with 1000 W/m^2 on the front of the module and 300 W/m^2 on the rear of the module to account for the additional power of the bifacial module.

Future Work:

- More data sites and cooperation with entities such as Sandia National Labs and NREL to improve the available data sets and knowledge base.

The most important aspects of the talk:

- Bifacial modules can significantly increase the kWh/kW yield of PV systems when they are installed in conditions that take advantage of their inherent ability to generate more energy from the additional energy reaching the rear of the module.
- The bifacial gain of bifacial modules is influenced by three main variables: height, tilt, and surface albedo. The maximum bifacial gain is reached in applications such as vertical tilts with the module oriented in an east/west configuration, or in high tilt conditions (+20 degrees) with high surface albedo.
- The lack of current bifacial standards makes the comparison of one manufacturer with another difficult. In addition, the current standards (IEC, UL/ Q+) fail to take into account the additional current/power that could be produced by bifacial modules, which may prove to be a safety issue.

3.5 Session 5: PV Modeling Applications: Modeling Tool Updates

This session was chaired by Jeffrey Newmiller from DNV GL.

Table 8: List of presentations and speakers for Session 5

Title	Presenter	Affiliation	Country
Latest Features of PVsyst	Bruno Wittmer	PVsyst	Switzerland
pvSpot - PV Simulation Tool for Operational PV Projects	Tomas Cebecauer	GeoModel Solar s.r.o.	Slovakia
Recent and Planned Improvements to the System Advisor Model (SAM)	Aron P. Dobos	National Renewable Energy Laboratory	USA
Helioscope	Paul Gibbs	Folsom Labs	USA
Performance Modeling of PV Systems in a Virtual Environment	Angele Reinders	University of Twente	Netherlands

3.5.1 Latest Features of PVsyst

Bruno Wittman of PVsyst presented an overview of new and upcoming features of the PVsyst software for the simulation of PV installations.

The features covered have been introduced into PVsyst since May 2014, which was the date of the last presentation of this kind at a Sandia PVPMC workshop.

At the time of the presentation, the current version of PVsyst was 6.39.

New features in V 6.39

1.   Meteorological Input

The built-in meteorological database of PVsyst was updated from Meteonorm 6.1 to Meteonorm 7.1. This new version has a larger underlying set of measurements covering a longer time span. It also uses an improved interpolation algorithm to calculate the climate at locations between measurement stations.

A tool was added to PVsyst that allows direct comparison of yearly meteorological input files. This comparison is useful to analyze the climate over several years, evaluate different data sources or compare the climate at different sites. It can be used to estimate the parameters needed for a meaningful P50/P90 analysis.

Furthermore, there is now the possibility to generate hourly meteorological input files based on a clear sky model. This allows a very easy cross-check of monitoring data against the simulation results on cloudless days, without having to actually measure the irradiance.

2.   Extended System Definitions

It is now possible to make simulations of systems that make use of power optimizers. Models of SolarEdge, AMPT and TIGO are supported. The optimizers are associated to the module types in the simulation, and their specific configuration can be defined in detail.

Inverters with several MPPT inputs can now be configured in a more flexible way. Previously, the distribution of the total nominal inverter power was assumed to be equal among all inputs. It is now possible to attribute specific fractions of the total power to each individual MPPT input.

3.   3D Editor

Several improvements have been made to the editing of 3D scenes (figure 1).

In the 3D editor, it is now possible to define groups of objects and edit their common properties at once.

The ground objects describing the topology, which previously could only be imported from external files, can now be edited directly in PVsyst.

Arbitrary polygonal filling zones can be defined. A filling algorithm populates the zones with PV tables according to configurable rules.

Up to now, the importing of scenes from the Helios3D software only recovered the sensitive PV tables. Now, also other shading objects are included and are imported into the PVsyst scene.

4.   Batch Simulations

The list of parameters that can be changed in batch simulations increased significantly. Around 40 different parameters are available covering meteorological input, orientation of the panels, shading details, system configuration, module properties and different losses.

5.   Optimization Scans

A new tool was added to simplify the creation of parametric scans. It is a simplified batch mode that integrates all steps from the creation of the parameter ranges through the execution of the simulations and finishing with the visualization of the results (figure 2). The available simulation parameters for this tool are tilt angle and azimuth of the PV panels, and the result variables that can be visualized are incident irradiance, PV power and power injected into the grid. The lists of simulation parameters and result variables will be expanded in the future.

6.   Other Tools

A new tool has been added to make a simple calculation of the carbon dioxide balance. The calculation is based on life cycle emissions (LCE) and can either be used easily with reasonable default values, or configured in great detail by the user.

A dialog has been added with a tool to study the behavior of the Incident Angle Modifier (IAM). The IAM describes the angular changes of the reflectance of the module surface. Different models are proposed for this description, including fully customized IAM curves. The effect on direct, diffuse and albedo irradiance can be visualized and the impact on the annual yield of the production of each of these components is estimated.

Upcoming features for V6.40 and higher

1.   Text-based file format

The format of the PVsyst files describing the PV system, its components and the results will change from binary to a text-based format. The purpose of this change is to increase compatibility between different PVsyst versions.

2.   3D editor and shading calculation

The algorithm to compute shading losses will be revised to increase the speed of calculation. The 3D editor will be based on the OpenGL library to allow faster rendering and a more fluid work flow, especially on scenes that are large or have a lot of details.

It will be possible to add background pictures to the 3D editor. These can be either photographs of the terrain or technical drawings. A set of drawing tools will allow a quick creation of 3D objects on top of the pictures, making it easier to create the 3D scene.

3.   Battery-Based Systems

The simulation of battery-based system is being revised to harmonize it with the grid-connected approach in PVsyst. Tools are being added to visualize the behavior of the battery controller, in order to obtain the optimal working thresholds quickly.

Li-ion batteries and controllers will be included in the system definitions.

On the long term, the simulation of hybrid systems will be possible (grid-connected with local storage).
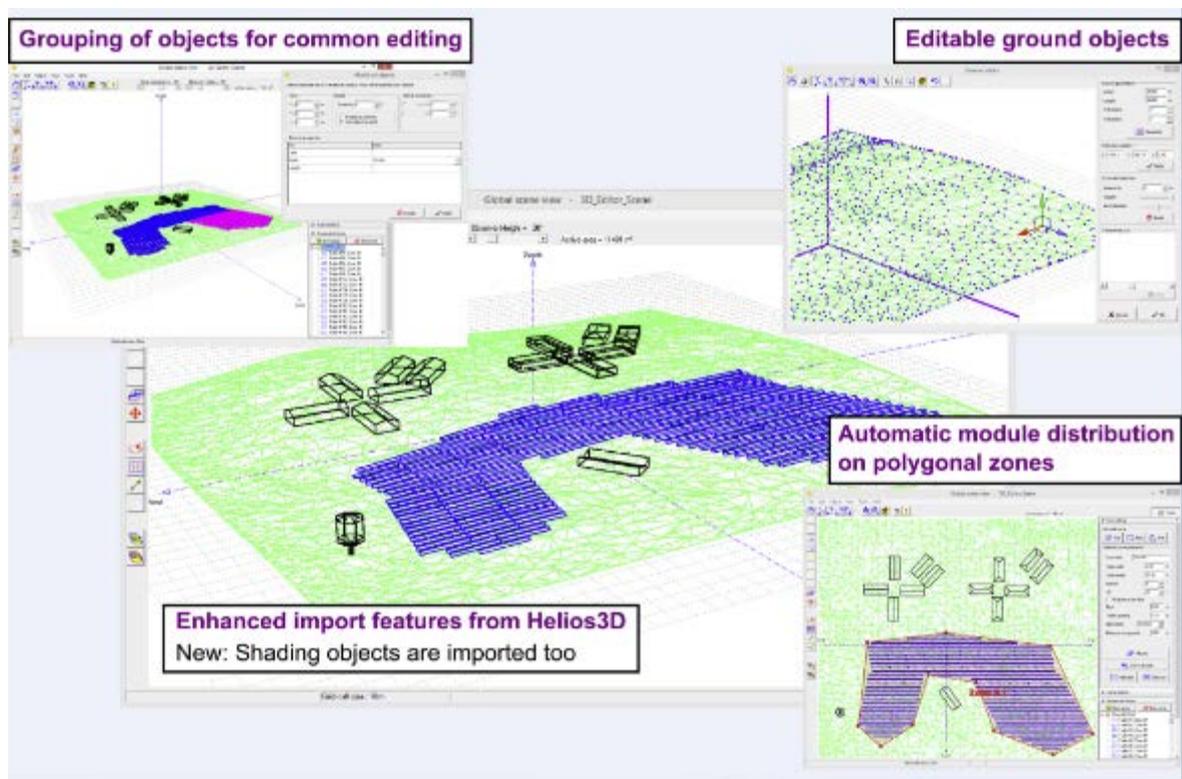

*Figure 51: New features for the PVsyst 3D editor Version 6.39.*
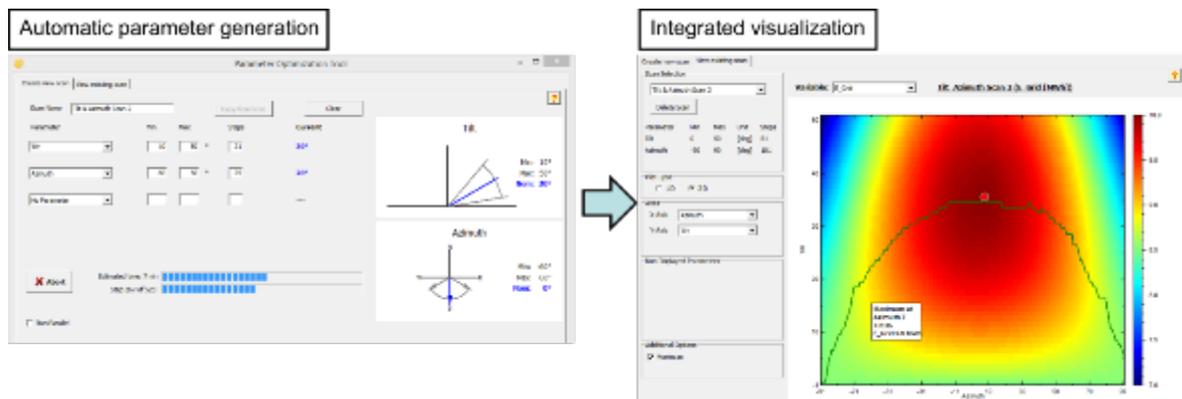
Figure 52: Tool for creating and visualizing parametric scans in PVsyst.

3.5.2   pvSpot - PV Simulation Tool for Operational PV Projects

Tomas Cebecauer of SolarGIS presented a new PV performance modeling capability called pvSpot that was developed by SolarGIS to offer PV performance estimates based on their worldwide irradiance database project, Solar GIS. pvSpot combines their irradiance data set with meteorological data, and terrain data to allow detailed performance models to be run and compared against monitoring data collected from operating systems. Systematic differences in these values may be useful in identifying performance issues with the system. The PV performance model approach is shown in *Figure 53*.
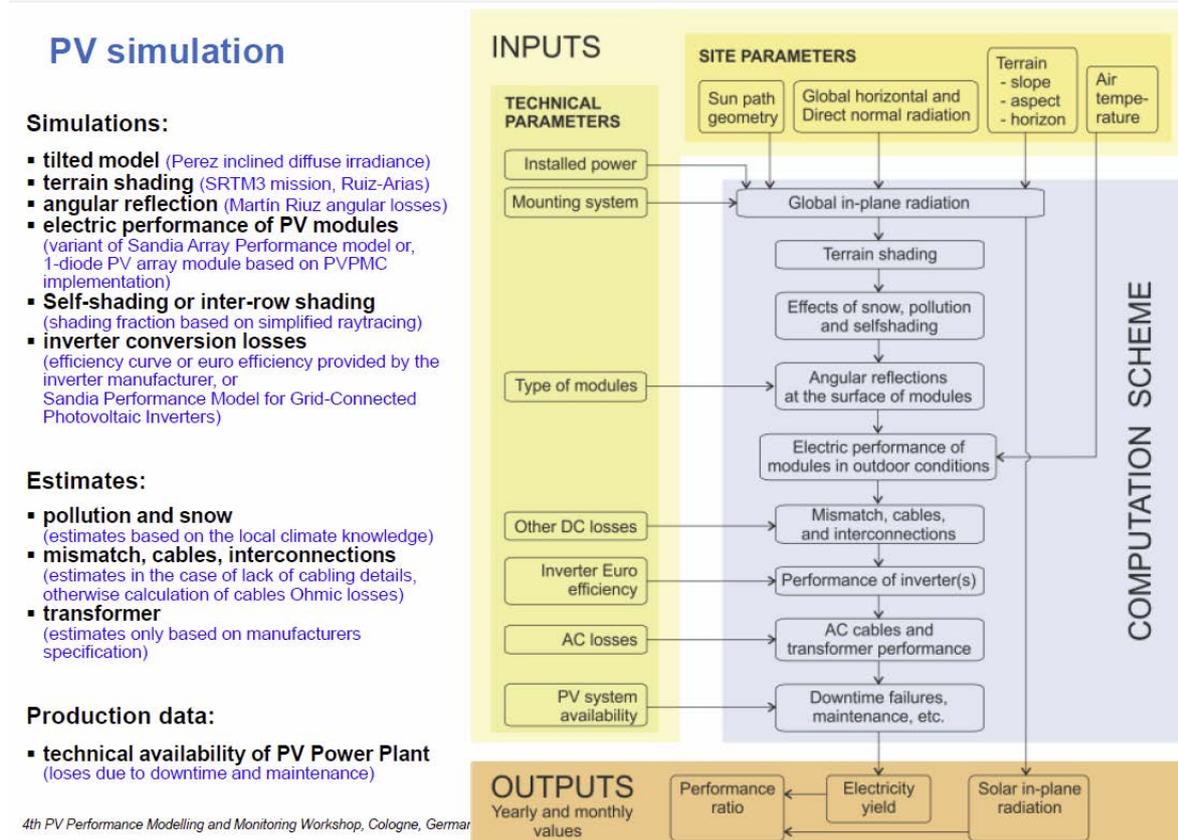

Figure 53: Details of pvSpot's approach to PV performance modeling.

This same modeling approach is also being applied to forecasting the future production of PV plants for more efficient participation in the energy market as well as longer-term forecasts that are used for financing of projects.

The model can be accessed as a web service or results can be automatically delivered via FTP and can be automated to track and forecast the performance of a fleet of as many as thousands of PV plants. *Figure 54* shows a comparison of a single plant's performance to the expected performance predicted by the model for 15-minute time intervals. It illustrates the model's very low bias error. The presentation also showed several examples of the model's ability to detect performance problems including snow losses, string failure, shading, and inverter clipping.
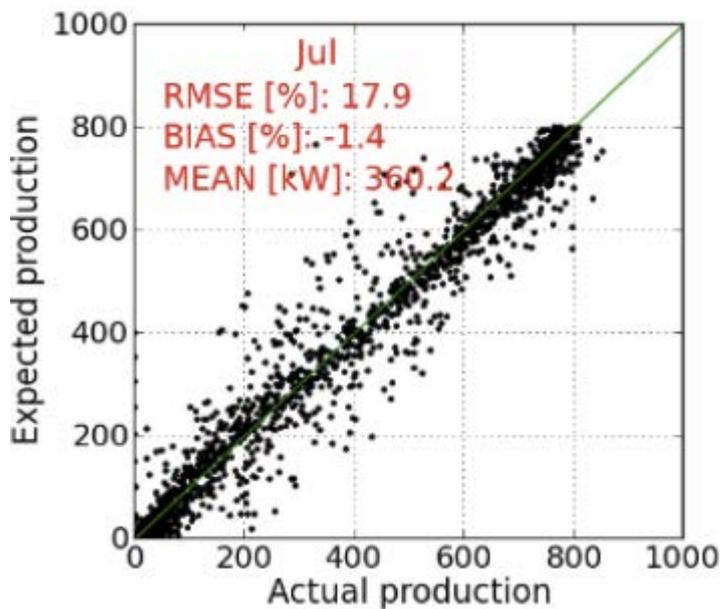
Figure 54: Comparison of expected production to measured production shows a low bias error.

3.5.3   Recent and Planned Improvements to the System Advisor Model (SAM)

Aron Dobos from NREL reviewed recent improvements to the System Advisor Model (SAM) for techno-economic modeling of photovoltaic systems.

The new battery model in SAM is designed for behind-the-meter analysis with complex utility tariff structures to help assess the economic viability of battery storage systems in conjunction with PV systems. The model considers lithium-ion and lead-acid technologies, and includes a flexible, manually scheduled dispatch controller along with several automatic dispatch strategies. In lifetime analysis mode, the effects of battery cycling and degradation are accounted for including the costs of replacement. The battery model was validated against laboratory measured test data for two different system types (*Figure 55*).

PV simulations can be run for up to 30 years at sub-hourly time steps. This new simulation mode allows detailed analysis of system DC/AC size ratio options with module degradation (*Figure 56*).

The new integrated 3D obstruction shading loss model in SAM is a simple-to-use tool for calculating beam and diffuse shading losses (*Figure 57*). The tool can underlay 2D aerial imagery, and future versions will include an option to estimate non-linear energy losses in systems with parallel-connected shaded strings.

Future work on SAM includes the addition of a plane-of-array (POA) irradiance input option for PV models, new automatic energy storage dispatch strategies, support for multiple input MPPT inverters, transient PV thermal models, 3D shade model validation and intercomparison, and improvements to spectral response models.
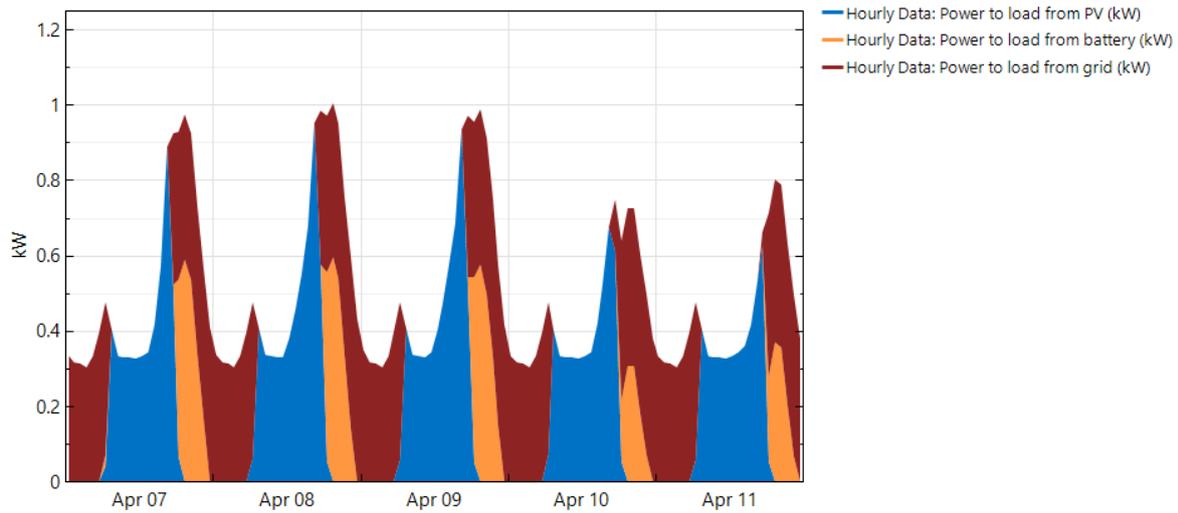
Figure 55: Example of modeling results from the System Advisor Model (SAM) for a PV-battery system.
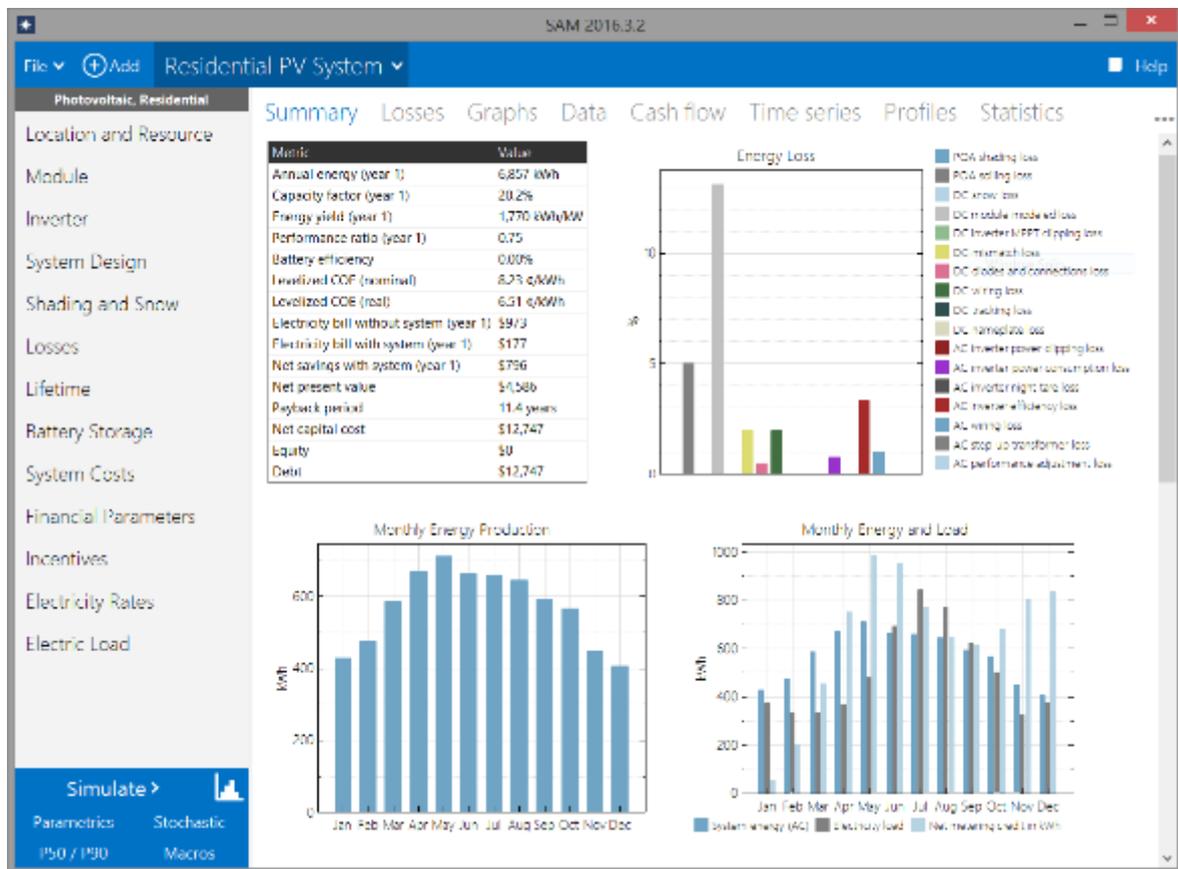

*Figure 56: The output summary screen in the System Advisor Model (SAM).*
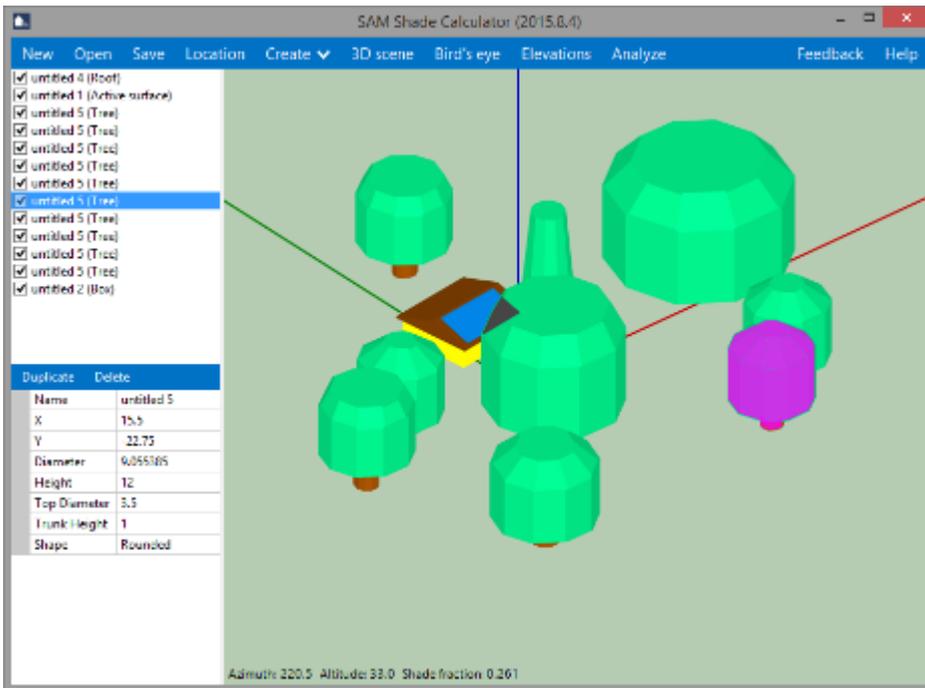
Figure 57: The 3-D interface Shade Calculator in the System Advisor Model (SAM).
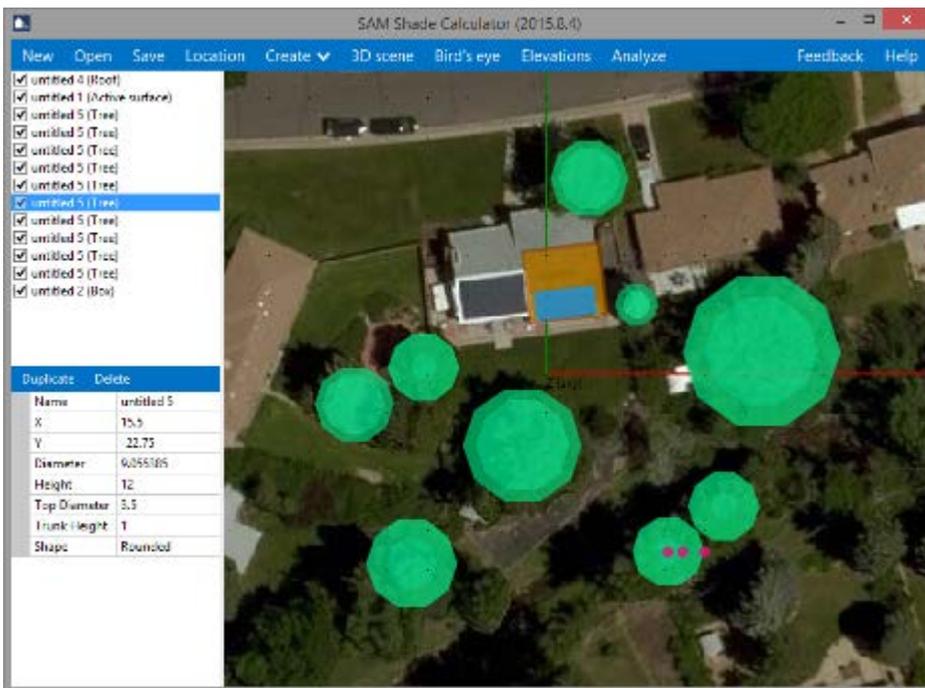
Figure 58: Shading objects can be drawn based on satellite imagery to capture the position of trees.

3.5.4   Helioscope

Paul Gibbs from Folsom Labs gave a live demonstration of the Helioscope modeling software. This web-hosted software aims to closely integrate the PV system design process with the optimization of PV performance. The user starts with a satellite image of the site and then uses basic drawing tools to layout the area of the PV array, which is located either on a rooftop or the ground. The next step is to choose the PV modules, type of racking, and inverters. Many important engineering constraints can be added to the design, such as minimum offsets from the roof edge. The program can also calculate and help avoid shading losses based on a Google

SketchUp model of the site. Once the components and constraints are defined, the software automatically designs the system, creating, on the fly, a bill of materials, including the wiring schedule. Inverters can be easily moved and stringing can be adjusted to minimize losses and wire needs. The performance model engine is compatible with PVsyst and accepts .PAN files as input.

3.5.5 Performance Modeling of PV Systems in a Virtual Environment

Angele Reinders presented on a new approach to PV performance modeling using virtual reality technologies. Virtual reality applications use sophisticated graphics engines to simulate a scene on a computer display. In order to make these simulations appear realistic to the human eye, they must be able to represent how light interacts with the objects in the scene. This talk describes research being done at the University of Twente to utilize such tools to simulate the light available to a PV system in a virtual environment. The advantage of using such a method is that it is easily capable of representing quite complex geometries while also being optimized for speed and mobile objects. For example, conventional PV performance models are not at all designed for use in designing mobile PV such as electric cars or boats. Because the virtual reality engines are designed to work with dynamic, high-speed video games, they can easily be used to simulate the light available to a mobile PV system.

The tool built at the University of Twente is called VR4PV and it is developed using Quest3D Virtual Reality Software. The simulations use rasterization techniques rather than ray tracing, which needs large computational resources. PV sub-models included in VR4PV include the solar position (Blanco-Muriel), solar decomposition (Orgill-Hollands), transposition (Liu-Jordan), PV temperature models (Skoplaki, Ross, King, and Veldhuis), and single-diode equivalent circuit models.

Validation of the model has been performed. Relative errors in the tilted irradiance was evaluated at four sites and shown to be <5%.

An example of a simulation was shown that considered four PV cells located on an outdoor solar light fixture with complex shade patterns (*Figure 59*). Each cell experiences a different irradiance pattern over time. The model was then run using inputs shown in *Figure 60*. The resulting output power from each cell is shown at the bottom of the figure. This type of simulation would be impossible using existing conventional PV simulations programs designed for ground or roof mounted systems.

As PV systems become less expensive and they are installed in more complex environments, new simulation tools will be needed to help support designs and deployments. VR4PV is an example of the type of tool that may prove very useful for such work.

POSITION OF SOLAR CELLS ON TOP OF STREET LIGHT
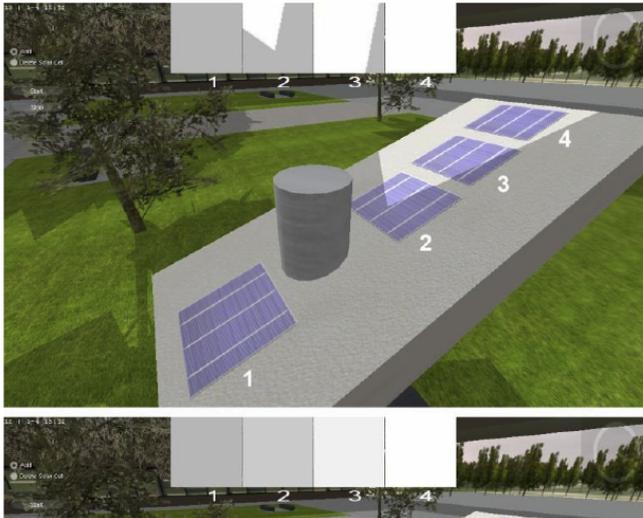
Three situations:

PV cell 1 is in full shadow:
It receives only the diffuse and ground reflected irradiance,

PV cell 2 and 3 are partly shaded:
They receive a fraction of the direct irradiance in addition to diffuse and ground reflected irradiance.

PV cell 4 is fully lit:
It receives the full amount of irradiance available.

UNIVERSITY OF TWENTE.

TUV-PVPerformanceModelling

Figure 59: Position of solar cells on a street light used as an example.

TIME SERIES, INPUT & OUTPUT DATA
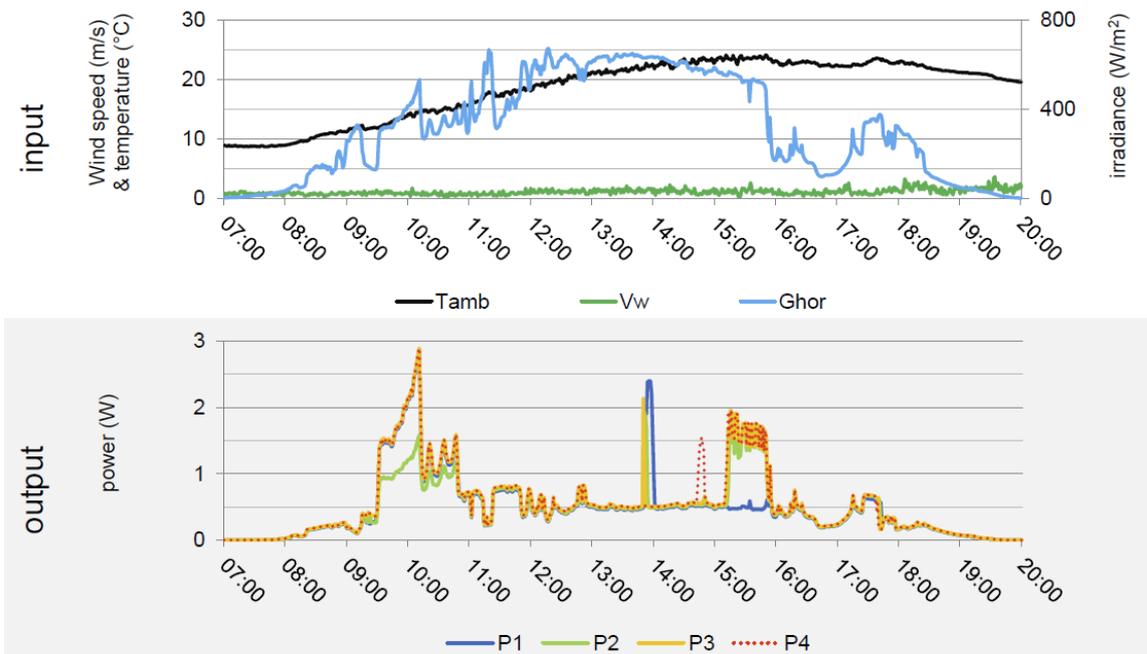
UNIVERSITY OF TWENTE.

TUV-PVPerformanceModelling

Figure 60: Examples of results of the VR4PV model.

3.6 Session 6: Field Monitoring and Validation of PV Performance Models

This session was chaired by Werner Knaupp from PV-plan.

Table 9: List of presentations and speakers for Session 6

Title	Presenter	Affiliation	Country
High-Speed Monitoring of Multiple Grid-Tied PV Array Configurations	Matthew Boyd	National Institute of Standards and Technology	USA
Field Data from Different Climates for the Validation of Module Performance Models	Gabi Friesen	SUPSI	Switzerland
Comparison and Validation of PV System and Irradiance Models	Benjamin Matthiss	Zentrum für Sonnenenergie- und Wasserstoff-Forschung Baden-Württemberg	Germany
The "best" PV Model Depends on the Reason for Modeling	Steve Ransome	SRCL UK	UK
Using Advanced PV and BoS Modeling and Algorithms to Optimize the Performance of Large Scale Utility Applications	Jürgen Sutterlueti	Gantner Instruments (GI)	Austria
System Performance and Degradation Analysis of Different PV Technologies	Yuzuru Ueda	Tokyo University of Science	Japan

3.6.1 High-Speed Monitoring of Multiple Grid-Tied PV Array Configurations

Matthew Boyd presented an overview of high-speed and resolution PV monitoring being done at the National Institute of Standards (NIST) in the USA. Three 73 kW to 271 kW mono-Si grid-connected arrays installed in different orientations and configurations have been monitored since August 2014 with research-grade instrumentation that is sampled and saved every 1 second. A local weather station was also constructed with redundant measurements of all main meteorological and solar components in addition to the full solar spectrum, UV, IR, and I-V traced reference modules in the same orientation as the arrays. Data availability for all systems is currently at 99 %. Cameras are also deployed at each array and weather station, taking high-resolution pictures of the shading and snow cover every 5 minutes as well as images of the full sky every 8 seconds.

Follow-up work underway includes setting up a public data portal for the data sets, and using the data sets to validate short-term irradiance forecasting and inverter/grid interaction models as well as examining dynamic electrical effects from irradiance enhancements and transitions. Modelers or analysts interested in using any of the data before the public data portal is available can contact Matthew Boyd at matthew.boyd@nist.gov .
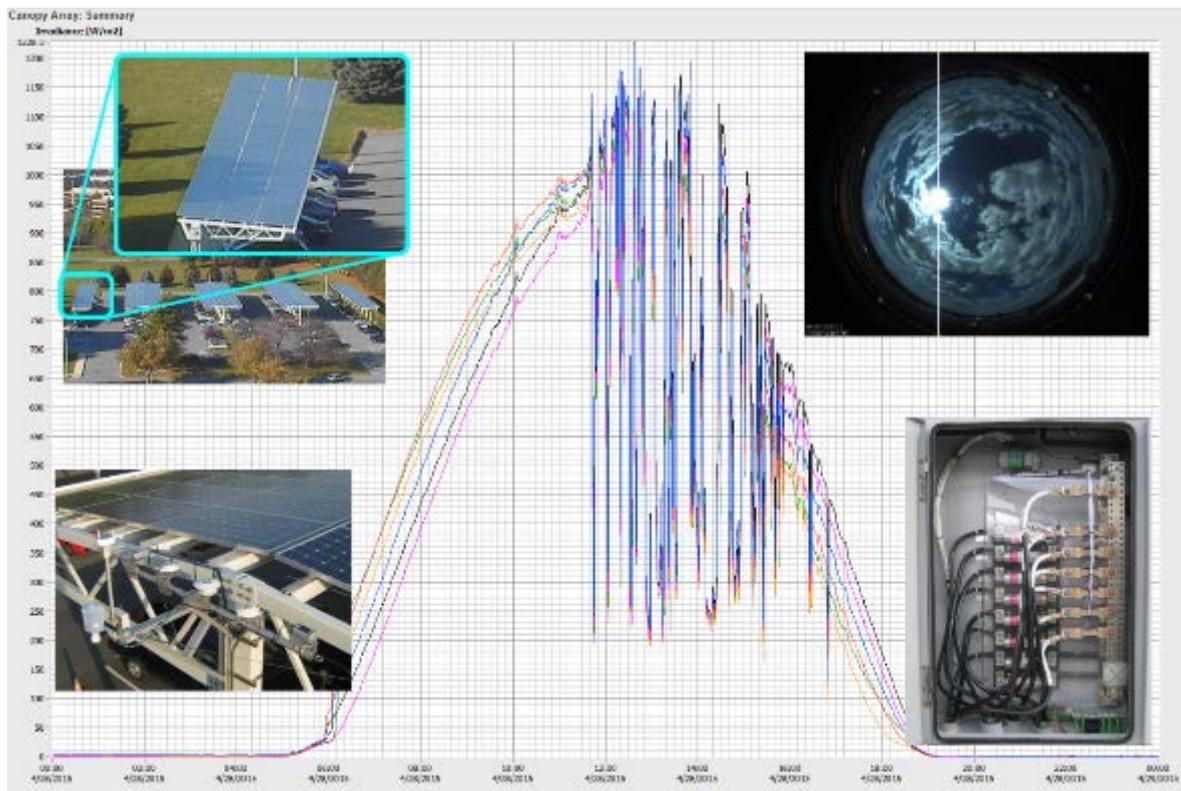
Figure 61: A selection of the irradiance and electrical measuring instruments and sample images from the cameras installed at one of the PV arrays.

Figure 62: The weather station, showing the various stationary and sun-tracking instruments as well as the I-V traced reference modules.

3.6.2 Field Data from Different Climates for the Validation of Module Performance Models

Gabi Friesen of SUPSI gave an overview of external parameters which can influence module energy yield measurements and benchmarking studies under different climates. At present, the lack of standardized guidelines for performing module yield measurements and analyses leads to misleading data being reported to the end user. It is emphasized that to better understand techno-

logical differences, reliable, accurate and comparable measurements are needed. Large discrepancies in measurement practice, uncertainty declarations and reporting can easily lead to contradictory results. For example, modules ranked as the 'best' in one study come out as 'average' in another study. Unfortunately, field data are often reported without any measurement uncertainty, which makes the validation of models very difficult. The presentation raised the question as to what is needed to improve the comparability of data measured outdoors under different climatic conditions (see *Figure 63*).
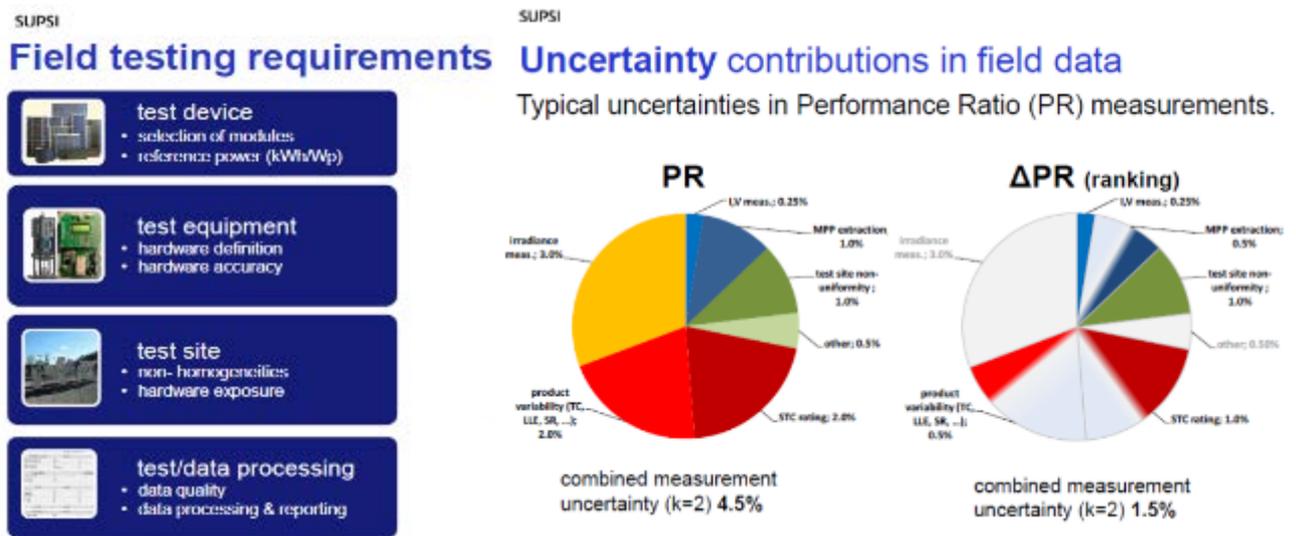

Figure 63: Field testing requirements and contributions to uncertainty in outdoor PV module yield measurements.

An example of typical measurement uncertainties for each contributing factor is given for absolute PR measurements and relative measurements (rankings) in *Figure 63*. The presentation discussed not only how the final measurement uncertainty is affected by the hardware specifications, but also by the experimental design, the sampling of modules, the test stand configuration, the operation and maintenance practice, the power rating, the irradiance measurement and last but not least, the data processing approach and quality control. In rankings, many of the uncertainties can be reduced or totally neglected. The harmonization of measurement practice helps in reducing the uncertainty contributions. Power rating remains however one of the major uncertainties and has to be approached separately.

At the end of the presentation, the IEA Task 13 activities of Subtask 3.2 were presented and potentially interested parties were invited to participate actively in the definition of a future guideline and the set-up of an open-source reference data base that aims to achieve better comparability of data with clear measurement uncertainties, better validation studies and models, and greater confidence in technology benchmarking. A standardized method for the assessment of field measurement uncertainties and the reporting of results is part of this.

3.6.3 Comparison and Validation of PV System and Irradiance Models

Benjamin Matthiss of the Zentrum für Sonnenenergie und Wasserstoff-Forschung in Baden-Württemberg presented on an approach for yield and self-consumption estimation in Germany. The goal was to estimate the total PV generation in Germany based on information about the installed capacity and location in combination with satellite irradiation data.

In a first step, various irradiation models were compared and validated to analyze their accuracy. Therefore, the tilted plane irradiation output of 6 irradiation models (Perez, Klucher, Hay&Davies, Isotrop, King, Reindl) were compared with high-resolution measurement data for a irradiation on a 40° tilted, south-facing plane. Best results were obtained with the Perez model for the given

location in southern Germany. Furthermore, the PV and inverter model were validated with measurement data.

For the ZIPcode-based Solar Power calculation (ZIPSoP), each zip code area was modeled with a distribution of PV system orientations. The size and approximate location of the PV system was known from a data base of the federal power grid agency. Unknown was the orientation, the PV technology and the inverter type.

The yearly yield was known for a subset of PV plants. This data was used to optimize various model parameters (temperature coefficient, orientation distribution, efficiency, scaling factor, minimum incident angle) with a non-linear optimization method, as shown in the figure below. The main problem with this approach was an overfitting with respect to the training year. Additionally, the input data set contained various obvious errors and inaccuracies which caused problems with the proper estimation of the coefficients. The accuracy reached with this version was between 1% and 10% depending on the training and validation year. With an older model of the ZIPSoP tool, accuracies between 3%-4% were achieved. The accuracy for a valid estimation of self-consumption in Germany should be constantly below 1%.

The three main points and results of the talk were:

- The Perez Model performed best in the irradiation model comparison for Germany.
- Yield estimation accuracy for Germany with the currently best performing yield prediction model is about 3%-4%.
- For the quality of the estimation, the input data has a key role.
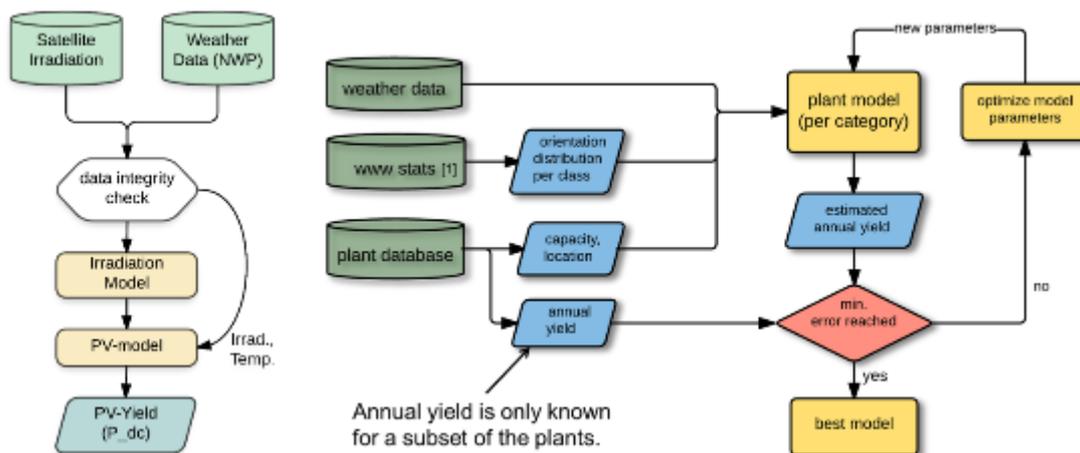
Figure 64: Data flow model showing how validation and comparison were performed.

3.6.4 The "best" PV Model Depends on the Reason for Modeling

Steve Ransome of SRCL presented an overview of criteria used to choose the best PV performance model for a given application. PV Performance Models should deliver unbiased performance understanding and prediction with best accuracy for optimized project assessments and reduced risk for the asset owner. Therefore, the appropriate model should be utilized.

The performance of PV modules/arrays in outdoor weather conditions can be modeled for many different reasons including:

1) Production process optimization (to minimize losses at Standard Test Conditions).
2) Determination of coefficients e.g. "PMAX vs. TMODULE", "Efficiency vs. Irradiance" etc.

3)   Overall system energy yield predictions vs. simulated weather inputs.
4)   Benchmarking different PV technologies (vs. differing PMAX, Low Light etc. coefficients).
5)   Validation of instantaneous performance (to prove the module or array is working correctly).
6)   Fault finding (if under-performing) – which model parameters are responsible?
7)   System output validation e.g. kWh/ year.
8)   Degradation rate vs. time, which parameters are degrading and at what rates?

PV Performance models derive their coefficients from IV curves taken at different irradiance values and temperatures, fitting either the entire IV curve (e.g. 1-Diode), a selection of points and gradients (e.g. Loss Factors Model and SAPM) or just modeling the maximum power point (e.g. Matrix method) as shown in *Figure 65*.
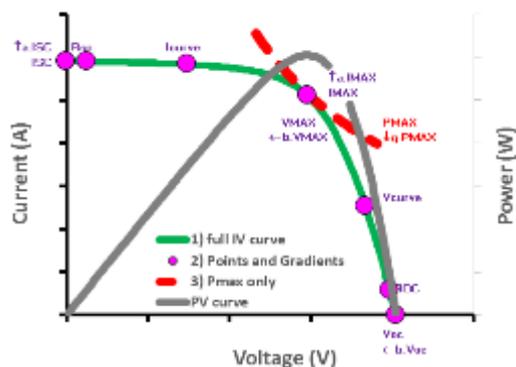

Figure 65: "Full IV curve" (green), Fitted "points and gradients" (purple), "PMAX only" (red), temperature coefficients (in brackets).

The ability of several models to differentiate the performance from IV curves over a range of technologies measured by NREL and Gantner Instruments outdoor was analyzed.

The performance of a good c-Si module, a good thin-film module and a poor thin-film module (with poor RSC and ROC) measured by NREL has been analyzed with all three models. The relative energy yield for Colorado is compared as an example.

These models are being studied as preparation for incorporation into Gantner Instruments' Web Portal software for optimum performance modeling and understanding. *Figure 66* shows how data from measured IV curves at different irradiance values and temperatures (top left) appear as parameters in a 1-diode model (top right), "points and gradients" model such as the loss factors model (LFM) (bottom right) and Matrix Method (bottom left).
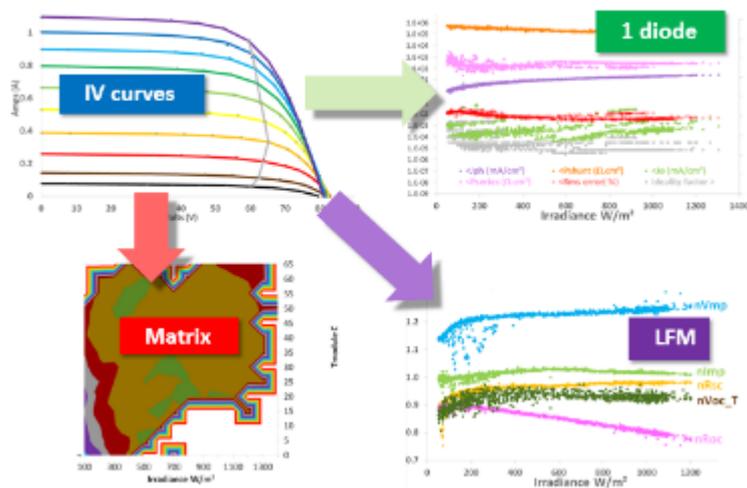
Figure 66: Processing sequence from IV curves vs. G_I and T_{MOD} to the three model types.

The 1-diode model was hard to analyze to identify the differences between the module types as some of the parameters were not monotonic (and thus were hard to fit), their magnitudes were very different (e.g. 10^{-10} to 10^{3}) and there was some difficulty in fitting (e.g. the ideality factor – green in *Figure 66* and saturation current – grey in *Figure 66* can compensate each other and appear as saw tooth shapes).

The Matrix method had less detail, as each temperature-irradiance bin was just an average of different values, so it was hard to see what the overall efficiency shape was, as it could have spikes due to bad data points. It could be characterized by the maximum efficiency and its location (irradiance and module temperature of the peak) plus the fall-off rates at both high (*I2.RSERIES) and low irradiance (LLEC) and also high temperature (Gamma).

The LFM was much easier to analyze for the differences in performance. An ideal module should have all parameters with a constant value with irradiance with values of 1 and this was near for the best c-Si module. The CdTe module shown in figure 2 is limited by poor nRoc (pink) at high irradiance which is caused by high RSERIES. The poorly performing thin-film module was shown to be limited also by poor nRSC at low irradiance which is due to a fall in RSHUNT.

Recommendations

- Normalize data to ensure easier understanding (e.g. ISC.MEAS/ISC.STC/GI).
- Use physically significant coefficients (e.g. nVOC: normalized VOC) rather than just polynomial fit coefficients.
- Ensure IV scans are of good quality, calibrated and plausible with little scatter.
- For simple kWh/kWp calculations at optimum sites the efficiency-only model may be enough.
- For a fast inline check, studying degradation/ non-optimum performance, a "points+gradients" model is better.
- For ultimate understanding, the full weighted point IV curves should be studied.

Needs for optimum modeling:

- To be able to differentiate "offsets between technologies" from "product variability within a type".
- To obtain curves that are easy to fit and recreate these curves with simple models.
- To quantify performance loss or optimization possible from sub-standard modules.

Future work

More data will be studied from the NREL dataset and also Gantner Instruments measurements. The models will be compared with a one-year data series residual analysis to show which ones fit modules under varying conditions best (i.e. not just a kWh/kWp measured vs. predicted value)

3.6.5 Using Advanced PV and BoS Modeling and Algorithms to Optimize the Performance of Large Scale Utility Applications

Jürgen Sutterlueti from Gantner Instruments presented an overview of their approach to PV system monitoring and introduced their Web-Portal application. When monitoring utility scale PV projects, some questions are commonly asked about the needs and benefits for investment. Here are some key requirements for understanding and implementation:

Performance understanding

In order to be able to do solid analysis and interpretation, one has to have a good understanding of PV performance.

Gantner Instruments has had its own research test site in Arizona, USA with data since 2010 as shown in *Figure 67*.

The aim of this Outdoor Test Facility (OTF) is to provide investors, EPCs and asset owners with recommendations on what parameters and methods they should be using to ensure their utility-scale solar projects achieve their full financial and energy yield potential.
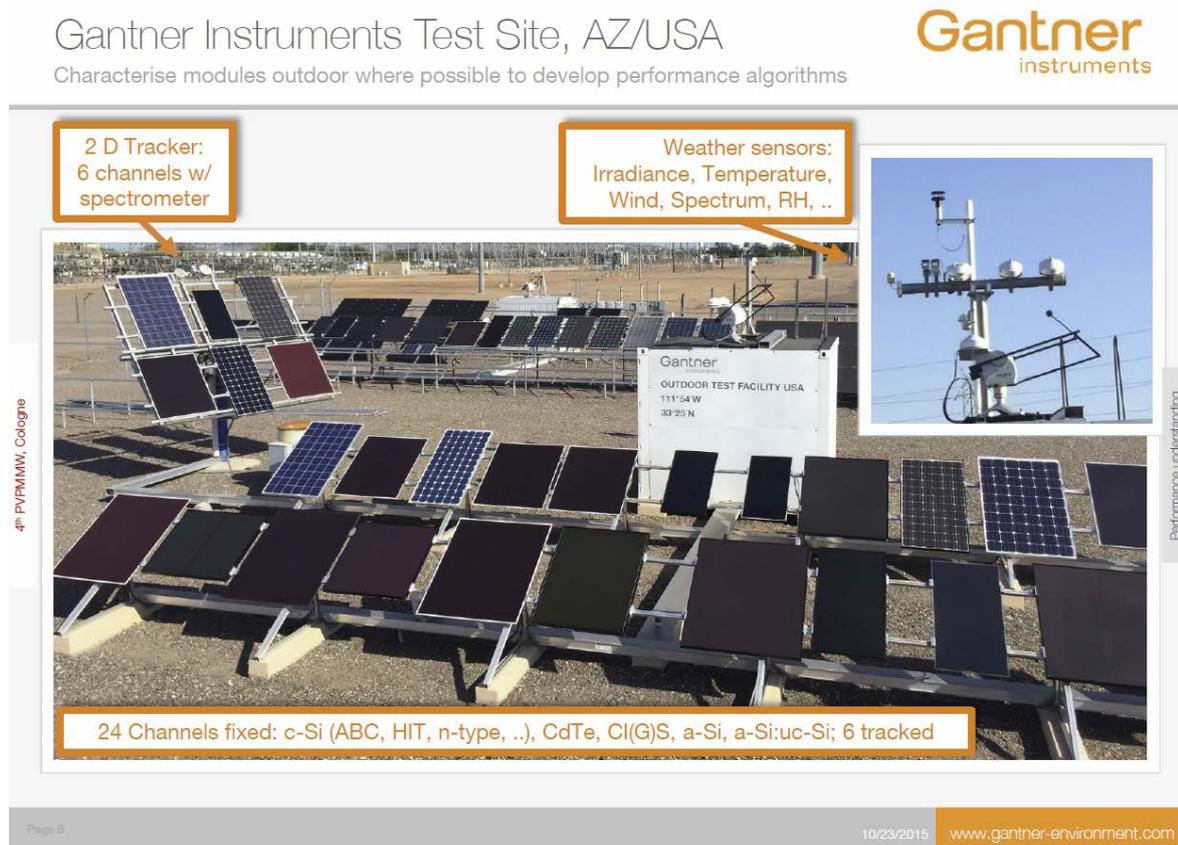

Figure 67: Gantner's OTF in Arizona, USA.

Key benefits from Gantner's OTF:

- PV Module performance track record since 2010
- Baseline for next generation of PV modeling and prediction of PV plant performance and monitoring
- Technology benchmark
- Bankability support for EPCs, Investors, Insurance
- Key for improved utility PV monitoring concepts
- Effective and repeatable analysis based on the LFM

Data from the OTF is analyzed with the LFM [21].

Data acquisition and handling

Market expectations: *Figure 68* illustrates a monitoring and control concept for cost-effective PV electricity generation and risk reduction used at Gantner Instruments.

Requirements:

- Multiple import data streams, standardized
- Fast check to validate all measurements sensors, inverters, strings etc. – first as plausible, then good.
- Automated checks (real time), constant performance
- Regular sanity checks
- PV power plant structure to identify losses
- Normalization of data sets for quick comparisons
- Good sanity check for all components (easier with normalized data)
- Redundant measurements of weather and electrical variables.
- Availability monitoring: For each component (inverter, system, sub-system, production batch, …) to support preventive maintenance strategies
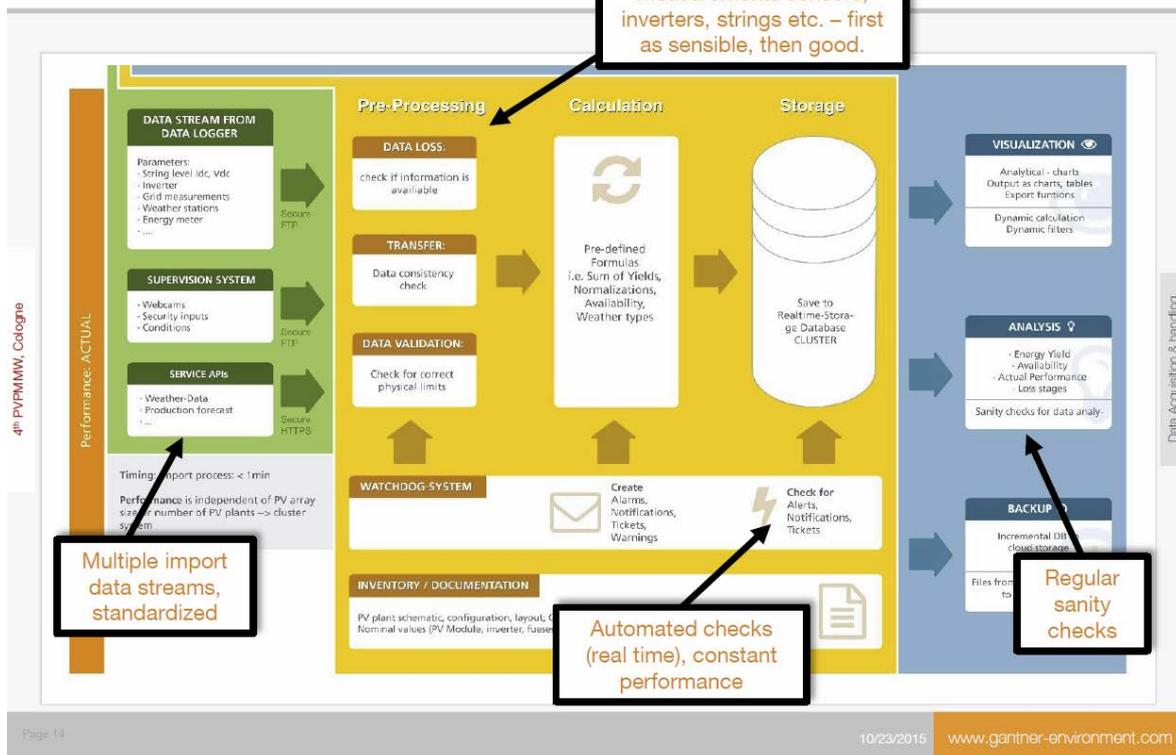
Figure 68: Process overview of the Gantner web portal.

Data Analysis

When it comes to data analysis, data consistency is key. Thus, the following steps are recommended:

- Perform real-time sanity checks for physically meaningful values
- Make uptime tracking / availability audits
- Provide overall sensor reviews for measurement validity
- Monitor irradiation sensor drift

Parameters and graphs should be shown with these aims:

1) Simplification of what is relevant in terms of $ (money) and kWh (energy)
2) Determining potential short, midterm impact,
3) Preventive maintenance

Performance prediction and optimization

Set up algorithms to predict instantaneous PV and BoS performance for measurement validity and energy yield predictions. The basic version already gives very useful results for system cross-checking and trend detection (soiling alerts, shading, …) which is very helpful for real-time error detection.

Investment vs. Benefit of Monitoring: Impact on system cost (CAPEX), O&M (OPEX) and LCoE

The case study shown in *Figure 69* is a system in Europe (10MWp AC) which includes a monitoring cost share of the system price:

~ 1.4% (0.013€/Wp, EU); this CAPEX of installed monitoring gives direct control of 17% of the LCoE Cost (O&M cost) and controls the performance of the inverter, cables and connections, …

The comparison with no monitoring vs. a PV power plant with monitoring shows that the monitored plant can deliver a 7.3% better energy yield, resulting in a 4.5% better LCoE.
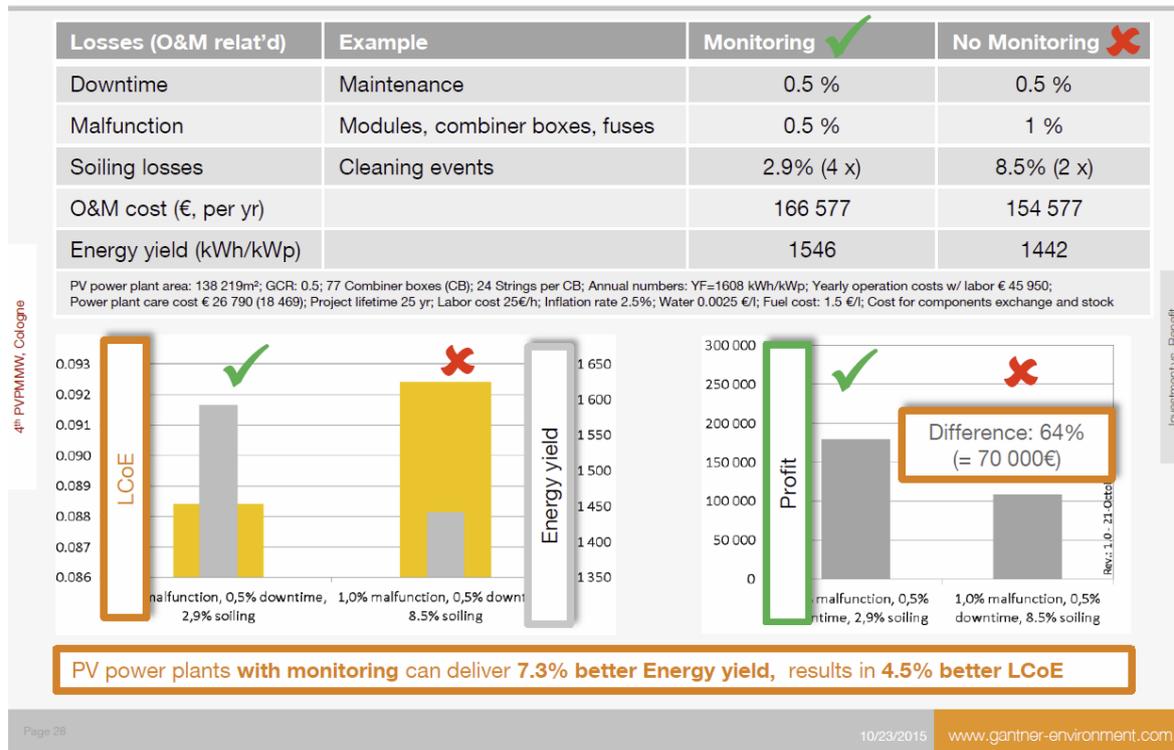

Figure 69: O&M cost. Energy yield and LCoE comparison of 2 monitoring scenarios: Monitoring vs. no monitoring.

Summary

Cost-effective monitoring solutions can:

- Reflect financial KPIs (performance guarantees, allowed maintenance, integrate simulations)
- Allow "real-time" data processing for availability, alarms, warnings
- Automate performance analysis and characterization in terms of kWh and $ (loss separation, sensitivity to irradiation, weather, cleaning, …)
- Implement preventive maintenance strategies

Advanced monitoring algorithms lead to:

- Providing investors with reliable information about O&M, track record & plant performance, control
- Separating and identifying losses where "actual vs. target" differs
- Optimizing plant performance during lifetime
- Reducing LCoE based on advanced monitoring design (characteristic trends, Loss Factor Model)
- Reducing risk for investors & Independent Power Producers (IPPs)

More details and references can be found at www.gantner-webportal.com.

3.6.6   System Performance and Degradation Analysis of Different PV Technologies

The presentation by Yuzuru Ueda from the Tokyo University of Science focused on two topics: (1) a performance modeling approach (the sophisticated verification (SV) method) that quantifies energy losses in a PV system and (2) a review of performance monitoring and degradation data collected as part of two long-term PV field deployment projects in Japan and the U.S.

The SV method focuses on defining a series of loss factors that are applied in series to the available insolation incident on the area of the PV array in order to calculate the AC electricity that is generated by the system. *Figure 70* shows the factors considered in the model and displays several of the equations used to determine the factors.

The second part of the presentation focused on long-term monitoring results from two PV field sites in Japan (*Figure 71*) and the U.S. (*Figure 72*). Performance ratios and effective peak power were used to compare performance levels over time at the Hokuto site (*Figure 73*). Effective peak power is the power measured at 1 000 W/m^2 corrected for temperature, spectrum, reflection, and DC wiring losses. Data influenced by shading, MPP mismatch and periods with high irradiance variability are filtered out. Effective peak power is used to estimate degradation rates. Results show degradation rates of -0.57%/year for sc-Si and -0.50%/year for mc-Si modules at the Hokuto site. The data set from the Los Alamos site, which begins in 2012, is not yet long enough to show clear degradation trends.
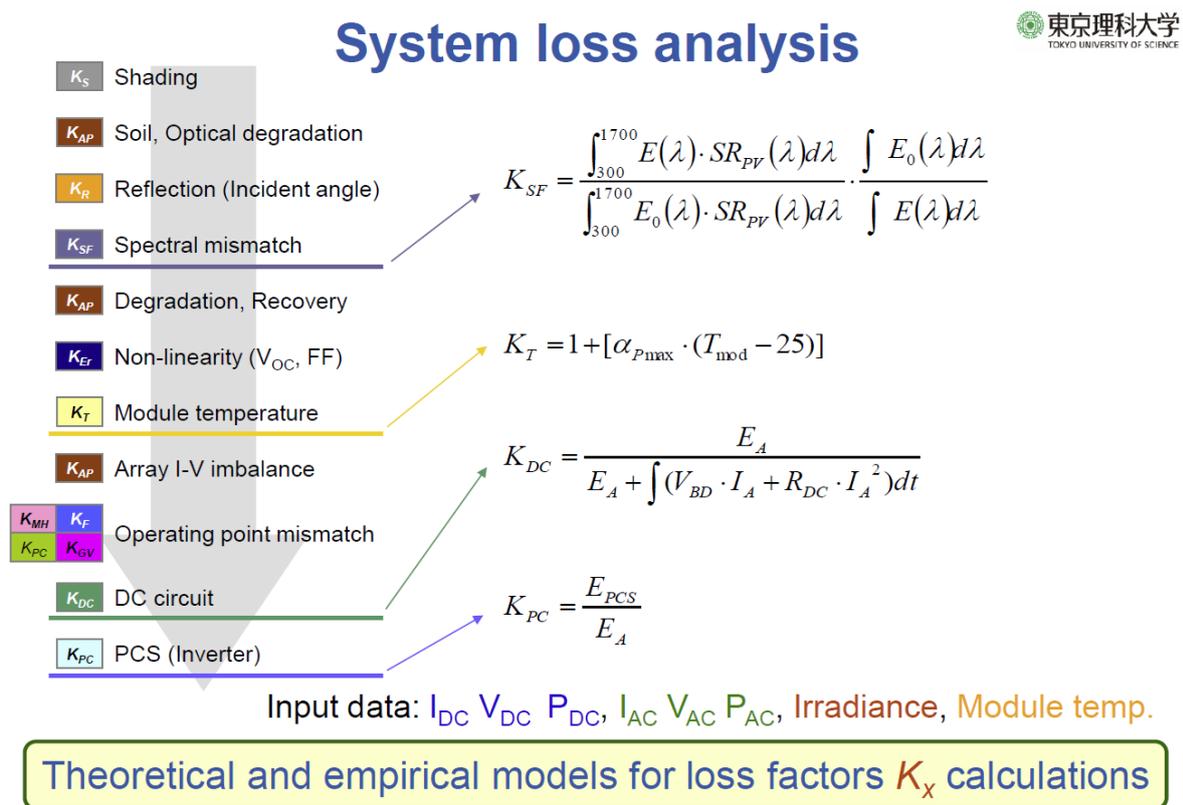
Figure 70: Diagram showing the loss factors considered by the SV method. The equations for several of the factors are shown.

84

Figure 71: The Hokuto testing site in Japan hosts modules from 26 different manufacturers.

*Figure 72: The Los Alamos testing site in New Mexico, USA.*
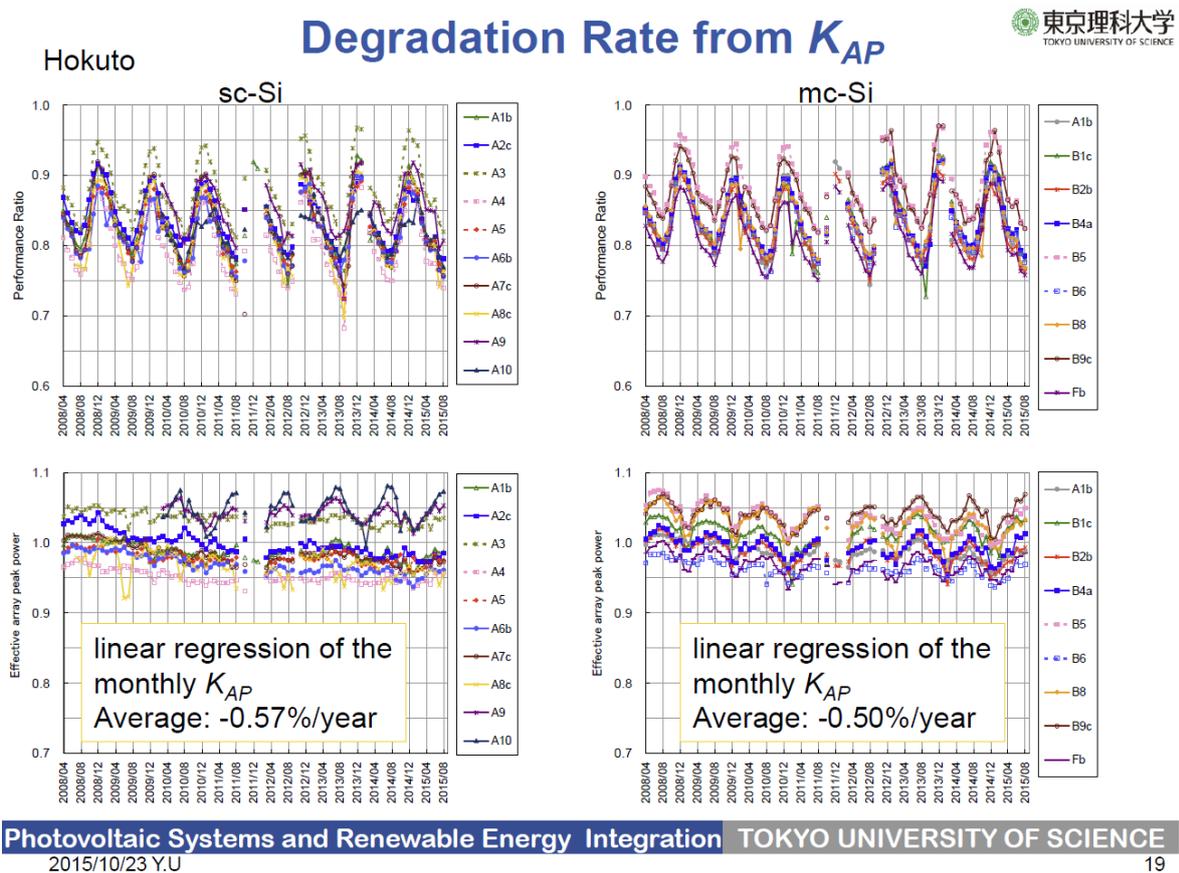
Figure 73: Summary of field-measured degradation of single crystalline (sc-Si) and multicrystalline Si (mc-Si) modules from the Hokuto site since 2008.

3.7 Poster Session

Each poster presenter had an opportunity to provide a 1-minute, 1-slide oral introduction to their poster in front of the entire workshop audience just prior to the general poster session. This format worked well to provide the audience with a general idea of the poster topics and the important results contained therein. The full list of posters is documented below in Table 10. Poster presenters were also offered the opportunity to submit a written summary of their poster to be included in this report. Only one of the presenters submitted a summary, which is included below. Readers interested in learning more about any of the posters are encouraged to contact the authors directly.

Table 10: List of poster presentations

#	Title	Authors	Affiliation	Country
P1	Investigating the Impact of Clouds on Solar Energy Production – Uncertainties for Yield Predictions by Using Satellite Data for Clouds	Ina Neher, Evandro Dresch, Khurshid Hasan, Bernd Evers-Dietze, Dieter Franke and Stefanie K. Meilinger	Hochschule Bonn-Rhein-Sieg	Germany
P2	Simulation of PV Power Output by Implementation of a Spectrally Dependent Photocurrent in the Double Diode Model	Evandro Dresch	Hochschule Bonn-Rhein-Sieg	Germany
P3	Spectral Analysis of Various Thin Film Modules Using High Precision Spectral Response Data and Solar Spectral Irradiance Data	Markus Schweiger, Ulrike Jahn, Werner Herrmann	TÜV Rheinland, Solar Energy	Germany
P4	Numerical Modeling of c-Si PV Modules by Coupling the Semiconductor with the Thermal Conduction, Convection and Radiation Equations	Malte Vogt	Institut für Solarenergieforschung GmbH	Germany
P5	Soiling and Self-Cleaning of PV Modules in Different Climates	Werner Herrmann	TÜV Rheinland, Solar Energy	Germany
P6	Bifacial Performance Field Data Analysis	Mike Francis, Teresa Zhang, Brandon Tracey	SunEdison	USA
P7	A New Software for PV Plant Modeling	Gianluca Corbellini	SUPSI	Switzerland
P8	Progress and Challenges of CPV Modeling	Tobias Gerstmaier, T. Zech, M. Röttger, C. Braun, A. Gombert	Soitec Solar GmbH	Germany
P9	Uncertainty and Sensitivity Analysis for Photovoltaic System Models	Clifford Hansen, Curtis Martin	Sandia National Laboratories	USA
P10	Data Requirements for Calibration of Photovoltaic System Models	Clifford Hansen, Kathrine Klise	Sandia National Laboratories	USA
P11	Comparing Measured Performance Data of PV Installations to Simulation Results	Bruno Wittmer	PVsyst	Switzerland
P12	Field Monitoring and Validation of PV Performance Models (tbc)	Frank Vignola, Fotis Mavromatakis	University of Oregon	USA
P13	Big-data Analytics of Real-world I-V, Pmp Time Series to Validate Models and Extract Mechanistic Insights to Lifetime Performance	Roger French, Tim Peshek	Case Western Reserve University	USA
P14	Effect of time-averaging on PV production estimates on systems with high DC to AC ratios	William Hobbs	Southern Company	USA

3.7.1 Big-data Analytics of Real-world I-V, Pmp Time Series to Validate Models and Extract Mechanistic Insights to Lifetime Performance

Authors: Roger H. French, Laura S. Bruckman, Timothy J. Peshek, Yang Hu, Nicholas R. Wheeler

Solar Durability and Lifetime Extension Research Center, Case Western Reserve University,

Cleveland, Ohio, USA.

The study of real materials systems undergoing real-world operation and degradation processes is a challenging problem in the area of mesoscale science. Our research focus is on the temporal evolution of electrical properties and behavior of photovoltaic energy materials, particularly crystalline silicon solar cells that contain a series of distinct and critically important interfaces, which play an essential role in the performance and degradation of PV modules over their lifetime. The central problem is that of incorporating real-world performance data, which is massive but informationally sparse (Pmp versus time for example), with laboratory-based data from confirmatory experiments, which can be informationally dense but suffers from low statistics. In the interfaces and chemical interactions among the screen-printed silver metallization grid on the front of the solar cells, which is applied as a paste consisting of silver nanoparticles, glass frit, various organic binders and subsequently fired, and corrosion from acetic acid produced in the ethylene vinyl acetate encapsulant in front of the c-Si cell, there are myriad interfaces and potentially non-linear overall responses. These responses can be studied microscopically in the laboratory but the relationship to real performance must be inferred.

Modeling the underlying performance and performance degradation of screen-printed silver contacts by a single diode and series and parallel resistances will likely miss the complexity of behavior because the diode model lacks the essential parameters for this complex materials system. The series resistance in particular comprises several contributors and is not unrelated to the shunt resistance or recombination current in real devices. However, by studying the massive real-world data streams themselves, new insights that are typically not modeled from physics-based models can provide new insights into complex behavior.

The behavior of the solar cells is determined by the IV curve shape, regardless of its relationship to the diode models. These shapes form the basis of what can be used for automated feature selection among huge data sets of IV curves. Further, there exist "change points", which are points in the IV curve where bypass diodes become forward-biased and turn on due to module heterogeneities. These heterogeneities can include cell cracking and hot spots for example and are more closely linked to the mesoscale degradation processes affecting localized areas.

Building upon the diode modeling, some researchers have utilized Simulation Programs with Integrated Circuit Emphasis (SPICE) to simulate behavior of the equivalent circuits. We invoked this type of modeling to rapidly step through simulation scenarios and test hypotheses related to heterogeneity to link real-world and laboratory datasets (e.g., Figure 74). Our models started with a single-diode model for each cell, with the ability to vary series and shunt resistors, diode parameters as well as illumination. This simple model was used to test the behavior of bypass diodes under forward and reverse bias conditions and simulate a large matrix of conditions related to changing the series and shunt resistors, photo-generated current, and any diode parameter we choose.

We simulated the performance of a 4-cell mini-module with high heterogeneity and then tested that simulation experimentally. The data support the interpretation that an increase in the series resistance, which itself comprises many factors, is linked to the shunt resistance in that the resistance cannot support fully the available current and more photo-generated carriers are recom-

bining even if the characteristic scattering time is unchanged in the bulk. The mini-module fabricated with the damaged cell showed bypass diode turn-on under uniform irradiance, due to the resistances of the cells being strongly non-uniform. This observation demonstrates the potential for real-world modules to show bypassing even under uniform illumination if a localized cell or interconnect becomes highly resistive. A scenario in which this observable may be found is localized hot spots, where positive thermal feedback occurs because the photo-generated carriers of a solar cell are thought of as a current source. At the SDLE SunFarm, over 1.5 million IV curves over 500 days have been acquired at an average interval of 10 minutes. Using automated analytics, we can statistically model the behavior of PV modules and strings in detail. The signatures of interest in the data were guided initially by the SPICE development, but machine learning techniques can explore the data in a supervised manner, and then group the data by recognizable features in the IV data sets.

A pairwise scatter and correlation matrix is a useful method for visualizing the lessons from these large amounts of data (e.g.,). As an example, *Figure 75* shows several variables including the currents at the intercept of each change point. Variables and their histograms are shown along the matrix diagonal. Below the diagonal are the pairwise scatter plots of the variables, and the corresponding pairwise linear correlation coefficient is shown above the diagonal. This visualization method allows for quick processing of big data.

Big data analytics is becoming a commonplace term today, and one that is being invoked in materials science. We have demonstrated the feasibility and novelty of studying large IV data sets using machine learning techniques, and those guided by mesoscopic insights into system-heterogeneous behavior. The IV curves form a linkage to the laboratory where hypothetical degradation scenarios can be verified and a more conventional materials characterization process can be undertaken to identify and understand the behavior and dynamics of mechanisms. These linkages then allow for an unbiased approach to mesoscale science applied rigorously to the vast scale of real-world photovoltaic deployment.
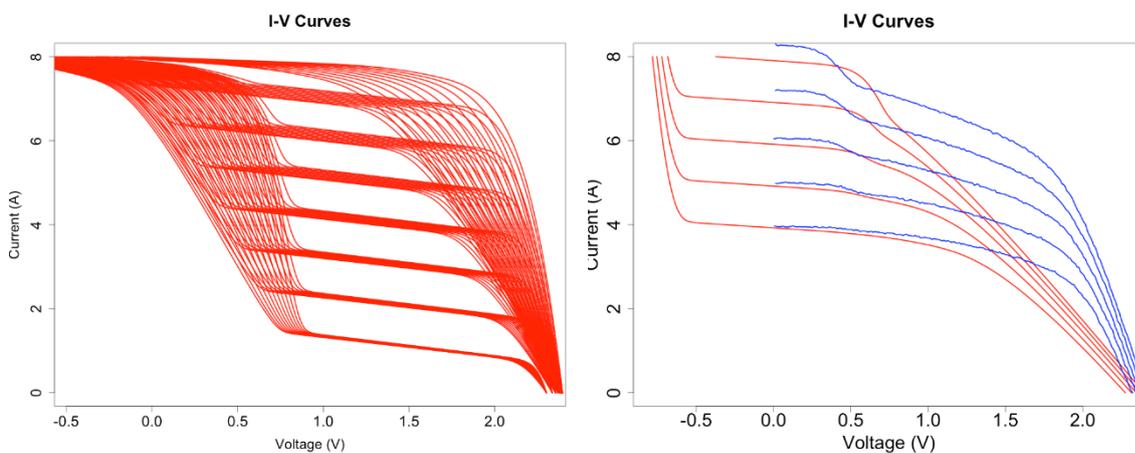

Figure 74: Examples of modeled (left) versus measured (right) IV curves.
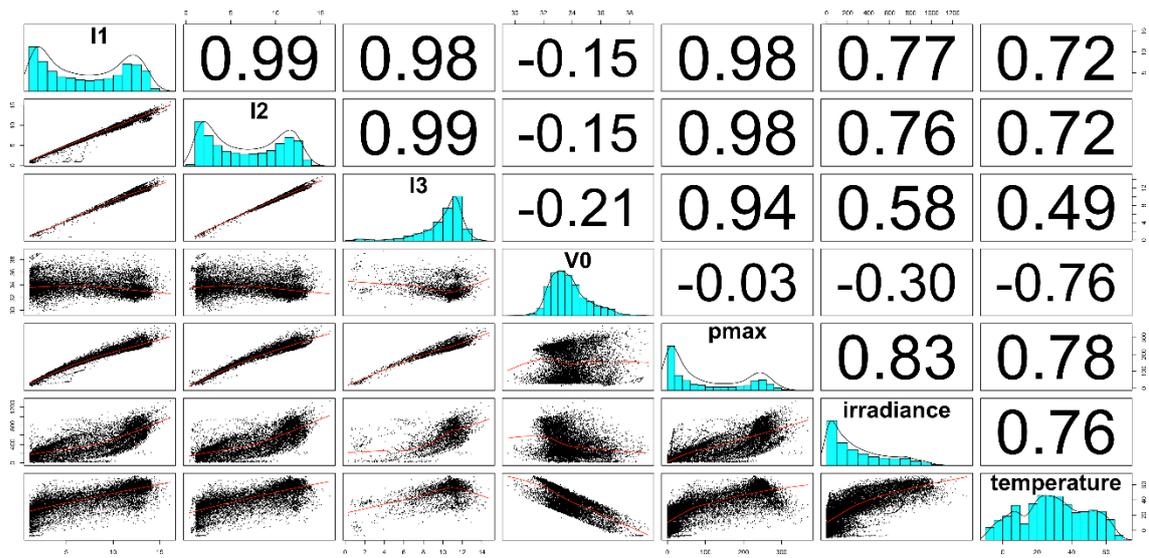
Figure 75: Example of a pairwise scatter and correlation matrix.

References

[1] "2015 4th PV Performance Modeling and Monitoring Workshop", *PV Performance Modeling Collaborative*, 2017. [Online]. Available: https://pvpmc.sandia.gov/resources-and-events/events/2015-4th-pv-performance-modeling-and-monitoring-workshop/. [Accessed: 27-Feb- 2017].

[2] Cameron, C., J. Stein and C. Tasca (2011). PV Performance Modeling Workshop Summary Report. Albuquerque, NM, Sandia National Laboratories. **SAND2011-3419**

[3] Box, G. E. P. and N. R. Draper (1986). Empirical model-building and response surface. New York, NY, John Wiley & Sons, Inc.

[4] Maxwell, E. L. (1987). A Quasi-Physical Model for Converting Hourly Global Horizontal to Direct Normal Insolation. Golden, CO, Solar Energy Research Institute.

[5] Perez, R., P. Ineichen, E. L. Maxwell, R. Seals and A. Zelenka (1992). "Dynamic Global-to-Direct Irradiance Conversion Models." ASHRAE Transactions **98**(1).

[6] "Albedo", *PV Performance Modeling Collaborative*, 2017. [Online]. Available: https://pvpmc.sandia.gov/modeling-steps/1-weather-design-inputs/plane-of-array-poa-irradiance/calculating-poa-irradiance/poa-ground-reflected/albedo/. [Accessed: 27- Feb- 2017].
[7] Hay, J. E. and J. A. Davies (1980). Calculations of the solar radiation incident on an inclined surface. First Canadian Solar Radiation Data Workshop. J. E. Hay and T. K. Won. Canada, Ministry of Supply and Services.

[8] Paltridge, G. W. and C. M. R. Platt (1976). Radiative processes in meteorology and climatology. New York, Elsevier Scientific Pub. Co.

[9] Reindl, D. T., W. A. Beckman and J. A. Duffie (1990). "Evaluation of Hourly Tilted Surface Radiation Models." Solar Energy **45**(1): 9-17.

[10] Perez, R., P. Ineichen and R. Seals (1990). "Modeling Daylight Availability and Irradiance Components from Direct and Global Irradiance." Solar Energy **44**(5): 271-289.

[11] Martin, N. and J. M. Ruiz (2001). "Calculation of the PV modules angular losses under field conditions by means of an analytical model." Solar Energy **70**: 25-38.

[12] "File:Solar spectrum ita.svg - Wikimedia Commons", *Commons.wikimedia.org*, 2017. [Online]. Available: http://commons.wikimedia.org/wiki/File:Solar_spectrum_ita.svg. [Accessed: 27- Feb- 2017].

[13] "Spectral Response", *PV Perfromance Modeling Collaborative*, 2017. [Online]. Available: https://pvpmc.sandia.gov/modeling-steps/2-dc-module-iv/effective-irradiance/spectral-response/. [Accessed: 27- Feb- 2017].

[14] King, D. L., E. E. Boyson and J. A. Kratochvil (2004). Photovoltaic Array Performance Model. Albuquerque, NM, Sandia National Laboratories. **SAND2004-3535**.

[15] Faiman, D. (2008). "Assessing the outdoor operating temperature of photovoltaic modules." Progress in Photovoltaics **16**(4): 307-315.

[16] Ross, R.G. and M.I. Smokler (1986). Flat-Plate Array Project – Final Report Vol. VI: Engineering Sciences and Reliability, JPL Pub. No. 86-31.

[17] Skoplaki, E. and J. A. Palyvos (2009). "Operating temperature of photovoltaic modules: A survey of pertinent correlations." Renewable Energy **34**(1): 23-29.

[18] Luketa-Hanlin, A. and J. S. Stein (2012). Improvement and Validation of a Transient Model To Predict Photovoltaic Module Temperature. World Renewable Energy Forum. Denver, CO.

[19] De Soto, W., S. A. Klein and W. A. Beckman (2006). "Improvement and validation of a model for photovoltaic array performance." Solar Energy **80**(1): 78-88.

[20] "Home", Pvsyst.com, 2017. [Online]. Available: http://www.pvsyst.com/en/. [Accessed: 27-Feb- 2017].

[21] Sellner, S., J. Sutterlueti, L. Schreier and S. Ransome (2012). "Advanced PV module performance characterization and validation using the novel Loss Factors Model." 38th IEEE PVSC: 2938-2943.

[22] Stein, J. S., J. Sutterlueti, S. Ransome, C. W. Hansen and B. H. King (2013). Outdoor PV Performance Evaluation of Three Different Models: Single-diode, SAPM and Loss Factor Model. 28th EU PVSEC. Paris, France.

[23] "PVWatts Calculator", Pvwatts.nrel.gov, 2017. [Online]. Available: http://pvwatts.nrel.gov/. [Accessed: 27- Feb- 2017].

[24] King, D. l., S. Gonzalez, G. M. Galbraith and W. E. Boyson (2007). Performance Model for Grid-Connected Photovoltaic Inverters. Albuquerque, NM, Sandia National Laboratories. **SAND2007-5036**.

[25] Driesse, A., P. Jain and S. Harrison (2008). Beyond the Curves: Modeling the Electrical Efficiency of Photovoltaic Inverters. 33rd IEEE PVSC San Diego, CA: 1935-1940.

[26] "CAMS radiation service - www.soda-pro.com", Soda-pro.com, 2017. [Online]. Available: http://www.soda-pro.com/web-services/radiation/cams-radiation-service. [Accessed: 27- Feb-2017].

[27] "ENDORSE FP7 project | ENDORSE (ENergy DOwnstRream SErvices)", Endorse-fp7.eu, 2017. [Online]. Available: http://www.endorse-fp7.eu/. [Accessed: 27- Feb- 2017].

[28] "Copernicus Atmosphere Monitoring Service |", Atmosphere.copernicus.eu, 2017. [Online]. Available: http://atmosphere.copernicus.eu/. [Accessed: 27- Feb- 2017].

[29] "MACC Project - Home", Gmes-atmosphere.eu, 2017. [Online]. Available: http://www.gmes-atmosphere.eu/. [Accessed: 27- Feb- 2017].

[30] "Home - OrPHEuS project", Orpheus-project.eu, 2017. [Online]. Available: http://www.orpheus-project.eu. [Accessed: 27- Feb- 2017].

[31] "Meteonorm: Irradiation data forevery place on Earth", Meteonorm.com, 2017. [Online]. Available: http://www.meteonorm.com. [Accessed: 27- Feb- 2017].

[32] "Homepage - GEBA", Geba.ethz.ch, 2017. [Online]. Available: http://www.geba.ethz.ch/. [Accessed: 27- Feb- 2017].

[33] Ineichen, P. (2008). "A broadband simplified version of the Solis clear sky model." Solar Energy **82**(8): 758-762.

[34] Marion, W., A. Anderberg, C. Deline, S. Glick, M. Muller, G. Perrin, J. Rodriguez, S. R. , K. Terwilliger and T. J. Silverman (2014). User's Manual for Data for Validating Models for PV Module Performance. Golden, CO, National Renewable Energy Laboratory. **NREL/TP-5200-61610**.

[35] Nelson, L., M. Frichtl and A. Panchula (2012). "Changes in cadmium telluride photovoltaic system performance due to spectrum." Journal of Photovoltaics **3**(1): 488-493.

[36] Haurwitz, B. (1946). "Insolation in Relation to Cloud Type." Journal of Meteorology **3**: 123-124.

[37] D. Ryberg and J. Freeman, "Integration, Validation, and Application of a PV Snow Coverage Model in SAM", National Renewable Energy Laboratory, 2015.

[38] Marion, B., R. Schaefer, H. Caine and G. Sanchez (2013). "Measured and modeled photovoltaic system energy losses from snow for Colorado and Wisconsin locations." Solar Energy **97**: 112-121.

[39] Winter, M. et al., "Impact of realistic illumination on optical losses in Si solar cell modules compared to standard testing conditions", EUPVSEC, 2015

[40] Ernst, M., H. Holst, M. Winter and P. P. Altermatt (2016). "SunCalculator: A program to calculate the angular and spectral distribution of direct and diffuse solar radiation." Solar Energy Materials and Solar Cells **157**: 913-922.

[41] Holst, H., M. Winter, M. R. Vogt, K. Bothe, M. Köntges, R. Brendel and P. P. Altermatt (2013). "Application of a New Ray Tracing Framework to the Analysis of Extended Regions in Si Solar Cell Modules." Energy Procedia **38**: 86-93.

For further information about the IEA Photovoltaic Power Systems Program and Task 13 publications, please visit www.iea-pvps.org.